ANALYSIS OF BIOPOLYMERS AND SYNTHETIC POLYMERS USING STRUCTURALLY SELECTIVE ANALYTICAL TECHNIQUES IN COMBINATION WITH MASS SPECTROMETRY

By

Rachel A. Harris

Dissertation

Submitted to the Faculty of the

Graduate School of Vanderbilt University

in partial fulfillment of the requirements

for the degree of

DOCTOR OF PHILOSOPHY

in

Chemistry

May 14, 2021

Nashville, Tennessee

Approved:

John A. McLean, Ph.D.

Ned A. Porter, Ph.D.

Lauren E. Buchanan, Ph.D.

Kevin L. Schey, Ph.D.

To my friends, family, and coworkers, whose support is invaluable to me.

ACKNOWLEDGEMENTS

I would like to start by thanking Dr. Gary Glish, who introduced me both to mass spectrometry and my dissertation advisor, Dr. John A. McLean. At the time, I never considered that an extra credit school project would lead me to my love of mass spectrometry and my future career. The mentorship I received in my undergraduate studies helped propel me to where I am today, and I am eternally grateful.

I would also like to thank Dr. McLean, who recruited me to Vanderbilt and provided me the opportunity to work in his research group over the past six years. I remember attending a guest lecture at the University of North Carolina at Chapel Hill hosted by Dr. McLean and being completely smitten with the research his lab was conducting, particularly the lab-on-a-chip research project. The opportunity to work in the McLean lab among bright fellow scientists and cutting-edge instrumentation, has been an incredibly special, although at times challenging, time in my life that I will never forget. Thank you again, Dr. McLean, for your mentorship and helping me develop into the scientist I am today.

I would like to acknowledge my dissertation committee members for their support and guidance on my dissertation research. The time they spent working with me is greatly appreciated and their advice invaluable. Thank you, Dr. Ned A. Porter, Dr. Kevin L. Schey, and Dr. Lauren E. Buchanan.

My collaborators over the years also deserve thanks and acknowledgment. I particularly want to thank Dr. Vicki H. Wysocki and Dr. Sophie R. Harvey for their aid on the SID project. This project began in my first year of graduate school and was very challenging, but Dr. Harvey was always available to help me troubleshoot issues I was having with the instrument, even going

could have done it without you. To my brother, thank you for brewing me beer; I still think we should combine our areas of expertise to open a brewery someday. Last but not least, thank you to my cat, Cleo, who kept me company during a long year of quarantine and "helped" me with my writing. I love all of you dearly.

TABLE OF CONTENTS

LIST OF TABLES

LIST OF FIGURES

LIST OF ABBREVIATIONS

HMDB ....The Human Metabolome Database

MS .... Mass spectrometry

LC ....Liquid chromatography

LC-MS .... Liquid chromatography-mass spectrometry

HPLC ....High pressure liquid chromatography

ESI... Electrospray ionization

MALDI ....Matrix assisted laser desorption ionization

CID...Collision-induced dissociation

EIEIO ....Electron impact excitation of ions from organics

PB... Paternò-Büchi

Oz..Ozonolysis

OzID... Ozone-induced dissociation

UVPD..Ultraviolet photodissociation

RDD ....Radical-directed dissociation

IM..Ion mobility spectrometry

IM-MS.. Ion mobility-mass spectrometry

CCS .... Collision cross section

$^{DT}CCS_{N2}$ .... Drift tube CCS measured in nitrogen drift gas

TWIMS .... Traveling wave ion mobility spectrometry

SLIM ....Structures for lossless ion manipulations

DMS .... Differential mobility spectrometry

CHAPTER 1

NEW FRONTIERS IN LIPIDOMICS USING STRUCTURALLY SELECTIVE ION

MOBILITY MASS SPECTROMETRY[*]

1.1   Introduction

Lipids are an incredibly diverse class of molecules that regulate cellular activity, act as

signaling molecules, and serve as the primary constituent of cell membranes, among other vital

biological functions. As understanding of their complex roles in biological systems increases,

lipids are gaining potential as therapeutic drug targets, especially given the intersection of lipid

metabolic pathways with disease states such as cancer and diabetes.[1–3] The increasing relevance

of lipids necessitates the development of analytical strategies for the discrimination and

identification of these species in biolo1gical samples. Lipidomics, the broad scale analysis of the

lipid content of a given system, poses unique analytical challenges due to the astounding structural

diversity amongst lipids.[3,4] This issue is further complicated in that many lipid species are

structural isomers, several examples of which are illustrated in Figure 1.1(A) for a common

phosphatidylcholine species. Potentially hundreds of thousands of unique lipid molecules exist in

biological samples, but only a small fraction of these have been putatively identified over recent

decades. The source of this discrepancy is largely due to lipidomic workflows being generally

developed for mass spectrometry (MS), a robust technology capable of identifying unknown

species by mass.[2–5] Although MS allows for high-throughput analyses of complex samples,

without a complementary separation method, MS measurements alone cannot distinguish isomeric components present in these samples. The necessity of the large degree of lipid isomerism produced in nature has yet to be determined; however, the specific, predictable lipid structural

motifs have a distinctly biological basis. As an example, fatty acids (FAs) are used in the biosynthesis of six of the eight categories of lipids defined by the LipidMaps Consortium and therefore represent a useful model system for understanding broader lipid structural trends.[6] Biological synthesis of FAs is a widely conserved process across all eukaryotes and some prokaryotes, and although specific enzymes may differ between species, catalyzed condensation of acetyl-CoA units for chain elongation is generally involved.[7,8] For this reason, most endogenous FA molecules contain an even number of carbon atoms, and additional biological rules govern placement of double bonds via desaturation pathways. Attention to these biological guidelines provides researchers with a powerful tool to leverage in bioinformatics approaches for more sophisticated hypotheses for lipid analyses. As previously stated, one challenge in the field of lipidomics is the discrimination of isomeric species. The true number of naturally occurring isomeric lipid species is unknown, but it is estimated to be in the tens of thousands. The Human Metabolome Database (HMDB) released its most comprehensive update in 2018, along with a new category of metabolites termed "Expected" to represent species of known structures that have yet to be detected in the human body or for which the precise isomer has yet to be formally identified.[9] Over 90% of the 82,274 compounds reported in this category are lipids, indicating the potential scale of the isomer issue. A simple enumeration equation for FAs (Figure 1.1(B)) was developed by the authors to estimate the number of theoretical double bond positional isomers (DBPI) and *cis/trans* geometric isomers (GI) that can exist for unmodified (e.g., no hydroxylation, methylation,

(A)

PC 16:0/18:1(9Z)	PC 16:0/18:1(9Z)	PC 16:0/18:1(9Z)	PC 16:0/18:1(9Z)
PC 18:1(9Z)/16:0	PC 16:0/18:1(10Z)	PC 16:0/18:1(9E)	PC 16:0/18:1(9Z)
sn-regioisomers	double bond positional isomers	*cis / trans* isomers	stereoisomers
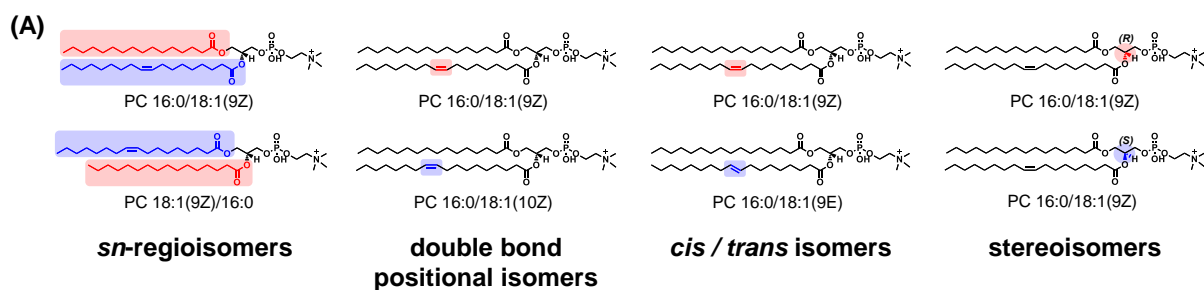
(B) **Enumeration Equations for C18:N Fatty Acid (FA) Isomers** (C = Carbons; N = Double Bonds)

$$DBPI = \sum_{i=1}^{C-2N} \frac{i(i+1)(i+2)}{6}(C-2N-i+1)$$

$$GI = 2^N \cdot DBPI - 2\left[\sum_{i=1}^{C-2N}\frac{1}{2}i(i+1)(C-2N-i+1)\right]$$

Double Bond Positional Isomers (DBPI)   *Geometric (cis / trans) Isomers (GI)*

Figure 1.1 (A) Visualization of potential isomeric forms of PC 34:1 including sn-regioisomers, double bond positional isomers, geometric cis/trans isomers, and chiral stereoisomers. **(B)** Enumeration equations for the determination of double bond positional isomers and geometric isomers for simple, straight-chain fatty acids.

oxidation), straight chain fatty acids containing 18 carbon atoms, which are among the most abundant FA chain lengths encountered in nature. Established rules governing typical lipid structure were followed, which excludes double bonds positioned at the α- and ω-carbons and adjacent to additional double bonds. Calculation results for these equations are summarized in Table 1.1 and indicate that hundreds to tens of thousands of possible isomers exist for even the simplest FA lipids. A more rigorous enumeration of lipid isomers has been reported by Schuster et al. using generalized Fibonacci numbers, which in addition to DPBI and GI, considers the allowance of allenic and cumulenic FAs as well as modifications to the carbon chain. In their analysis, a C18 FA can have over 1×10^9 possible forms.[10] Although only a fraction of these theoretical FA isomer species are expected to occur biologically, it is currently unknown to what extent. Therefore, chemical separation and analysis approaches capable of differentiating various isomeric forms are necessary in order to improve current lipidomic strategies and expand the breadth of analytical information that can be obtained. Moreover, detailed knowledge of experimentally-observed lipid structural trends present in multidimensional analytical data will become critically important in guiding the development of predictive informatic tools and improve the confidence in lipid annotation and identification.

1.2   New Directions in Lipidomic Analyses

Recent advances in mass spectrometry and related analytical techniques have helped drive the field of lipidomics forward. In particular, ion activation/fragmentation techniques such as collision-induced dissociation (CID) and electron impact excitation of ions from organics (EIEIO) have enabled the discrimination of *sn*-regioisomers.[11–13] Additionally, techniques which promote carbon-carbon double bond cleavage have been developed in conjunction with MS to identify

double bond position, in particular the Paternò-Büchi (PB) and ozonolysis (Oz) reactions.[14–16] However, at this time there is no single technique capable of resolving all types of isomers commonly encountered in lipid samples (Figure 1.1(A)).[5,17] Therefore, integration of multiple approaches is necessary to expand lipidome coverage and to differentiate isomeric species. In this chapter, we focus predominantly on the utilization of ion mobility-mass spectrometry (IM-MS) for lipidomic analyses and its combination with orthogonal analytical techniques. IM is particularly suited to tackling the specific structural issues endemic to lipidomics discussed previously. The IM technique separates gas-phase ions based on differences in their collision cross section (CCS), a parameter that correlates to the two-dimensional cross sectional area of the molecule in the gas phase.[18] Prior studies indicate that the multidimensional separations resulting from IM-MS analyses are capable of differentiating isomers and delineating molecules into respective biomolecular classes.[19,20] When applied to lipids, IM-MS analyses have previously revealed specific and reproducible mobility-mass correlations related to differences in headgroup, acyl chain length, and degree of unsaturation.[21] The relationship between lipid structure and gas-phase conformation via IM-MS analysis are explored in the following section, with subsequent expansion towards predictive approaches and complementary analytical techniques.

In this chapter, we focus predominantly on the utilization of ion mobility-mass spectrometry (IM-MS) for lipidomic analyses and its combination with orthogonal analytical techniques. IM is particularly suited to tackling the specific structural issues endemic to lipidomics discussed previously. The IM technique separates gas-phase ions based on differences in their collision cross section (CCS), a parameter that correlates to the two-dimensional cross sectional area of the molecule in the gas phase.[18] Prior studies indicate that the multidimensional separations

Table 1.1 Theoretical number of double bond positional isomers and *cis*/*trans* isomers for unmodified, straight chain fatty acids containing 18 carbon atoms and 0-5 double bonds. Isomer numbers are calculated from the equations presented in **Figure 1.1 (B)**.

Fatty Acid (FA)	Molecular Formula	Exact Mass (Da) ([M-H]$^-$)	Number of Carbons	Number of Double Bonds	Number of Possible Double Bond Isomers	Number of Possible *cis* / *trans* Isomers
FA 18:0	$C_{18}H_{36}O$	283.2637	18	0	0	0
FA 18:1	$C_{18}H_{34}O$	281.2480	18	1	16	30
FA 18:2	$C_{18}H_{32}O$	279.2324	18	2	105	392
FA 18:3	$C_{18}H_{30}O$	277.2167	18	3	364	2756
FA 18:4	$C_{18}H_{28}O$	275.2011	18	4	715	11000
FA 18:5	$C_{18}H_{26}O$	273.1854	18	5	792	25104

resulting from IM-MS analyses are capable of differentiating isomers and delineating molecules into respective biomolecular classes.[19,20] When applied to lipids, IM-MS analyses have previously revealed specific and reproducible mobility-mass correlations related to differences in headgroup, acyl chain length, and degree of unsaturation.[21] The relationship between lipid structure and gas-phase conformation via IM-MS analysis are explored in the following section, with subsequent expansion towards predictive approaches and complementary analytical techniques.

1.3   Mobility-Mass Trends and Prediction of CCS for Lipid Analyses

One of the more interesting aspects of IM-MS data is the existence of empirical correlations between the analyte ion size (mobility) and its mass, i.e., chemical class trendlines which correspond to the specific conformation that the analyte ion adopts within the anhydrous, gas-phase environment of the IM spectrometer. These mobility-mass correlations are related to the primary structure of the analyte and thus are highly-specific for each biomolecular class.[20,22–27] For lipids, it has been shown that gas-phase packing is inefficient, resulting in a relatively large size-to-mass ratio that allows lipids to be readily differentiated from other molecules within a 2-dimensional IM-MS spectrum. Recent developments in commercial IM-MS instrumentation have allowed for larger numbers of lipids to be measured with high precision and reproducibility, which has facilitated the development of IM-MS lipidomic databases incorporating both size (CCS) and mass measurement information.[28,29] This in turn, has allowed for numerous sub-classes of lipids to be analyzed for specific size-mass trends which can be quantitatively-mapped in support of utilizing IM information for identifying and characterizing unknowns.[28–31]

Recent work from the authors' laboratory has focused on mapping IM-MS structural trends for broad classes of lipids (Figure 1.2(A)), yielding over 450 CCS measurements ($^{DT}CCS_{N2}$) for

217 unique lipid species obtained from four classes of glycerophospholipids (PC, PE, PS, PA) and three classes of sphingolipids (GlcCer, Cer, SM).[28] This dataset was sufficiently large to allow specific structural trends to be quantitatively mapped for each lipid sub-class as well as for different ion forms (e.g., H^+, Na^+, H^-, etc.) within each class, shown in Figure 1.2(B) for glucosylceramides. As with trends observed in smaller IM-MS studies using DTIMS[32–34] and TWIMS,[35,36] the conformational orderings of lipids were found to be well-represented by linear functions[37] and reproducibly influenced by polar headgroup (lipid class), acyl chain length, degree of unsaturation, and ion form. Similar to previous findings[36], sphingolipids were found to adopt larger gas-phase conformations than phospholipids (quantitatively, by approximately 2-6% increase in CCS), with this observation being attributed to the limited degrees of unsaturation in sphingolipids due to the constraint imposed by the $sn1$ sphingosine backbone.[28] Linear equations were fitted to groups of lipids differing only in their number of double bonds or acyl chain carbon atoms, and it was found that variations in degree of unsaturation were three to four times as influential on the CCS as alkyl chain length for similar masses. The influence of the ion form on the CCS was found to be correlated to the size of the charge-carrier adduct, i.e., $[M+2Na-H]^+$ > $[M+K]^+$ > $[M+Na]^+$ > $[M+H]^+$ > $[M-H]^-$.

Zhu and coworkers have recently developed a machine learning model to predict lipid CCS_{N2} values.[29] Using a commercial DTIMS, the authors first empirically measured 458 lipid $^{DT}CCS_{N2}$ values across ten classes of glycerophospholipids (PC, PE, PG, PS, PI, PA, LPC, LPE, LPI, LPS), two classes of glycerolipids (TG, DG), and three classes of sphingolipids (SM, Cer, GlcCer). Linear trends for acyl chain length and degree of unsaturation were observed, such as is shown for PE lipids in Figure 1.2(C). Using this large pool of CCS data, the authors then developed
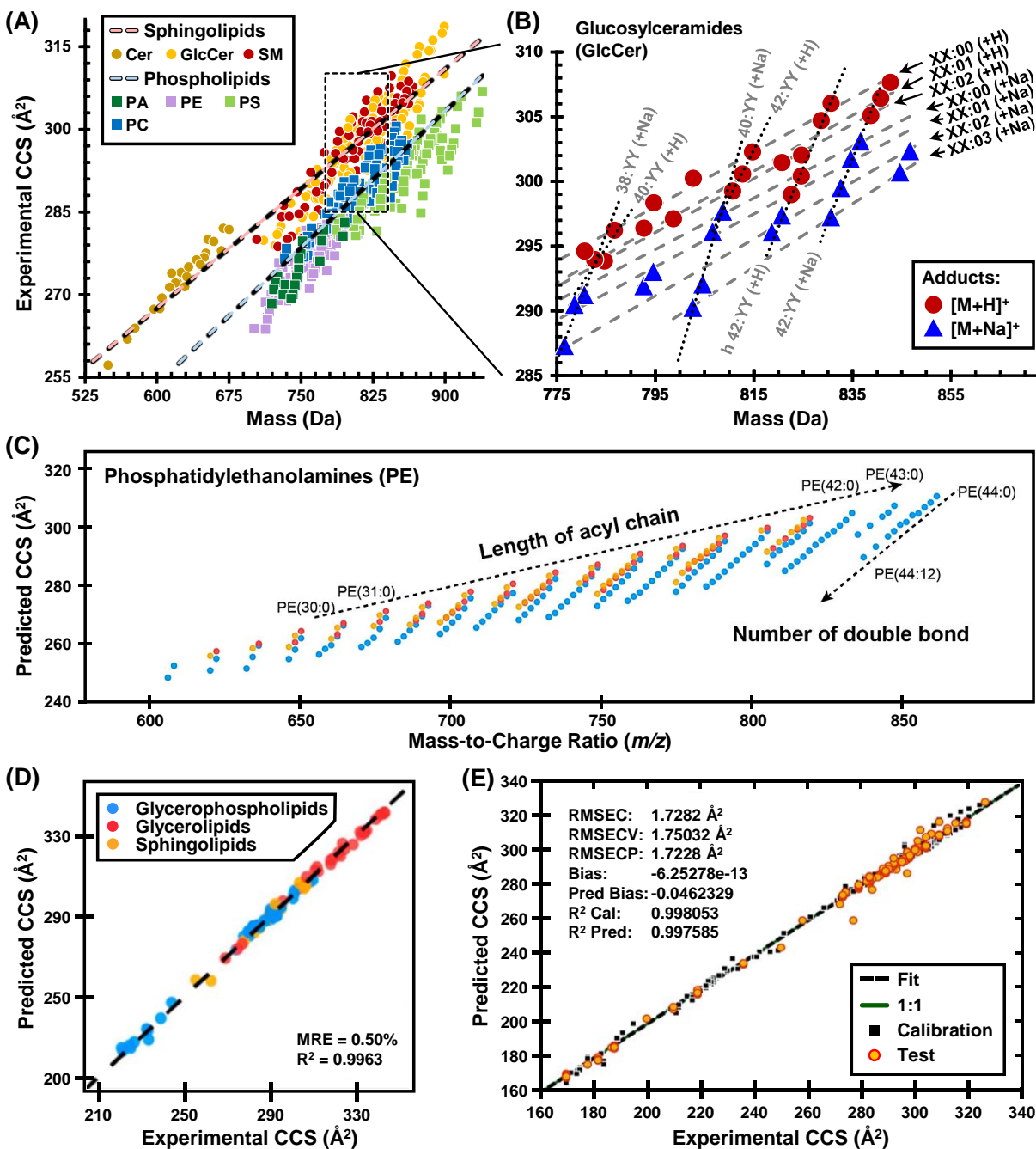
Figure 1.2 (**A**) Experimentally measured $^{DT}CCS_{N2}$ vs mass measurements and linear regressions plotted for the two lipid categories, sphingolipids and phospholipids. (**B**) Quantitative correlations observed within GlcCer cation data corresponding to variation in either acyl chain length (*i.e.* XX:00) or degree of unsaturation (*i.e.* 42:YY). (**C**) Linear trends for three common PE lipid modifications (colored markers) to investigate the effect of acyl chain length and degree of unsaturation in [M+H]$^+$ ions . (**D**) Intra-lab validation for correlation of predicted and experimental $^{DT}CCS_{N2}$ values for cations of three lipid classes. (**E**) Correlation of cross validation (CV)-predicted and experimental $^{TW}CCS_{N2}$ with root mean square error of calibration (RMSEC), cross validation (RMSECV), and test set prediction (RMSECP), as well as bias and fitness.

a prediction model called LipidCCS Predictor which was capable of predicting lipid CCS values with an externally validated median relative error of ca. 1% (Figure 1.2(D)). The support vector regression-based prediction models were built using optimized molecular descriptors (45 for cations and 66 for anions) to generate a large-scale, theoretical database of lipid CCS values, containing 63,434 predicted lipid CCS values covering 22 common lipid classes.[29] Both the LipidCCS Predictor and LipidCCS database are freely-accessible. For CCS_{N2} prediction, users can input SMILES structures into LipidCCS Predictor, which currently supports prediction for five commonly observed, singly charged adducts including $[M+H]^+$, $[M+Na]^+$, $[M+NH_4]^-$, $[M+COOH]^-$, and $[M-H]^-$.

Fernandez and coworkers recently demonstrated another machine-learning approach for predicting lipid CCS values using only 2-dimensional molecular descriptors (numerical representatives of chemical structure) as inputs.[30] From a database of $^{TW}CCS_{N2}$ measurements published by Astarita and coworkers,[38] 195 values representing a wide variety of lipids were selected. An initial machine learning step prioritized 68 molecular descriptors of shape, symmetry, connectivity, chemical diversity, etc. upon which partial least squares (PLS) linear multivariate regression models were used to accurately predict CCS from 2D structures with a root mean square error for CCS prediction (RMSECP) of 1.72 $Å^2$ (Figure 1.2(E)).[30] These and other machine learning approaches to CCS prediction are critically important for populating large databases of lipid CCS values where experimental measurements cannot be obtained, such as the case for the near 100,000 lipids which are only theoretically predicted to exist.[9]

While the numbers of high-quality, experimentally-measured lipid CCS values have increased drastically within the last few years, there are relatively few initiatives to integrate this data into lipidomic informatic workflows. Recently, McLean and coworkers compiled over 3,800

experimental $^{DT}CCS_{N2}$ values into an online, interactive resource called the Unified CCS Compendium. In addition to a large number of peptides, carbohydrates, and small molecule metabolites, this Compendium includes over 800 lipid CCS values, all of which have been scaled to reference values in order to make this resource self-consistent.[31] Regression models and predictive statistics were used in the Compendium to describe empirical size-mass correlations, and these mathematical relationships can serve as an identification filter in untargeted experimental workflows. As an example, the identification of an unknown biochemical species from a human serum sample was narrowed from 325 potential chemical formulas to 21 PC lipid isomers using the IM-MS information from the Compendium. This CCS filtering workflow results in higher confidence assignment of chemical class, and the predictive capabilities will support annotation of unknown chemical isomers which are commonly encountered in lipidomic and metabolomic studies. For lipid-specific analysis, Zhu and coworkers have recently developed a software tool known as LipidIMMS Analyzer to support the accurate identification of lipids using IM-MS.[39] The software incorporates a multi-dimensional database comprised of over 260,000 theoretical lipids annotated with predicted *m/z*, retention time, CCS, and fragmentation information and currently supports multiple data acquisition approaches and IM-MS instrumentation types. A test data set comprised of both lipid standards and biological samples yielded 500-600 lipid identifications through LipidIMMS Analyzer and indicated the increased identification confidence gained by utilizing a multidimensional approach.[39] While these and other IM-MS approaches provides important information for supporting the identification of lipids from untargeted studies, comprehensive lipidomics, however, requires more structural detail than can yet be gleaned from trend and predictive analyses of CCS, thus more structurally-specific analytical techniques need to be employed, such as those addressed in the following section.

11

1.4 Diagnostic Double Bond Cleavage Coupled to IM-MS and Other Fragmentation Approaches

Given the strong influence of molecular structure on biological function, the discrimination of lipid double bond positional isomers (Figure 1.1(A)) is an analytical challenge of great interest to the lipidomic community. Analyses combining MS and X-ray crystallography have shown that the position and degree of unsaturation of a lipid's acyl chain(s) affect the ability of that species to fit in the binding pocket of an interacting protein partner.[40,41] Given the potential existence of thousands of double bond positional isomers in biological samples, the identification and separation of these species is a laborious yet crucial task. Therefore, it is beneficial to combine multiple stages of analytical techniques to enhance lipid isomer separation and identification.[17]

While IM has been successfully applied to the separation of *cis/trans* lipid isomers, the differences in CCS of double bond positional isomers is generally too small to be resolved with current IM instrumentation.[25,42] Thus, to distinguish between double bond positional isomers, alternative strategies are necessary. While multiple analytical strategies have been developed for this purpose, including radical-derived processes such as ultraviolet photodissociation (UVPD),[43] electron impact excitation from organics (EIEIO),[13] and radical-directed dissociation (RDD),[44] here we will focus primarily on ion-molecule reactions that specifically target the C=C double bond.

Ozonolysis (Oz)[15,16,45–49] and Paternò-Büchi (PB) reactions[14,50–53] have both been utilized to target sites of unsaturation in lipids. When interfaced with MS, Oz and/or PB reactions induce fragmentation at the C=C double bond, resulting in diagnostic fragment ions whose mass pinpoints the double bond location in the lipid precursor ion. The two approaches have been utilized in both shotgun[16,46,48,54] and HPLC-coupled workflows[55–58] and are capable of readily identifying a

multitude of lipid C=C isomers in complex samples. In order to facilitate data analysis, custom software have been developed by both the Xia and Mitchell groups to automate the annotation of reaction products originating from Oz and PB reactions.[57,59]

More recently, ozonolysis has been combined with DTIM-MS as an orthogonal dimension of separation, and the implementation of ozonolysis on a drift tube IM-MS instrument is described in Chapter 2 of this work.[58,60–62] Generally, ozonolysis may be performed either prior to or after separation via IM. For example, differential mobility spectrometry (DMS) as a front-end separation technique for ozonolysis has been used for the structural characterization of unsaturated PCs, as well as 1-deoxysphingosine and its isomers.[60–62] Conversely, ozonolysis can also be performed prior to IM as part of an LC-Oz-IM-MS workflow (Figure 1.3(A)). In this case, IM separates the diagnostic ozonolysis fragment ions produced by the reaction, allowing further structural discrimination and improving sensitivity for low abundance fragments. For this workflow, the ozonolysis reaction can be performed either in solution or in the gas phase, with the latter implementation termed OzID.[56,58] The solution-phase method utilizes a low-pressure mercury lamp mounted parallel with the fluidics to convert dissolved oxygen gas into ozone that reacts with lipids before ionization in the ESI source. Conversely, the gas phase approach requires modification of the IM-MS instrument such that ozone is introduced into the trapping ion funnel, allowing controlled reactions of ozone with lipid ions on timescales of 1-90 ms prior to injection into the IM drift tube. Because the rate of reaction is sufficiently fast, ozonolysis and OzID product ions can be correlated to precursors based on common retention times when LC separation is included.
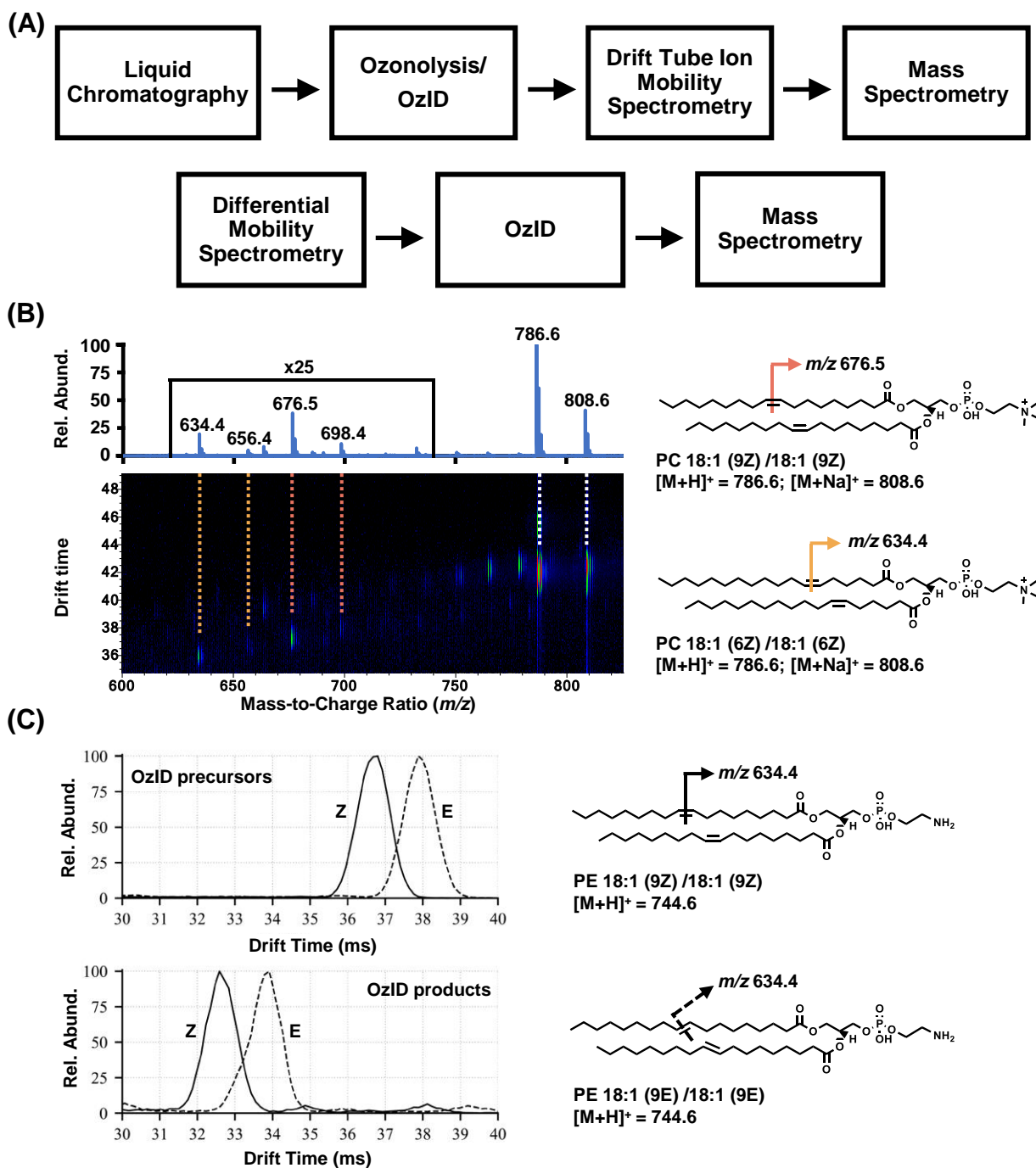
Figure 1.3 (A) Example workflows combining IM and ozonolysis techniques. **(B)** A mixture of PC double bond positional isomers is converted to diagnostic products using Oz-IM-MS. **(C)** IM elution order of *cis*/*trans* PE isomers is retained post-ozonolysis, allowing for identification of precursors.

An example of how ozonolysis can be used to elucidate double bond location is depicted in Figure 1.3(B), where the IM-MS spectrum of a mixture of PC 18:1(9Z)/18:1(9Z) and PC 18:1(6Z)/18:1(6Z) double bond positional isomers is shown. The primary spectral peaks at *m/z* 786.6 and *m/z* 808.6 represent the [M+H]$^+$ and [M+Na]$^+$ cations, respectively. The isomer with double bonds at the 9Z positions reacted with ozone to form products at *m/z* 676.5 [M+H]$^+$ and *m/z* 698.4 [M+Na]$^+$, while the isomer with double bonds at the 6Z positions gave products at *m/z* 634.4 [M+H]$^+$ and *m/z* 656.4 [M+Na]$^+$. Each of these species possesses a unique drift time, which corresponds to the time taken for that particular ion to traverse through the drift tube. This drift time is proportional to the size and shape of the molecule in the gas phase, and it has previously been observed that changing the position and orientation of a lipid species' double bond changes the molecule's resulting drift time.[25]

Blanksby and coworkers have demonstrated that differences in unique drift times for *cis*/*trans* isomer precursors allows for correlation to and identification of their product ions in combined OzID-IM experiments.[56] When running a mixture of PE *cis*/*trans* isomers, namely PE 18:1(9Z)/18:1(9Z) and PE 18:1(9E)/18:1(9E), it was observed that the *cis* isomer exhibited a lower drift time than the *trans* isomer (Figure 1.3(C)). This relationship was retained post-OzID in the fragment ions, and although the two resulting products had the same mass, they could be identified based upon their IM elution order.

Ion mobility separations and ozonolysis reactions exist as orthogonal techniques, and when combined serve as a powerful analytical tool for lipid isomer discrimination and identification. The work described here illustrates that combined LC-Oz/OzID-IM-MS workflows allow for the differentiation of both *cis*/*trans* isomers and double bond positional isomers, two of the four isomer types described in Figure 1.1(A). The ongoing work to integrate these techniques into a standard

LC-MS lipidomics workflow will rely on the development of bioinformatics software for the automated assignment of spectral peaks that, once completed, will enable thousands of lipid identifications from a single experiment, bringing the field closer to the capability of cataloguing the entirety of the lipidome.

Although this section has primarily focused thus far on the identification of double bond position and the discrimination of double bond position isomers, the presence of other forms of isomerism in lipid biological extracts including *cis/trans* isomers, *sn*-regioisomers, and stereoisomers necessitate the development of a multi-pronged analytical approach to expand lipidomic coverage, which in turn will lead to more accurate biological predictions.[5,17] To that end, our lab has explored the utilization of alternative fragmentation techniques for improved lipid structural characterization. Two strategies we have focused in particular to increase lipid structural information content include the implementation of surface induced dissociation (SID), an alternative to collision induced dissociation, and the utilization of energy-resolved ion breakdown curves (ERIBC). SID, which will be explored in depth in Chapter 3, is a fragmentation mechanism in which energy is imparted to the target molecule via collision with a solid surface. The technique may be utilized in combination with IM, and similarly to ozonolysis as discussed earlier in this section, can be implemented either before or after mobility separation.[63] By utilizing a comparatively massive surface as a collision partner, SID is considered to have more efficient energy transfer to the analyte than CID, which is generally limited by the mass of the collision partner.[64,65] Additionally, SID occurs on a faster timescale than CID fragmentation, lowering the probability of rearrangement reactions, and is therefore is potentially able to access fragmentation pathways unavailable to CID for certain classes of molecules.[66] For these reasons, our lab was

interested in exploring the utility of SID for the analysis of lipids, which have not previously been studied using this analytical technique.

Energy-resolved ion breakdown curves (ERIBC) are another strategy our lab has utilized for in-depth analysis of lipid fragmentation pathways. Sometimes alternatively referred to as "breakdown curves" or "energy-resolved mass spectrometry," ERIBC are a fragmentation data visualization strategy that has been utilized in the field of mass spectrometry for decades and serve as a graphical representation of how the fragmentation spectrum of an analyte changes as a function of increasing collision energy. They are constructed by plotting the relative intensities of the most abundant fragment ions as a function of either lab frame collision energy or center of mass collision energy (E_{COM}). Historically, ERIBC have been utilized mainly for the comparison of different fragmentation mechanisms for a single analyte (e.g. SID versus CID) as well as a means of discriminating isomeric compounds.[67–69] Comparing the ERIBC of two isomers can illuminate subtle differences in the relative rates of different decomposition mechanisms that may not be immediately apparent when viewing individual fragmentation spectra.[70,71] For example, a specific fragmentation mechanism leads to the generation of product ion A, while a competing mechanism produces ion B. Therefore, the isomeric compounds 1 and 2 can be subsequently distinguished by differences in their relative rates of production of ions A and B in their ERIBC. Alternatively, isomers can be differentiated based on differences in appearance energy (the collision energy at which a given fragment ion appears in the mass spectrum) in the ERIBC for a particular fragment, which is also indicative of the relative stabilities of the two compounds. In this way, projecting the fragmentation data in the form of ion breakdown curves provides additional information in terms of specific decomposition pathways and comparison of ERIBC can help elucidate differences in isomeric structures.

1.5   Conclusions

Lipidomics as a field has experienced enormous growth in past decades, but still faces critical challenges due to the structural complexity of lipid species and the high degree of isomerism hindering putative identifications. New analytical developments leverage the highly-conserved rules of lipid biosynthesis on expected lipid structure to more fully characterize lipid samples. In particular, IM-MS analysis of lipids reveals quantitative structural trends based on headgroup, acyl chain length, and degree of unsaturation. Combining IM with targeted ion-molecule reactions such as Oz and PB or alternative fragmentation techniques such as SID provide orthogonal dimensions of separation for further discrimination of isomeric species. Future directions to further interrogate lipid structural trends include bioinformatics approaches, such as predicting CCS, and the integration of IM and novel ion activation techniques into existing lipidomic workflows, both of which will promote improved identifications and expansion of the current lipidomic landscape.

1.6   Extension of Methodology to Analysis of Polymers

While this chapter has principally focused on the challenges inherent in the structural analysis of lipids for improving lipidomic workflows, several of the methodologies discussed in the preceding sections can also be applied to the analysis of synthetic polymers. As is the case with lipids, comprehensive analysis of synthetic polymers is challenging due to the high level of structural heterogeneity present in samples.[72–74] Industrially, polymers are synthesized in a process known as "melt polymerization" that results in a complex mixture of leftover starting material and a distribution of oligomers of varying sizes. Further complicating analysis, some polymers such as polyurethanes exist as copolymers consisting of two or more repeat units. For polyurethanes, the

repeat units are typically comprised of "hard" blocks that increase structural rigidity and flexible polyol "soft" blocks; the polymer's overall properties are a direct function of the number of and sequence of these blocks.[72,75] However, the ability to determine the sequence of units is incredibly challenging via mass spectrometry, along with the ability to distinguish sequence structural isomers. For example, two polyurethane oligomers containing a single hard block unit and four soft block units might differ in the placement of the hard block unit in the chain but have the same overall mass and are thus indistinguishable via mass spectrometry. The utilization of alternative analytical techniques sensitive to the three-dimensional structure of the analyte is therefore necessary for improving the characterization of synthetic polymer samples. As has been discussed previously in the context of lipid analysis, IM and targeted fragmentation are strategies attuned to molecular structure that both help reduce mass spectral complexity and allow for discrimination of isomeric species. The application of IM-MS and MS/MS for the analysis of three isomeric polyurethane oligomers is discussed in depth in Chapter 4 of this work and serves as a model workflow for the analysis of more complex polymer samples in the future.

1.7   Objectives of Dissertation Research

Mass spectrometry is a key tool for the analytical characterization of unknown samples; however, it lacks the level of structural fidelity necessary for the discrimination of isomers. The overarching goal of this work is the development and application of state-of-the-art analytical strategies complementary to traditional mass spectrometry workflows in order to improve the structural characterization of both lipids and polymer samples. These strategies, which include IM and fragmentation mechanisms such as ozonolysis, SID, and CID, increase the information content gained in a single experiment and provide additional structural information to aid in the

discrimination of isomeric species. Chapter 2 begins with the development of an online ozonolysis device that when interfaced with an IM-MS instrument allows for the determination of lipid double bond position. In this implementation of the technique, the ozonolysis reaction occurs in the solution phase prior to the ionization of the sample in the source of the mass spectrometer. The device performance was characterized in terms of conversion efficiency at a given flow rate for several lipid standards via direct infusion. The full LC-Oz-IM-MS workflow combines the benefits of its constituent analytical techniques and was demonstrated to allow for the discrimination of both cis/trans isomers and double bond positional isomers in a single run for a mixture of PC lipid standards. With further refinement, the workflow will be utilized for the untargeted lipidomic analysis of biological samples and provide a higher level of structural fidelity in feature assignments than traditional lipidomic approaches.

Chapter 3 continues under the thematic methodology of combining analytical techniques for more comprehensive analysis by exploring the utility of SID-IM-MS for the structural analysis of lipids, as an alternative to the LC-Oz-IM-MS workflow described in Chapter 2. Seven lipid standards from four major lipid subclasses were analyzed via this approach to determine whether SID provided fragmentation information unavailable using more traditional CID fragmentation methods. Building off of previous work in analyzing Oz-IM-MS data, the utilization of IM post-SID led to a mobility-mass correlation between the fragmentation products and their precursor, a relationship that proved critical for the validation of lipid fragments and rejection of interfering species present in the sample. Other data projection strategies, including energy-resolved ion breakdown curves (ERIBC) and Kendrick mass defect analysis, were explored in this work for the analysis of lipid decomposition pathways and how they differed between SID and CID.

Chapter 4 utilizes the several of the tools developed in the preceding sections to characterize synthetic polymer samples rather than lipids. As described in section 1.6, the analysis of polymers using mass spectrometry presents similar challenges as lipids due to polydispersity and a high degree of isomerism. Many strategies developed herein for the structural characterization of lipids, such as fragmentation in conjunction with mobility separation, can be applied to polymer analysis. In this particular study, three isomeric polyurethane oligomers were characterized in terms of their fragmentation spectra (visualized using the ERIBC as in Chapter 3) and the CCS of both their +1 and +2 sodium-adducted charge states. It was observed that the three oligomers could be distinguished based on differences in their ERIBC and the CCS of the +2 charge states, while the +1 charge states had differences in CCS that were too small to resolve using the current instrument platform. While small in scope, this study demonstrates the utility of combining analytical techniques, in this case MS/MS and IM, for the analysis of polymers and the discrimination of sequence isomers in block copolymers. The limitations in separating the +1 charge states of the three isomeric oligomers indicates the continued need for improvements and innovations in mass spectrometry instrumentation, as improvements in instrumentation and their complementary analytical workflows often go hand-in-hand. To that end, Chapter 5, following a summary of the preceding chapters, discusses future directions for several ongoing projects and the field of IM-MS in general.

1.8   Acknowledgements

1.9   References

(1)   Evans, J. F.; Hutchinson, J. H. Seeing the Future of Bioactive Lipid Drug Targets. *Nat. Chem. Biol.* **2010**, *6* (7), 476–479.

(2)   Rolim, A. E. H.; Henrique-Araújo, R.; Ferraz, E. G.; de Araújo Alves Dultra, F. K.; Fernandez, L. G. Lipidomics in the Study of Lipid Metabolism: Current Perspectives in the Omic Sciences. *Gene* **2015**, *554* (2), 131–139.

(3)   Wenk, M. R. The Emerging Field of Lipidomics. *Nat. Rev. Drug Discov.* **2005**, *4* (7), 594–610.

(4)   Navas-Iglesias, N.; Carrasco-Pancorbo, A.; Cuadros-Rodríguez, L. From Lipids Analysis towards Lipidomics, a New Challenge for the Analytical Chemistry of the 21st Century. Part II: Analytical Lipidomics. *TrAC Trends Anal. Chem.* **2009**, *28* (4), 393–403.

(5)   Zheng, X.; Smith, R. D.; Baker, E. S. Recent Advances in Lipid Separations and Structural Elucidation Using Mass Spectrometry Combined with Ion Mobility Spectrometry, Ion-Molecule Reactions and Fragmentation Approaches. *Curr. Opin. Chem. Biol.* **2018**, *42*, 111–118.

(6)   Fahy, E.; Subramaniam, S.; Brown, H. A.; Glass, C. K.; Merrill, A. H.; Murphy, R. C.; Raetz, C. R. H.; Russell, D. W.; Seyama, Y.; Shaw, W.; et al. A Comprehensive Classification System for Lipids. *J. Lipid Res.* **2005**, *46*, 839–861.

(7)   Smith, S.; Witkowski, A.; Joshi, A. K. Structural and Functional Organization of the Animal Fatty Acid Synthase. *Prog. Lipid Res.* **2003**, *42* (4), 289–317.

(8)   White, S. W.; Zheng, J.; Zhang, Y.-M.; Rock, C. O. The Structural Biology of Type Ii Fatty Acid Biosynthesis. *Annu. Rev. Biochem.* **2005**, *74* (1), 791–831.

(9)   Wishart, D. S.; Feunang, Y. D.; Marcu, A.; Guo, A. C.; Liang, K.; Rosa, V.; Sajed, T.; Johnson, D.; Li, C.; Karu, N.; et al. HMDB 4 . 0 : The Human Metabolome Database for

2018. **2018**, *46* (November 2017), 608–617.

(10) Schuster, S.; Fichtner, M.; Sasso, S. Use of Fibonacci Numbers in Lipidomics – Enumerating Various Classes of Fatty Acids. *Nat. Publ. Gr.* **2017**, No. January, 1–9.

(11) Blanksby, S. J.; Mitchell, T. W. Advances in Mass Spectrometry for Lipidomics. *Annu. Rev. Anal. Chem.* **2010**, *3* (1), 433–465.

(12) Murphy, R. C.; Axelsen, P. H. Mass Spectrometric Analysis of Long-Chain Lipids. *Mass Spectrom. Rev.* **2011**, *30* (4), 579–599.

(13) Campbell, J. L.; Baba, T. Near-Complete Structural Characterization of Phosphatidylcholines Using Electron Impact Excitation of Ions from Organics. *Anal. Chem.* **2015**, *87* (11), 5837–5845.

(14) Ma, X.; Xia, Y. Pinpointing Double Bonds in Lipids by Paternò-Büchi Reactions and Mass Spectrometry. *Angew. Chemie - Int. Ed.* **2014**, *53* (10), 2592–2596.

(15) Thomas, M. C.; Mitchell, T. W.; Harman, D. G.; Deeley, J. M.; Murphy, R. C.; Blanksby, S. J. Elucidation of Double Bond Position in Unsaturated Lipids by Ozone Electrospray Ionization Mass Spectrometry. *Anal. Chem.* **2007**, *79* (13), 5013–5022.

(16) Thomas, M. C.; Mitchell, T. W.; Harman, D. G.; Deeley, J. M.; Nealon, J. R.; Blanksby, S. J. Ozone-Induced Dissociation: Elucidation of Double Bond Position within Mass-Selected Lipid Ions. *Anal. Chem.* **2008**, *80* (1), 303–311.

(17) Hancock, S. E.; Poad, B. L. J.; Batarseh, A.; Abbott, S. K.; Mitchell, T. W. Advances and Unresolved Challenges in the Structural Characterization of Isomeric Lipids. *Anal. Biochem.* **2017**, *524*, 45–55.

(18) Mason, E. A.; McDaniel, E. W. *Transport Properties of Ions in Gases*; Wiley-VCH Verlag GmbH & Co. KGaA: Weinheim, FRG, 1988; Vol. 374.

(19) Fenn, L. S.; Kliman, M.; Mahsut, A.; Zhao, S. R.; McLean, J. A. Characterizing Ion Mobility-Mass Spectrometry Conformation Space for the Analysis of Complex Biological Samples. *Anal. Bioanal. Chem.* **2009**, *394* (1), 235–244.

(20) May, J. C.; Goodwin, C. R.; Lareau, N. M.; Leaptrot, K. L.; Morris, C. B.; Kurulugama, R. T.; Mordehai, A.; Klein, C.; Barry, W.; Darland, E.; et al. Conformational Ordering of Biomolecules in the Gas Phase: Nitrogen Collision Cross Sections Measured on a Prototype High Resolution Drift Tube Ion Mobility-Mass Spectrometer. *Anal. Chem.* **2014**, *86* (4), 2107–2116.

(21) Kliman, M.; May, J. C.; McLean, J. A. Lipid Analysis and Lipidomics by Structurally Selective Ion Mobility-Mass Spectrometry. *Biochim. Biophys. Acta - Mol. Cell Biol. Lipids* **2011**, *1811* (11), 935–945.

(22) Tao, L.; McLean, J. R.; McLean, J. A.; Russell, D. H. A Collision Cross-Section Database

of Singly-Charged Peptide Ions. *J. Am. Soc. Mass Spectrom.* **2007**, *18* (7), 1232–1238.

(23) Fenn, L. S.; McLean, J. A. Biomolecular Structural Separations by Ion Mobility-Mass Spectrometry. *Anal. Bioanal. Chem.* **2008**, *391* (3), 905–909.

(24) McLean, J. A. The Mass-Mobility Correlation Redux: The Conformational Landscape of Anhydrous Biomolecules. *J. Am. Soc. Mass Spectrom.* **2009**, *20* (10), 1775–1781.

(25) Kyle, J. E.; Zhang, X.; Weitz, K. K.; Monroe, M. E.; Ibrahim, Y. M.; Moore, R. J.; Cha, J.; Sun, X.; Lovelace, E. S.; Wagoner, J.; et al. Uncovering Biologically Significant Lipid Isomers with Liquid Chromatography, Ion Mobility Spectrometry and Mass Spectrometry. *Analyst* **2016**, *141* (5), 1649–1659.

(26) May, J. C.; McLean, J. A. The Conformational Landscape of Biomolecules in Ion Mobility– Mass Spectrometry. In *Ion mobility spectrometry-mass spectrometry: theory and applications*; Wilkins, C. L., Trimpin, S., Eds.; CRC press, 2010; pp 326–342.

(27) Woods, A. S.; Ugarov, M.; Egan, T.; Koomen, J.; Gillig, K. J.; Fuhrer, K.; Gonin, M.; Schultz, J. A. Lipid/Peptide/Nucleotide Separation with MALDI-Ion Mobility-TOF MS. *Anal. Chem.* **2004**, *76* (8), 2187–2195.

(28) Leaptrot, K. L.; May, J. C.; Dodds, J. N.; McLean, J. A. Ion Mobility Conformational Lipid Atlas for High Confidence Lipidomics. *Nat. Commun.* **2019**, *10* (985), 1–9.

(29) Zhou, Z.; Tu, J.; Xiong, X.; Shen, X.; Zhu, Z.-J. LipidCCS: Prediction of Collision Cross-Section Values for Lipids with High Precision To Support Ion Mobility–Mass Spectrometry-Based Lipidomics. *Anal. Chem.* **2017**, *89* (17), 9559–9566.

(30) Soper-Hopper, M. T.; Petrov, A. S.; Howard, J. N.; Yu, S. S.; Forsythe, J. G.; Grover, M. A.; Fernández, F. M. Collision Cross Section Predictions Using 2-Dimensional Molecular Descriptors. *Chem. Commun.* **2017**, *53* (54), 7624–7627.

(31) Picache, J. A.; Rose, B. S.; Balinski, A.; Leaptrot, K. L.; Sherrod, S. D.; May, J. C.; McLean, J. A. Collision Cross Section Compendium to Annotate and Predict Multi-Omic Compound Identities. *Chem. Sci.* **2019**, *10* (4), 983–993.

(32) Jackson, S. N.; Ugarov, M.; Post, J. D.; Egan, T.; Langlais, D.; Schultz, J. A.; Woods, A. S. A Study of Phospholipids by Ion Mobility TOFMS. *J. Am. Soc. Mass Spectrom.* **2008**, *19* (11), 1655–1662.

(33) Trimpin, S.; Tan, B.; Bohrer, B. C.; O'Dell, D. K.; Merenbloom, S. I.; Pazos, M. X.; Clemmer, D. E.; Walker, J. M. Profiling of Phospholipids and Related Lipid Structures Using Multidimensional Ion Mobility Spectrometry-Mass Spectrometry. *Int. J. Mass Spectrom.* **2009**, *287* (1), 58–69.

(34) Jackson, S. N.; Barbacci, D.; Egan, T.; Lewis, E. K.; Schultz, J. A.; Woods, A. S. MALDI-Ion Mobility Mass Spectrometry of Lipids in Negative Ion Mode. *Anal. Methods* **2014**, *6* (14), 5001–5007.

(35) Kim, H. I.; Kim, H.; Pang, E. S.; Ryu, E. K.; Beegle, L. W.; Loo, J. A.; Goddard, W. A.; Kanik, I. Structural Characterization of Unsaturated Phosphatidylcholines Using Traveling Wave Ion Mobility Spectrometry. *Anal. Chem.* **2009**, *81* (20), 8289–8297.

(36) Paglia, G.; Angel, P.; Williams, J. P.; Richardson, K.; Olivos, H. J.; Thompson, J. W.; Menikarachchi, L.; Lai, S.; Walsh, C.; Moseley, A.; et al. Ion Mobility-Derived Collision Cross Section as an Additional Measure for Lipid Fingerprinting and Identification. *Anal. Chem.* **2015**, *87* (2), 1137–1144.

(37) Zhang, F.; Guo, S.; Zhang, M.; Zhang, Z.; Guo, Y. Characterizing Ion Mobility and Collision Cross Section of Fatty Acids Using Electrospray Ion Mobility Mass Spectrometry. *J. mass Spectrom.* **2015**, *50* (7), 906–913.

(38) Paglia, G.; Williams, J. P.; Menikarachchi, L.; Thompson, J. W.; Tyldesley-Worster, R.; Halldórsson, S.; Rolfsson, O.; Moseley, A.; Grant, D.; Langridge, J.; et al. Ion Mobility Derived Collision Cross Sections to Support Metabolomics Applications. *Anal. Chem.* **2014**, *86* (8), 3985–3993.

(39) Zhou, Z.; Shen, X.; Zhu, Z.-J.; Tu, J.; Chen, X.; Xiong, X. LipidIMMS Analyzer: Integrating Multi-Dimensional Information to Support Lipid Identification in Ion Mobility—Mass Spectrometry Based Lipidomics. *Bioinformatics* **2018**, *35* (July 2018), 698–700.

(40) Shinzawa-Itoh, K.; Aoyama, H.; Muramoto, K.; Terada, H.; Kurauchi, T.; Tadehara, Y.; Yamasaki, A.; Sugimura, T.; Kurono, S.; Tsujimoto, K.; et al. Structures and Physiological Roles of 13 Integral Lipids of Bovine Heart Cytochrome c Oxidase. *EMBO J.* **2007**, *26* (6), 1713–1725.

(41) Brown, S. H. J.; Mitchell, T. W.; Oakley, A. J.; Pham, H. T.; Blanksby, S. J. Time to Face the Fats: What Can Mass Spectrometry Reveal about the Structure of Lipids and Their Interactions with Proteins? *J. Am. Soc. Mass Spectrom.* **2012**, *23* (9), 1441–1449.

(42) Groessl, M.; Graf, S.; Knochenmuss, R. High Resolution Ion Mobility-Mass Spectrometry for Separation and Identification of Isomeric Lipids. *Analyst* **2015**, *140* (20), 6904–6911.

(43) Klein, D. R.; Brodbelt, J. S. Structural Characterization of Phosphatidylcholines Using 193 Nm Ultraviolet Photodissociation Mass Spectrometry. *Anal. Chem.* **2017**, *89* (3), 1516–1522.

(44) Pham, H. T.; Ly, T.; Trevitt, A. J.; Mitchell, T. W.; Blanksby, S. J. Differentiation of Complex Lipid Isomers by Radical-Directed Dissociation Mass Spectrometry. *Anal. Chem.* **2012**, *84* (17), 7525–7532.

(45) Sun, C.; Zhao, Y. Y.; Curtis, J. M. A Study of the Ozonolysis of Model Lipids by Electrospray Ionization Mass Spectrometry. *Rapid Commun. Mass Spectrom.* **2012**, *26* (8), 921–930.

(46) Pham, H. T.; Maccarone, A. T.; Thomas, M. C.; Campbell, J. L.; Mitchell, T. W.; Blanksby,

S. J. Structural Characterization of Glycerophospholipids by Combinations of Ozone- and Collision-Induced Dissociation Mass Spectrometry: The next Step towards "Top-down" Lipidomics. *Analyst* **2014**, *139* (1), 204–214.

(47) Vu, N.; Brown, J.; Giles, K.; Zhang, Q. Ozone-Induced Dissociation on a Traveling Wave High-Resolution Mass Spectrometer for Determination of Double-Bond Position in Lipids. *Rapid Commun. Mass Spectrom.* **2017**, *31* (17), 1415–1423.

(48) Barrientos, R. C.; Vu, N.; Zhang, Q. Structural Analysis of Unsaturated Glycosphingolipids Using Shotgun Ozone-Induced Dissociation Mass Spectrometry. *J. Am. Soc. Mass Spectrom.* **2017**, *28* (11), 2330–2343.

(49) Stinson, C. A.; Zhang, W.; Xia, Y. UV Lamp as a Facile Ozone Source for Structural Analysis of Unsaturated Lipids Via Electrospray Ionization-Mass Spectrometry. *J. Am. Soc. Mass Spectrom.* **2017**, *2*.

(50) Ma, X.; Chong, L.; Tian, R.; Shi, R.; Hu, T. Y.; Ouyang, Z.; Xia, Y. Identification and Quantitation of Lipid C=C Location Isomers: A Shotgun Lipidomics Approach Enabled by Photochemical Reaction. *Proc. Natl. Acad. Sci.* **2016**, *113* (10), 2573–2578.

(51) Stinson, C. A.; Xia, Y. Method of Coupling Paternò-Büchi Reaction with Direct Infusion ESI-MS/MS for Locating C=C Bond in Glycerophospholipids. *Analyst* **2016**, *141*, 3696–3704.

(52) Ma, X.; Zhao, X.; Li, J.; Zhang, W.; Cheng, J. X.; Ouyang, Z.; Xia, Y. Photochemical Tagging for Quantitation of Unsaturated Fatty Acids by Mass Spectrometry. *Anal. Chem.* **2016**, *88* (18), 8931–8935.

(53) Murphy, R. C.; Okuno, T.; Johnson, C. A.; Barkley, R. M. Determination of Double Bond Positions in Polyunsaturated Fatty Acids Using the Photochemical Paternò-Büchi Reaction with Acetone and Tandem Mass Spectrometry. *Anal. Chem.* **2017**, *89* (16), 8545–8553.

(54) Ren, J.; Franklin, E. T.; Xia, Y. Uncovering Structural Diversity of Unsaturated Fatty Acyls in Cholesteryl Esters via Photochemical Reaction and Tandem Mass Spectrometry. **2017**, 1432–1441.

(55) Kozlowski, R. L.; Campbell, J. L.; Mitchell, T. W.; Blanksby, S. J. Combining Liquid Chromatography with Ozone-Induced Dissociation for the Separation and Identification of Phosphatidylcholine Double Bond Isomers. *Anal. Bioanal. Chem.* **2015**, *407* (17), 5053–5064.

(56) Poad, B. L. J.; Zheng, X.; Mitchell, T. W.; Smith, R. D.; Baker, E. S.; Blanksby, S. J. Online Ozonolysis Combined with Ion Mobility-Mass Spectrometry Provides a New Platform for Lipid Isomer Analyses. *Anal. Chem.* **2018**, *90* (2), 1292–1300.

(57) Batarseh, A. M.; Abbott, S. K.; Duchoslav, E.; Alqarni, A.; Blanksby, S. J.; Mitchell, T. W. Discrimination of Isobaric and Isomeric Lipids in Complex Mixtures by Combining Ultra-High Pressure Liquid Chromatography with Collision and Ozone-Induced Dissociation. *Int.*

J. Mass Spectrom. **2018**, *431*, 27–36.

(58)　Harris, R. A.; May, J. C.; Stinson, C. A.; Xia, Y.; McLean, J. A. Determining Double Bond Position in Lipids Using Online Ozonolysis Coupled to Liquid Chromatography and Ion Mobility-Mass Spectrometry. *Anal. Chem.* **2018**, *90* (3), 1915–1924.

(59)　Zhang, W.; Zhang, D.; Chen, Q.; Wu, J.; Ouyang, Z.; Xia, Y. Online Photochemical Derivatization Enables Comprehensive Mass Spectrometric Analysis of Unsaturated Phospholipid Isomers. *Nat. Commun.* **2019**, *10* (1), 1–9.

(60)　Maccarone, A. T.; Duldig, J.; Mitchell, T. W.; Blanksby, S. J.; Duchoslav, E.; Campbell, J. L. Characterization of Acyl Chain Position in Unsaturated Phosphatidylcholines Using Differential Mobility-Mass Spectrometry. *J. Lipid Res.* **2014**, *55* (8), 1668–1677.

(61)　Steiner, R.; Saied, E. M.; Othman, A.; Arenz, C.; Maccarone, A. T.; Poad, B. L. J.; Blanksby, S. J.; von Eckardstein, A.; Hornemann, T. Elucidating the Chemical Structure of Native 1-Deoxysphingosine. *J. Lipid Res.* **2016**, *57* (7), 1194–1203.

(62)　Poad, B. L. J.; MacCarone, A. T.; Yu, H.; Mitchell, T. W.; Saied, E. M.; Arenz, C.; Hornemann, T.; Bull, J. N.; Bieske, E. J.; Blanksby, S. J. Differential-Mobility Spectrometry of 1-Deoxysphingosine Isomers: New Insights into the Gas Phase Structures of Ionized Lipids. *Anal. Chem.* **2018**, *90* (8), 5343–5351.

(63)　Zhou, M.; Wysocki, V. H. Surface Induced Dissociation: Dissecting Noncovalent Protein Complexes in the Gas Phase. *Acc. Chem. Res.* **2014**, *47*, 1010–1018.

(64)　Laskin, J.; Denisov, E.; Futrell, J. A Comparative Study of Collision-Induced and Surface-Induced Dissociation. 1. Fragmentation of Protonated Dialanine. *J. Am. Chem. Soc.* **2000**, *122* (40), 9703–9714.

(65)　Zhou, M.; Huang, C.; Wysocki, V. H. Surface-Induced Dissociation of Ion Mobility-Separated Noncovalent Complexes in a Quadrupole/Time-of-Flight Mass Spectrometer. *Anal. Chem.* **2012**, *84* (14), 6016–6023.

(66)　Wysocki, V. H.; Joyce, K. E.; Jones, C. M.; Beardsley, R. L. Surface-Induced Dissociation of Small Molecules, Peptides, and Non-Covalent Protein Complexes. *J. Am. Soc. Mass Spectrom.* **2008**, *19* (2), 190–208.

(67)　Fetterolf, D. D.; Yost, R. A. Energy-Resolved Collision-Induced Dissociation in Tandem Mass Spectrometry. *Int. J. Mass Spectrom. Ion Phys.* **1982**, *44* (1–2), 37–50.

(68)　Miller, S. A.; Riederer, D. E.; Cooks, R. G.; Cho, W. R.; Lee, H. W.; Kang, H. Energy Disposal and Target Effects in Hyperthermal Collisions of Ferrocene Molecular Ions at Surfaces. *J. Phys. Chem.* **1994**, *98* (1), 245–251.

(69)　Harrison, A. G. Energy-Resolved Mass Spectrometry: A Comparison of Quadrupole Cell and Cone-Voltage Collision-Induced Dissociation. *Rapid Commun. Mass Spectrom.* **1999**, *13* (16), 1663–1670.

(70)   Stow, S. M.; Crescentini, T. M.; Forsythe, J. G.; May, J. C.; McLean, J. A.; Hercules, D. M. Structural Characterization of Methylenedianiline Regioisomers by Ion Mobility-Mass Spectrometry, Tandem Mass Spectrometry, and Computational Strategies. 3. MALDI Spectra of 2-Ring Isomers. *Anal. Chem.* **2017**, *89* (18), 9900–9910.

(71)   Crescentini, T. M.; Stow, S. M.; Forsythe, J. G.; May, J. C.; McLean, J. A.; Hercules, D. M. Structural Characterization of Methylenedianiline Regioisomers by Ion Mobility-Mass Spectrometry and Tandem Mass Spectrometry. 4. 3-Ring and 4-Ring Isomers. *Anal. Chem.* **2018**, *90* (24), 14453–14461.

(72)   Gies, A. P.; Hercules, D. M. Collision Induced Dissociation Study of Ester-Based Polyurethane Fragmentation Reactions. *Anal. Chim. Acta* **2014**, *808*, 199–219.

(73)   Murgasova, R.; Hercules, D. M. Polymer Characterization by Combining Liquid Chromatography with MALDI and ESI Mass Spectrometry. *Anal. Bioanal. Chem.* **2002**, *373* (6), 481–489.

(74)   Nielen, M. W. F. Maldi Time-of-Flight Mass Spectrometry of Synthetic Polymers. *Mass Spectrom. Rev.* **1999**, *18* (5), 309–344.

(75)   Crescentini, T. M.; May, J. C.; McLean, J. A.; Hercules, D. M. Mass Spectrometry of Polyurethanes. *Polymer.* **2019**, *181* (3), 121624.

CHAPTER 2

DETERMINING DOUBLE BOND POSITION IN LIPIDS USING ONLINE

OZONOLYSIS COUPLED TO LIQUID CHROMATOGRAPHY AND ION MOBILITY

MASS SPECTROMETRY[†]

2.1 Introduction

Mass spectrometry-based lipidomic approaches are emerging as an increasingly important analytical strategy for characterizing the varied and critical roles lipids play in biological systems.[1–3] Like other 'omics techniques, lipidomic studies aim to generate a comprehensive snapshot of the lipid content of a given system, identifying and quantifying individual components and attempting to interpret the intermolecular interactions in coordination with relevant biological functions. Common lipidomic workflows often combine liquid chromatography and tandem mass spectrometry (LC-MS/MS) in broad-scale, untargeted analyses.[2,4,5] However, the immense structural diversity of the lipidome often precludes putative identification of species, especially given the potential presence of a myriad of isomeric and isobaric species at a given mass-to-charge ratio. For example, phosphatidylcholine (PC) 14:0/20:1 and PC 18:0/16:1 are alkyl chain isomers that have identical chemical formulas ($C_{42}H_{82}NO_8P$) and thus cannot be differentiated via mass measurement alone. Nevertheless, these two isomeric species can be distinguished by tandem MS/MS experiments via product ion scanning for diagnostic fatty acid fragments in negative mode

---

electrospray ionization.[6] Other classes of lipid isomers, such as *sn*-regioisomers and double bond positional isomers, are much more challenging to assign a specific chemical structure.[7] As a result, there is no single analytical method currently available that can resolve all the possible configurations of lipid species that may exist in a given sample. For this reason, the combination and integration of several analytical techniques into a single workflow is often necessary to identify isomeric lipid species and expand lipidome coverage.[8]

Ozonolysis is a chemical reaction that has long been utilized by organic chemists to cleave carbon-carbon double bonds, and has more recently been adopted by analytical chemists for the localization of lipid double bonds by mass spectrometry.[9–11] The reaction may be performed in one of several ways, including online in the solution-phase or directly in the ionization source of the instrument.[12,13] Most prominently, the Blanksby group at the Queensland University of Technology has developed a family of techniques known as "OzID" in which ozonolysis is performed on mass-selected ions in the gas phase in either a collision cell or a trapping region of the instrument.[14,15] In recent publications, Blanksby and coworkers have demonstrated the capabilities of ozonolysis combined with MS on a variety of instrument platforms.[15–17] Advantages of the technique include high reaction yield (product ion intensity ca. 20% of the precursor ion in the most recent iteration) and the ability to combine successive collision-induced dissociation (CID) and OzID experiments for increased structural characterization and lipid coverage.[14–17] One drawback preventing widespread adoption of OzID is the instrument modifications that are necessary to perform the experiments, which typically include the addition of a gas manifold and ozone generator to the mass spectrometer.

Other chemical reactions that cleave carbon-carbon double bonds have also been utilized for double bond localization in mass spectrometry. Of recent note is the Paternò-Büchi reaction,

which the Xia group at Purdue coupled to MS via UV irradiation of the tip of the nano-ESI emitter containing a lipid sample in the presence of an acetone cycloaddition reagent.[18–21] A low-pressure mercury lamp is used to generate UV radiation to activate the acetone (primarily via a 254 nm band), resulting in the addition of an acetone radical to the double bond and forming an oxetane.[18] Collision-induced dissociation of the oxetane is then used to enact retro-PB, resulting in two product ions spaced 26 Da apart that are diagnostic of the double bond position in the original lipid molecule.[18] Given the relatively low quantum yield of acetone, the PB reaction yields are typically less than 50%. The non-quantitative chemical conversion can increase spectral complexity for mixture analysis and limit the identification of low abundance unsaturated lipids, in particular for lipid species containing multiple sites of unsaturations, although careful choice of solvent composition can minimize side reaction products.[19,20,22] In recent work by Murphy and coworkers, double bond cleavage products were observed for 9,12,15-octadecatrienoic acid and 6,9,12-octadecatrienoic acid prior to enacting retro-PB via CID.[22] They hypothesized that these cleavage products were a result of ozonolysis due to the fact that the peaks were no longer observed upon degassing of sample solution prior to analysis but did not explore these observations further.

Ion mobility (IM) is an analytical technique that is gaining widespread use towards the structural analysis of lipids.[23,24] When interfaced with a mass spectrometer, IM allows for the separation of isomeric lipid species based on differences in their collision cross section (CCS) which provides a structurally-selective measurement that is orthogonal to mass analysis. For example, using IM, Baker and coworkers were able to distinguish *sn*-positional isomers and cis/trans isomers for several ceramide standards, and Groessl et. al. demonstrated IM separation of phosphatidylcholine acyl-chain regioisomers via silver-cationized forms of the natural lipid species present in a porcine brain extract.[25,26] Double bond positional isomers have also been

resolved via IM-MS; however, the analytical specificity was only demonstrated for fatty acids and more biologically uncommon species such as PC 18:1(9Z)/18:1(9Z) and PC 18:1(6Z)/18:1(6Z).[25,26] Moreover, lipid isomers in a complex mixture may have CCS differences that are too small to exhibit baseline separation using current instrument platforms.[27] For these reasons, it was hypothesized that combining ozonolysis and IM-MS would provide for multiple dimensions of isomer structural discrimination. Ozonolysis provides the basis for determination of double bond position, while IM-MS facilitates separation of the ozonolysis products based upon differences in CCS and mass. Together, these analytical tools have the potential for enabling high confidence in identification and discrimination of lipid isomers in complex samples. Recently, the combination of IM-MS with OzID has been demonstrated by the Blanksby group in collaboration with PNNL, highlighting the potential of the combined techniques for the analysis of isomeric lipid species.[28] Our work aims to further examine the benefits of utilizing IM in conjunction with ozonolysis, but rather than modifying the mass spectrometer for gas-phase OzID, we have implemented ozonolysis on a low- cost, portable solution-phase device.

In this work, we have developed an ozonolysis device that combines the immediacy of double bond cleavage with the simplicity of online ozone generation without instrument modification. The device is a continuation of our previous work[29] and contains a flow-cell in which analyte solution is irradiated by the mercury lamp, producing solution-phase ozonolysis products that then are ionized in the source of the mass spectrometer. As in the ozonolysis and Paternò-Büchi experiments described previously, these products are diagnostic in that they can be used to determine the double bond position in the lipid precursor species when analyzed via mass spectrometry. Following ozonolysis in the device, IM-MS allows for separation of the ozonolysis products to aid in the deconvolution of isomeric signals. Here, we explore the utility of ozonolysis

32

combined with ion mobility-mass spectrometry for the analysis of three distinct lipid systems: (1) a PC standard containing a single double bond, (2) a fatty acid standard containing multiple double bonds, and (3) a complex mixture in the form of chicken egg PC lipid extract. Additionally, given the importance of separation via liquid chromatography in many lipidomic workflows, the utilization of LC in combination with the ozonolysis device was demonstrated using a simple mixture of three isomeric PC standards.

2.2 Experimental Methods

2.2.1 Sample Preparation

Phosphatidylcholine standards 1-hexadecanoyl-2-(9Z-octadecenoyl)-sn-glycero-3-phosphocholine (PC 16:0/18:1(9Z)), 1-palmitoyl-2-stearoyl-sn-glycero-3-phosphocholine (PC 16:0/18:0), 1,2-di-(6Z-octadecenoyl)-sn-glycero-3-phosphocholine (PC 18:1(6Z)/18:1(6Z)), 1,2-di-(9Z-octadecenoyl)-sn-glycero-3-phosphocholine (PC 18:1(9Z)/18:1(9Z)), 1,2-di-(9E-octadecenoyl)-sn-glycero-3-phosphocholine (PC 18:1(9E)/18:1(9E)), and a total TLC fraction of a phosphatidylcholine lipid extract (PC, chicken egg) were purchased from Avanti Polar Lipids. Docosahexaenoic acid (FA 22:6) was purchased from Cayman Chemical. Prior to analysis, individually infused samples were diluted to working concentrations ranging from 0.1 to 10 μM in 7:3 acetonitrile/water (Optima LC/MS grade, Fisher Scientific), while the three isomeric PC lipids were combined in equimolar ratios and diluted to approximately 6 μM in the solvent composition utilized at the beginning of the RPLC separation gradient. Formic acid (0.1%, Optima grade, Fisher Scientific) was added to PC lipids analyzed in positive ion mode to facilitate the formation of protonated species. A saturated phosphatidylcholine standard, PC 16:0/18:0, was spiked into the lipid extract at 1 μM due to low abundance of the fully saturated species inherent

in the sample fraction. For mass calibration, a mixture of hexakis-(fluoroalkoxy) phosphazines (ESI-Low Concentration Tuning Mixture, Agilent Technologies) was purchased and diluted by a factor of 10 in a 59:1 (v/v) solution of acetonitrile/water.

2.2.2 Instrumentation and Parameters

Experiments were performed on a uniform field drift tube IM-MS (6560, Agilent) with nitrogen as the drift gas in both positive and negative ionization modes.[30] The IM-MS instrument was tuned for high sensitivity in standard mass mode (*m/z* 50-1700) and mass calibrated prior to analysis using the Agilent tuning mixture. The drift tube was operated at ca. 300 K with an electric field strength of 14.7 V/cm which represents conditions yielding optimal IM resolving power.[31] For analysis of the fatty acid standard which displayed low ionization efficiency in negative mode, the ion mobility trap release time was increased from 150 μs to 450 μs, increasing signal with a slight loss in mobility resolving power (ca. 2% for *m/z* 261.1). Samples were directly infused into the electrospray source (ESI, Agilent Jet Stream) at various flow rates ranging from 5 μL/min to 500 μL/min. The source was operated with a capillary voltage of 3500V and nozzle voltage of 2000V. Nitrogen sheath and drying gases were heated to 275°C and 325°C at flow rates of 12 L/min and 8 L/min, respectively. For LC experiments, 5-10 μL of sample was injected onto a C-18 2.1 mm x 50 mm (1.8 μm) analytical column with the flow rate set to 250 μL/min. Mobile phase A consisted of water with 0.1% formic acid, and mobile phase B consisted of 3/2 isopropanol: acetonitrile with 0.1% formic acid. The gradient elution profile was based upon conditions for analyzing hydrophobic compounds as described by Cruickshank-Quinn et. al.[32]

Ozonolysis reactions were carried out in the solution-phase prior to ionization in the ESI source. A custom built, mechanically stable device was constructed in-house to support and align the low-pressure mercury lamp (81-1057-51, BHK Inc.) which is used to catalyze the relevant reaction (Figure 2.1). This particular lamp produces several emission bands spanning from 185 nm to 579 nm; however, previous studies have shown that the 185 nm band is responsible for the production of ozone necessary for these experiments.[33,34] The custom support housing allows up to two lamps to be used, although only one is utilized in this current study. The device is constructed such that the entire length of the lamp(s) irradiates a polyimide-coated fused silica line (ID 220 μm, OD 363 μm, SGE Analytical Science) positioned in the center of the device parallel to the lamp(s). This silica line has been "windowed" by thermally removing the polyimide coating along the length of the lamp to allow UV transmission into the inner capillary. The fused silica is fixed securely in the device using PEEK microtight fittings (1/32'' OD, Upchurch). Although not shown in Figure 2.1, the device is covered during operation such that UV radiation is blocked from sight for safety. The distance between the device and the IM-MS instrument (~20 cm) contributes to an observed "dead time" before reaction products are detected. Experiments were performed such that data acquisition was initiated concurrent to the lamp being turned on.

2.2.3 Data Analysis

Data was analyzed using MassHunter IMS Browser and Qualitative Analysis software (B.07.02 and B.07.00, Agilent Technologies). For the variable flow rate studies, precursor and ozonolysis product peaks at a given flow rate were extracted as ion chromatograms and normalized as a percent conversion over time. Replicates at each flow rate, collected in triplicate, were time-aligned and percent conversions were averaged. The equilibrium conversion was determined as
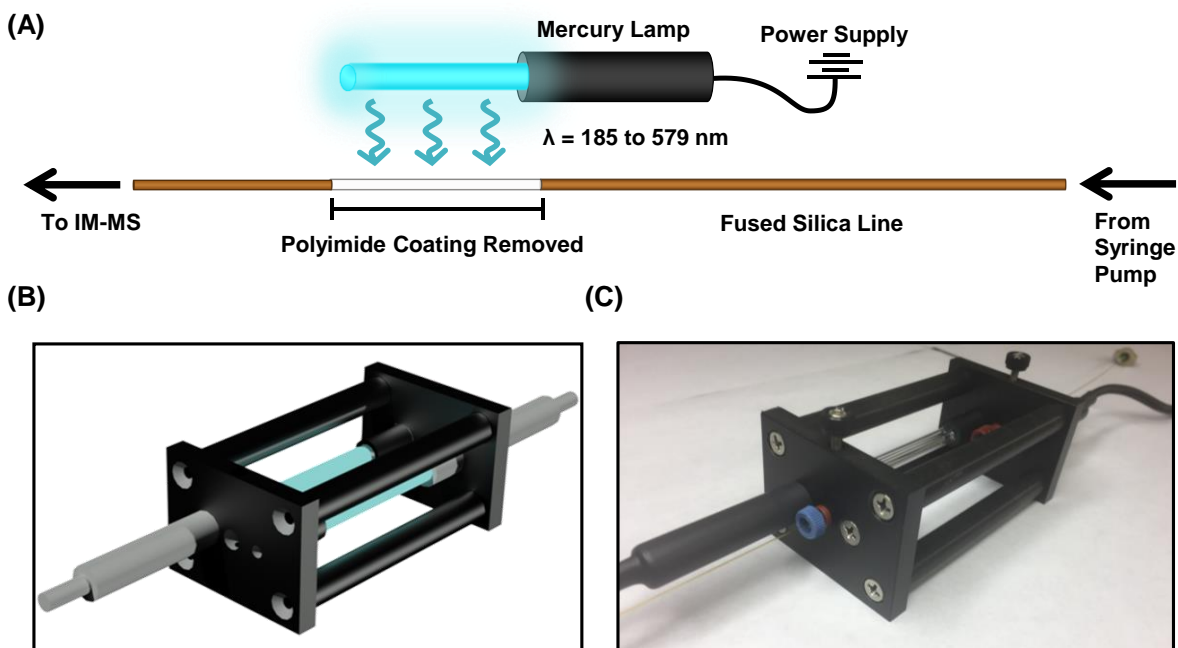
Figure 2.1 (A) A diagram of the ozonolysis apparatus utilizing a low-pressure mercury lamp and fused silica line with a portion of the polyimide coating removed to permit transmission of UV radiation. **(B)** A rendered schematic of the mechanically-stable housing for the ozonolysis device. **(C)** Photograph of the completed device with inclusion of thumb screws and capillary fittings for precise alignment of the silica line relative to the lamp.

the maximal conversion reached after precursor/product ion ratios ceased to vary with time. For LC experiments, relevant extracted ion chromatograms (EIC's) were extracted, smoothed, and integrated. Background subtracted mass spectra were subsequently extracted from each of the integrated LC peaks.

2.3   Results and Discussion

2.3.1   *Conversion of a Glycerophospholipid Standard*

For initial characterization purposes, a commonly studied phosphatidylcholine standard, PC 16:0/18:1(9Z), was directly infused through the device and into the instrument source at a flow rate of 10 µL/min. It was observed that the precursor protonated lipid peak at *m/z* 760.6 underwent a reaction to form a product aldehyde species at *m/z* 650.4 which is representative of double bond cleavage at the ninth carbon atom of the eighteen-carbon length alkyl chain (Figure 2.2(A)). Extracted mass spectra averaged over 0.3 min before and after the reaction confirm a transition of approximately ~110.1 Da, which is indicative of an ozonolysis reaction corresponding to a loss of 18 hydrogen and 9 carbon atoms from the alkyl chain, as well as an oxygen atom gained during the cycloaddition of ozone as per the Criegee mechanism.[35] Although a detailed analysis of the mechanism that gives rise to the diagnostic aldehyde product ion is not within the scope of this paper, the results are consistent with solution phase ozonolysis, in which an aldehyde and carbonyl oxide are produced following reaction with ozone.[36] The unstable carbonyl oxide subsequently reacts with water and rearranges to form additional aldehyde product and hydrogen peroxide, such that the aldehyde product is the only product detectable via MS. Similar rearrangements have also been demonstrated using methanol as a solvent in other ozonolysis-coupled MS studies.[12] In the experiments described here where no methanol is used, the presence of a single primary diagnostic

ozonolysis product ion simplifies spectral interpretation.[29] However, as seen in Figure 2.2(B), other minor product ions are also observed. These minor side products primarily include sodiated and potassiated forms of the aldehyde at m/z 672.4 and 688.4, respectively, as well as other observed peaks in the mass spectrum possibly indicative of solvent adduction processes (see Supplementary Figure B.1).[11,12,37] Nonetheless, the major process observed involves conversion of the glycerophosphocholine precursor to an aldehyde product representative of cleavage at the 9Z position, a process that approaches 95% completion at 10 μL/min (Figure 2.2(C)). Even at this relatively low flow rate, the ozonolysis process is rapid and reaches a steady-state equilibrium in less than a minute. The high degree of reaction conversion efficiency, fast reaction kinetics, and low degree of reaction side products highlights several analytical advantages of this online, solution-phase method.

2.3.2   Influence of Flow Rate on Conversion Efficiency

Using the same phosphatidylcholine standard, the transition from m/z 760.6 to 650.4 was monitored as a function of time for flow rates ranging from 5 to 500 μL/min. The conversion-time profile displayed sigmoidal behavior, with an observed deadtime (Figure 2.2(C)) corresponding to the length of tubing between the exit of the ozonolysis device and the source of the mass spectrometer. At sufficiently high flow rates, e.g. ~75 μL/min with 30 cm of tubing, this deadtime becomes negligible (ca. 5 seconds or less), with observed product being formed and detected almost immediately after turning the lamp on. As the reaction kinetics reach equilibrium with the device flow rate (Figure 2.2(C)), the observed conversion from precursor to product ion plateaus to a fixed conversion rate. The extent to which the reaction proceeds is thus dependent on flow rate, with lower flow rates engendering greater maximum conversion (Figure 2.3(A)). As the flow
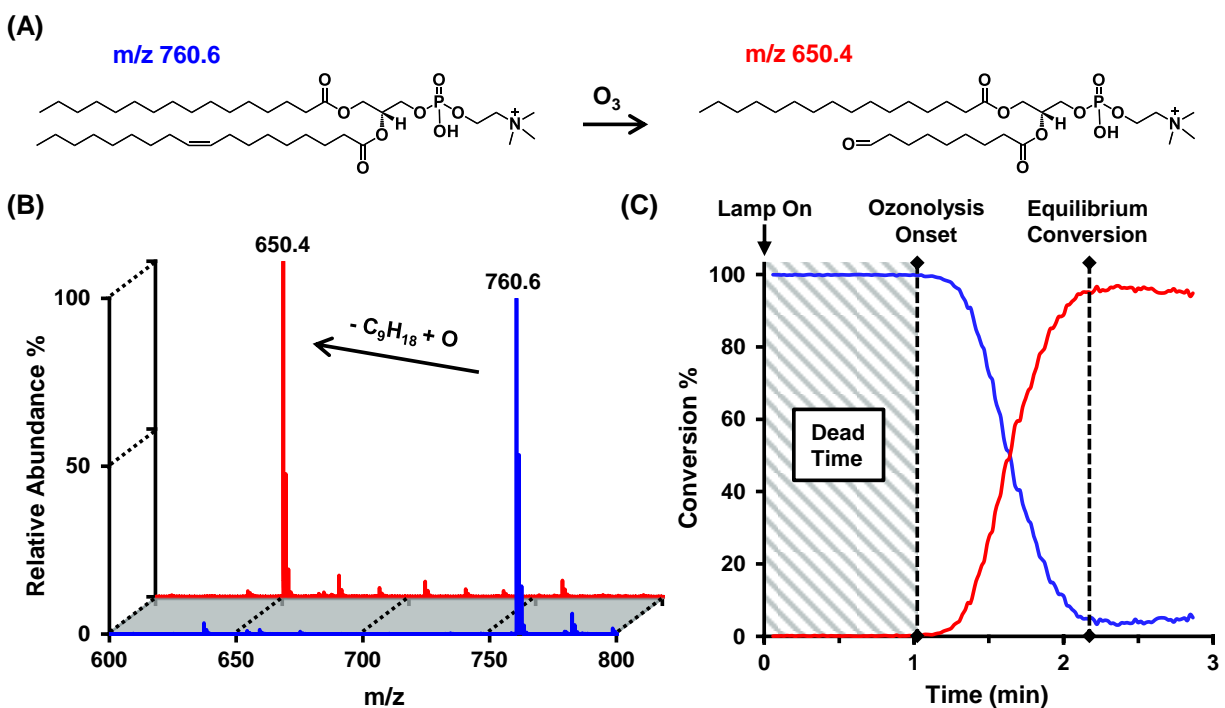
Figure 2.2 (A) The conversion of a glycerophospholipid to a diagnostic aldehyde product ion indicative of double bond position was demonstrated using PC 16:0/18:1 (9Z)). **(B)** Following irradiation, the IM-MS spectrum contained a representative peak at m/z 760.6 that decreased in intensity as the sample was infused through the device. Another peak, m/z 650.4, increased in intensity in response to the turning the lamp on, the latter corresponding to cleavage of a double bond at the ninth carbon atom of one alkyl chain. **(C)** A plot of percent conversion over time which indicates that conversion to the aldehyde product at 10 µL/min reached ca. 95% completion after about 1 minute following observed onset of reaction.

rate through the device is increased, the observed conversion percentage from precursor to product decreases due to the fact that the reaction can no longer proceed to completion during the limited time spent in the cell. This inverse relationship between sample flow rate and product conversion is demonstrated in Figure 2.3(B). The measured conversion-flow rate relationship of the device has been divided into three characteristic regions based upon suggested useful operating conditions. In the nano flow regime (defined here as flow rates less than 10 μL/min), the reaction approaches 100% completion. From 10 to 300 μL/min (i.e., direct infusion conditions), the conversion efficiency decreases as a function of increasing flow rate. Finally, at the upper end of flow rates surveyed (the flow injection regime, ≥400 μL/min), the observed maximum conversion varies very little with flow rate. In this region of behavior, the high flow rate limits the observed conversion to approximately ~25%; however, the generation of the maximal conversion at a given flow rate in this regime is nearly instantaneous, allowing for fast "on-off" switching of the device. This characteristic fast response of the device at high flow rates has the greatest implication for integration with liquid chromatography approaches. The reaction kinetics are such that the device could be toggled on and off during the elution of a chromatographic peak, facilitating identification via IM-MS of both the precursor and the product ion for each LC time bin, with the observed product allowing for determination of double bond position in the precursor.

2.3.3   Conversion in a System Containing Multiple Double Bonds

The fatty acid docosahexaenoic acid (FA 22:6 (Δ4, 7, 10, 13, 16, 19)) was chosen for evaluating the device for localizing multiple double bonds as this lipid contains six sites of unsaturation at positions Δ4, 7, 10, 13, 16, and 19 in the carbon chain (Figure 2.4(B)). To address the increased complexity of this system, ion mobility was utilized post ozonolysis reaction to gain
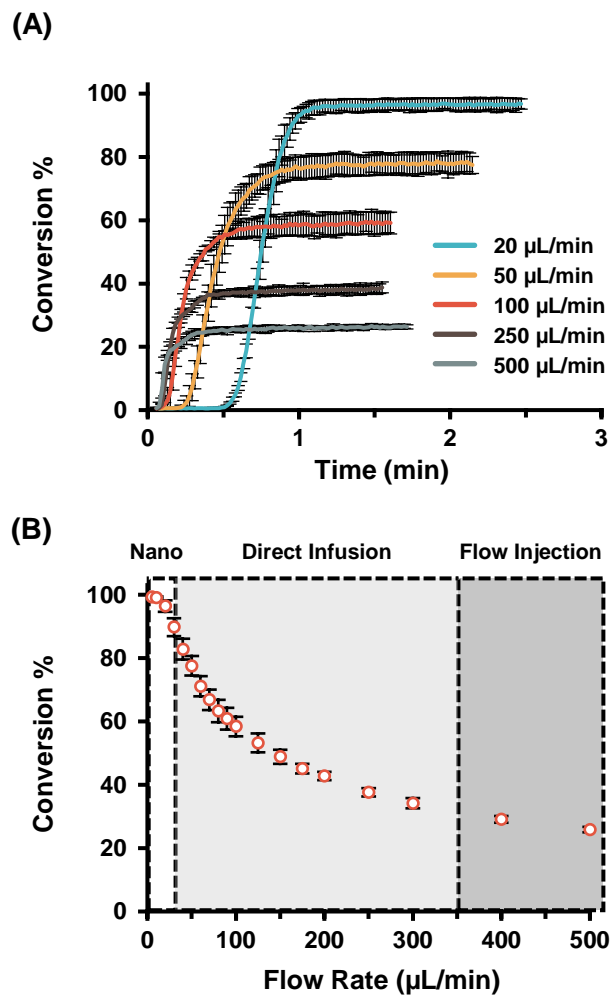
Figure 2.3 The performance of the ozonolysis device was evaluated as a function of flow rate. **(A)** The conversion of phosphatidylcholine precursor to an aldehyde product characteristic of double bond position was monitored, with the lamp switched on at a time corresponding to zero minutes. Five representative flow rates are shown here with error bars representing triplicate measurements. **(B)** Across the range of flow rates measured (5 to 500 µL/min) conversion efficiency was observed to decrease as flow rate increased

an additional dimension of separation of the ozonolysis products prior to mass analysis. Figure 2.4(A) contains a negative mode IM-MS spectrum for ozonolysis of deprotonated FA 22:6 at 10 µL/min. In contrast to the PC 16:0/18:1 described previously, the ozonolysis reaction is distributed across multiple possible reaction channels leading to a series of diagnostic product ions, but a decreased conversion efficiency for any single product ion channel. Additionally, fatty acids appear less reactive than glycerophosphocholines, as it was observed that while 10 µL/min was sufficient to convert nearly 100% of the PC 16:0/18:1 precursor to its single product ion, the same flow rate for FA 22:6 only converted about 45% of the precursor to the six possible product ions. However, upon increasing the device flow rate, the conversion percentage decreased in a manner analogous to the phosphatidylcholine described in Figure 2.3 (Figure 2.4(C)). The differential reactivity of various lipid species has been noted by Blanksby and coworkers and has been suggested as a possible means for quantitation via ozonolysis but has not been further explored in this work due to the sensitivity of product generation via this technique to flow rate.[15] Additionally, as discussed in the group's OzESI work, because sample ionization occurs after ozonolysis, ion abundances are biased due to differences in ionization efficiency, making quantitation challenging, particularly in complex mixtures where ion suppression is prevalent.[10,12]

Because the double bonds are symmetrically distributed along the fatty acid acyl tail (spaced 3 carbons apart), the ozonolysis products generated are linearly spaced in 40 Da intervals in the mass spectrum. These products ions each contain a negatively charged carboxylic acid moiety on one end and are truncated with an aldehyde corresponding to ozonolysis cleavage at a given double bond position. From the IM-MS spectra in Figure 2.4(A), it was observed that there exists a mobility-mass correlation for the ozonolysis fragments and the fatty acid precursor which allows for the isolation of product-specific mass and mobility spectra and thus improves the signal-
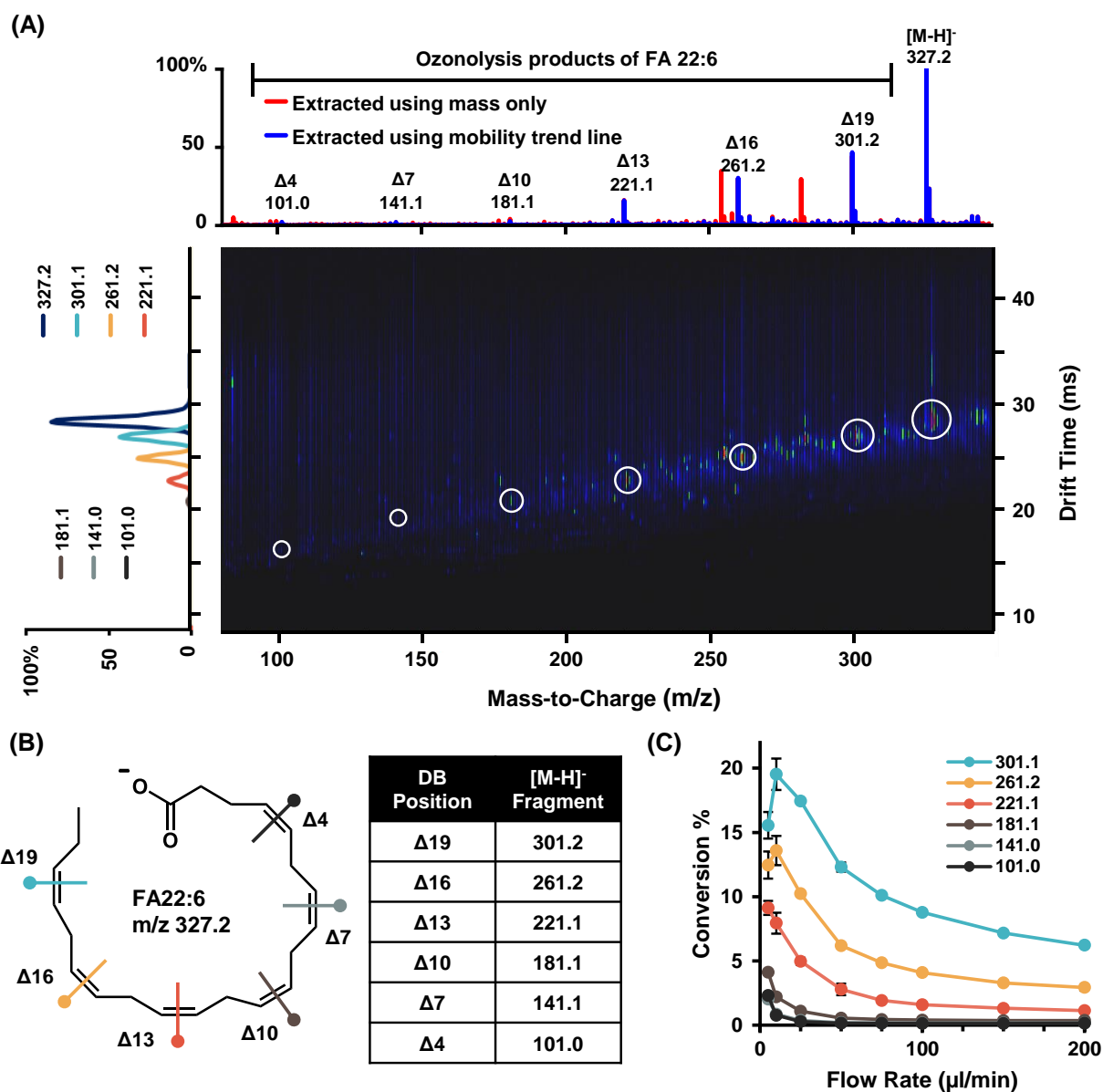
Figure 2.4 The highly-unsaturated fatty acid docosahexaenoic acid (FA 22:6) was examined using the flow-cell ozonolysis device in negative ion mode. **(A)** IM-MS spectrum of FA 22:6 following ozonolysis at a flow rate of 10 µL/min. The six products detected displayed a linear trend in both mass and drift time dimensions and correspond to fragmentation at double bond locations as depicted in **(B)**. Isolation of this particular mobility-mass correlation increases the signal of the ozonolysis fragments versus the background noise. **(C)** Conversion versus flow rate plots for each of the products trend similarly to the single double bond containing species depicted in **Figure 2.3**.

to-noise ratio for the ions of interest, especially for that of the low intensity products resulting from cleavage at the Δ4, 7, and 10 positions. This highlights the utility of IM separation for localization of double bond position in complex samples, as previous studies have discussed the difficulty of double bond assignment in polyunsaturated fatty acids due to low signal-to-noise of product fragments.[19,20,22] Moreover, the intensity of each product fragment correlates to the propensity for the reaction at each double bond position. Specifically, the product ion intensities decrease relative to a given double bond's proximity to the fatty acid head group, such that in this example the ozonolysis reaction occurs most readily at the 19-carbon position (farthest from the head group) and least readily at the 4-carbon position (closest to the head group).We hypothesize that this observed decreased reaction efficiency near the lipid head group is likely due to the slight electron-withdrawing character of the carboxylate group of the fatty acid decreasing the nucleophilicity of the double bond near the head group of the molecule, which decreases the probability of ozonolysis. The mechanism of ozonolysis is generally thought to occur by an electrophilic 1,3-addition of ozone, with reaction rates a function of electron density around the double bond, which supports our hypothesis.[38–40]

2.3.4 Analysis of a Lipid Extract

The utility of the ozonolysis device was further explored by analyzing a phosphatidylcholine lipid extract which contains a distribution of PC lipids of various degrees of saturation. Due to the low natural abundance of saturated lipids, a fully saturated lipid standard, PC 16:0/18:0, which should not undergo ozonolysis was spiked into the extract prior to analysis. In this role, PC 16:0/18:0 acts as a negative control for ozonolysis in a biological sample. The resulting IM-MS spectra for the lamp on and off are contained in Figure 2.5. The two IM-MS

spectra highlight a region corresponding to the series of phosphatidylcholines containing 34 alkyl chain carbon atoms and 0-4 alkyl chain double bonds (PC 34:x, x = 0-4). When the lamp is off (Figure 2.5(A)), all five of the species are readily detectable, and their peak centroids display a characteristic mobility-mass correlation consistent with previous IM lipid studies.[41-43] This observed decrease in drift time with an increase the number of double bonds is due to changes in the gas-phase packing efficiency of the lipid as the degree of unsaturation increases. The addition of a cis double bond to the alkyl chain of a lipid introduces a kink in the structure that allows the lipid tail to wrap around the molecule, resulting in a more compact gas-phase structure.[26] The further addition of a second or third double bond causes additional compaction and further reduces the drift time; however, this phenomenon has diminishing returns as additional double bonds (≥3) result in more modest compaction of the gas-phase structure.

When the lamp is switched on (Figure 2.5(B)) all four of the unsaturated lipid species in this IM-MS region deplete as expected due to ozonolysis. Two of the lipid precursors (PC 34:4 and PC 34:3) are no longer detectable, and the other two lipids containing sites of unsaturation (PC 34:2 and PC 34:1) are depleted to the extent that the fully saturated species PC 34:0 at m/z 762.6 becomes the dominant species in this region of the spectrum. Hence, as earlier hypothesized, the ozonolysis device readily identifies fully saturated lipid species in a mixture by converting only the unsaturated species to product ions.

The utility of the ozonolysis device to analyze a complex lipid mixture is also demonstrated in the resulting narrower IM peak profiles observed following the reaction. Normally, the overlapping of isotopic envelopes between adjacent lipid species introduces drift profile peak broadening and can lead to shifts in the drift peak's measured centroid (Figure B.2). As such, this isotopic overlap can result in inaccurate calculations of collision cross section for closely related
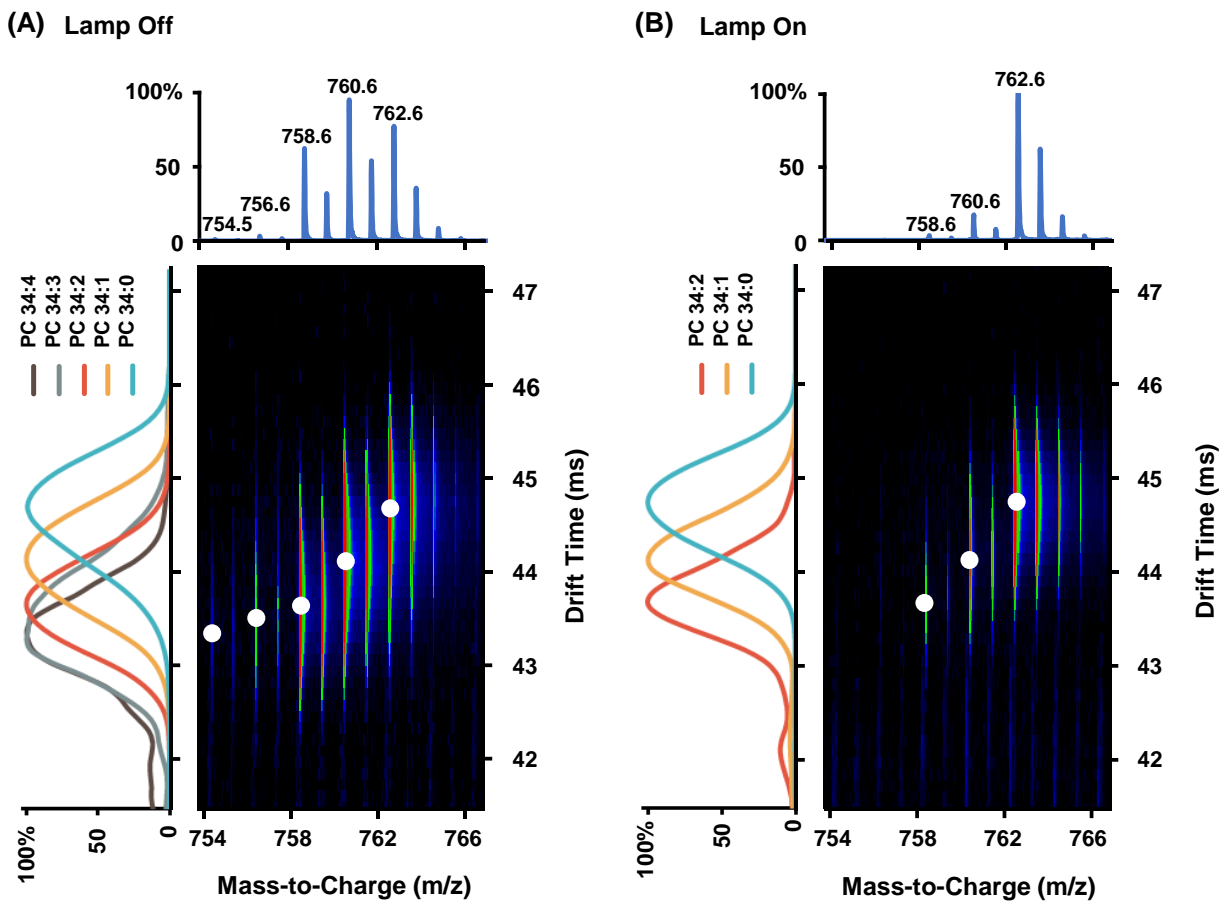
Figure 2.5 A phosphatidylcholine lipid extract from chicken egg spiked with a saturated lipid standard (PC 34:0) was irradiated using the device. **(A)** The lipid signals observed in the IM-MS spectrum correspond to a series of phosphatidylcholines containing 34 alkyl chain carbons with 0-4 alkyl chain double bonds. **(B)** The four species containing double bonds were found to deplete upon irradiation, with low intensity species completely converted. However, the fully saturated lipid standard at m/z 762.6 did not decrease in intensity, clearly identifying saturated versus unsaturated lipids within a complex lipid sample.

lipid species. As increasing efforts are made to establish collision cross section as a discriminating identifier in metabolomic and lipidomic workflows, the generation of CCS databases that are both comprehensive and accurate is becoming increasingly important.[42-45] Ozonolysis in this setting provides an additional analytical tool for minimizing isobaric interferences and thus resulting in more accurate CCS measurements.

Although not depicted in Figure 2.5, several other series of phosphatidylcholines were also detected in the lipid extract, such as PC 38:X (X = 3-8) and PC 18:X (X = 0-4). In contrast to traditional post-mobility collision induced dissociation (IM/CID-MS) where product and precursor ions are drift time correlated, the ozonolysis reactions in this work occur prior to source ionization. Thus, the product ions created via the mercury lamp cannot be time-aligned to a lipid precursor ion, resulting in challenging fragment association and identification. In fact, multiple precursors could generate a given product ion, and additionally if a precursor contains multiple double bonds it can generate multiple product ions, as demonstrated in Figure 2.4. For these reasons, the resulting post-ozonolysis product spectrum for a mixture is challenging to analyze and double bond positions in the precursor are difficult to assign (Figure B.3 and B.4). These findings indicate that chromatographic separation prior to ozonolysis (LC-Oz-IM-MS) would facilitate improved characterization of double bond position in complex mixtures. A recent review by Hancock et. al. concludes that initial separation by chromatography, followed by online ozonolysis and IM-MS, should be sufficient not only for determination of double bond position, but for near complete structural characterization of the lipidome.[7] This assertion lends further credence to the strength and potential impact of our online ozonolysis approach via the low-pressure mercury lamp, especially when coupled to chromatography for broad-scale lipidomic analyses.

2.3.5   Demonstration of a Simple Chromatography Experiment in Conjunction with Ozonolysis

As described in the preceding section, chromatographic separation is crucial to the application of the ozonolysis technique to the identification of double bond position in complex mixtures. To illustrate the analytical utility of performing ozonolysis following LC separation, a mock mixture of three isomeric glycerophosphocholines (PC 18:1 (9E)/18:1 (9E), PC 18:1 (9Z)/18:1 (9Z), and PC 18:1 (6Z)/18:1 (6Z)) was prepared and analyzed by LC-Oz-IM-MS. The results of this experiment are depicted in Figure 2.6. The chromatographic separation consisted of a simple linear gradient, and in lieu of interleaving on-off experiments the analysis was performed twice: in the first, the ozonolysis device remained off, and in the second it was activated for the duration of the experiment. Performing two parallel experiments facililatated simpler correlation of precursors and products and thus allowed easier interpretation of the data. Note that in both experiments, the degasser apparatus was bypassed so as to not remove oxygen from the solvent and decrease ozonolysis reaction efficiency. Low inter-run variability allowed for the alignment of the two resulting extracted ion chromatograms (EICs) for the isomer species at *m/z* 786.6, although only the EIC corresponding to the second experiment with the lamp on is displayed in Figure 6B for simplicity. With the device off (Figure 2.6(A)), it is unclear from the EIC of *m/z* 786.6 that three isomeric species are present since only two chromatographic peaks are observed. However, once the ozonolysis device is switched on (Figure 2.6(B)), the background subtracted extracted mass spectra corresponding to each chromatographic peak reveal the existence of an additional third isomer present in the second chromatographic peak. Evidence supporting the assignment of two isomers in the second peak arises from the diagnostic ozonolysis fragments at *m/z* 634.4 and 676.6 corresponding to aldehyde products resulting from cleavage at the 6Z and 9Z positions on the fatty acid chain. However, other ozonolysis products in addition to the aldehyde
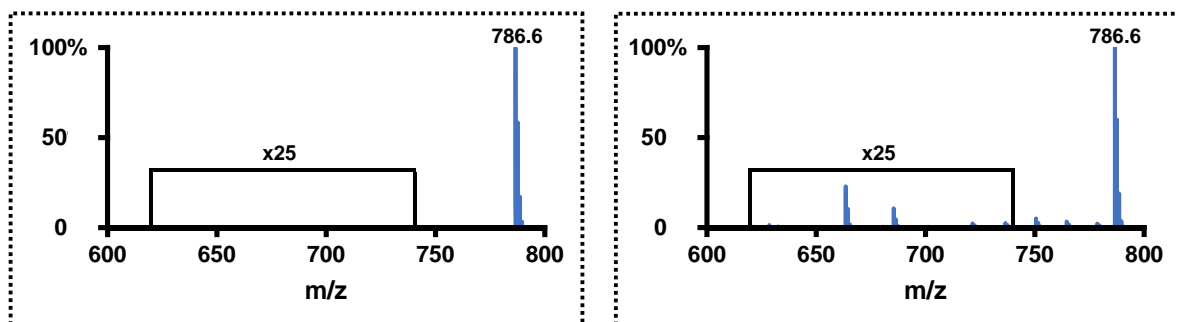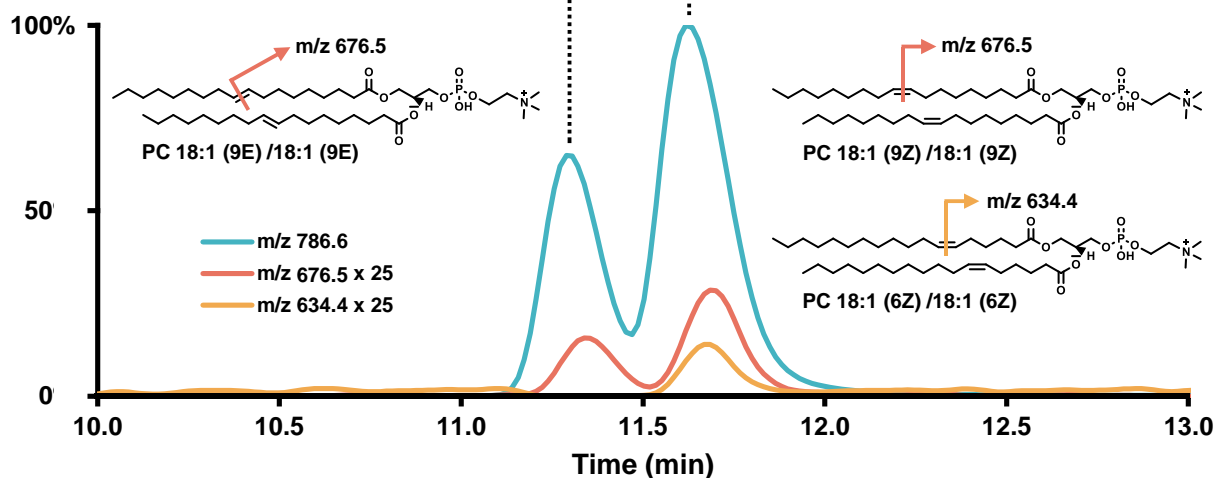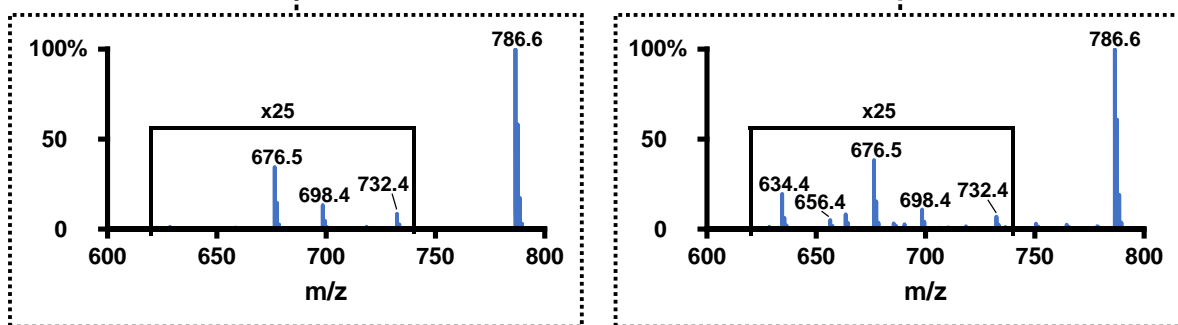
Figure 2.6 A mock mixture of three isomeric glycerophosphatidylcholines was analyzed via LC-Oz-IM-MS. **(A)** With the device turned off, the EIC trace of m/z 786.6 shows separation into cis and trans isomers, and no diagnostic ozonolysis fragments are detected. **(B)** Activation of the ozonolysis device reveals the presence of two distinct cis double bond positional isomers at the 6Z and 9Z positions, with diagnostic aldehyde fragments at m/z 634.4 and 676.6, respectively, underneath the second LC peak in the EIC trace.

49

product are also detected at masses approximately 22 and 56 Da above that of the aldehyde and are thought to correspond to sodiated and solvent adducted species (Figure B.5).

Interestingly, this experiment highlights how neither chromatographic nor ozonolysis approaches alone are sufficient to resolve this system of isomers: liquid chromatography separates the *cis* and *trans* isomers via differences in their retention time, and ozonolysis produces fragments diagnostic of double bond location to identify the 6Z and 9Z position isomers. Moreover, though not specifically illustrated in this particular example, ion mobility separation provides an additional dimension of separation to further increase the signal-to-noise of the ozonolysis fragments. In this way, multiple techniques serve complementary roles within a combined analytical platform for more comprehensive lipid coverage.

2.4   Conclusions

The online flow-cell device developed here allows for determination of double bond position in multiple lipid species in both positive and negative ionization modes. Post-ozonolysis ion mobility separation imparts further structural information regarding the aldehyde product ions and may in the future aid in identification of other classes of lipid isomers. Characterization of the device's performance revealed that the rate of production of diagnostic product ions as well as total observed conversion of precursor to product displayed a high degree of dependence on the sample flow rate. Moreover, preliminary experiments indicate that the flow rates achievable through the device are complementary with liquid chromatographic approaches. The LC-Oz-IM-MS separation of three lipid isomers was able to differentiate the presence of each isomer, thus demonstrating the utility of combining several analytical dimensions within a single experiment. Overall, the use of a low-pressure mercury lamp to induce ozonolysis in

glycerophosphatidylcholines and fatty acids resulted in fast reaction kinetics and high product yield under the conditions studied. Moreover, the platform is low-cost and simple to implement on any instrument because it requires no instrument modifications and does not require an ozone generator. For these reasons, this device has the potential for wide adoption into existing MS-based lipidomic workflows.

2.5   Acknowledgements

2.6   References

(1)   Wenk, M. R. The Emerging Field of Lipidomics. *Nat. Rev. Drug Discov.* **2005**, *4* (7), 594–610.

(2)   Navas-Iglesias, N.; Carrasco-Pancorbo, A.; Cuadros-Rodríguez, L. From Lipids Analysis towards Lipidomics, a New Challenge for the Analytical Chemistry of the 21st Century. Part II: Analytical Lipidomics. *TrAC Trends Anal. Chem.* **2009**, *28* (4), 393–403.

(3)   Rolim, A. E. H.; Henrique-Araújo, R.; Ferraz, E. G.; de Araújo Alves Dultra, F. K.; Fernandez, L. G. Lipidomics in the Study of Lipid Metabolism: Current Perspectives in the Omic Sciences. *Gene* **2015**, *554* (2), 131–139.

(4)   Pulfer, M.; Murphy, R. C. Electrospray Mass Spectrometry of Phospholipids. *Mass Spectrom. Rev.* **2003**, *22* (5), 332–364.

(5)   McDonald, J. G.; Ivanova, P. T.; Brown, H. A. Approaches to Lipid Analysis. In *Biochemistry of Lipids, Lipoproteins and Membranes*; Elsevier, 2016; pp 41–72.

(6)   Blanksby, S. J.; Mitchell, T. W. Advances in Mass Spectrometry for Lipidomics. *Annu. Rev. Anal. Chem.* **2010**, *3* (1), 433–465.

(7)   Hancock, S. E.; Poad, B. L. J.; Batarseh, A.; Abbott, S. K.; Mitchell, T. W. Advances and Unresolved Challenges in the Structural Characterization of Isomeric Lipids. *Anal. Biochem.* **2017**, *524*, 45–55.

(8)   May, J. C.; McLean, J. A. Advanced Multidimensional Separations in Mass Spectrometry: Navigating the Big Data Deluge. *Annu. Rev. Anal. Chem.* **2016**, *9* (1), 387–409.

(9)   Harrison, K. A.; Murphy, R. C. Direct Mass Spectrometric Analysis of Ozonides: Application to Unsaturated Glycerophosphocholine Lipids. *Anal. Chem.* **1996**, *68* (18), 3224–3230.

(10)   Brown, S. H. J.; Mitchell, T. W.; Blanksby, S. J. Analysis of Unsaturated Lipids by Ozone-Induced Dissociation. *Biochim. Biophys. Acta - Mol. Cell Biol. Lipids* **2011**, *1811* (11), 807–817.

(11)   Sun, C.; Zhao, Y. Y.; Curtis, J. M. The Direct Determination of Double Bond Positions in Lipid Mixtures by Liquid Chromatography/In-Line Ozonolysis/Mass Spectrometry. *Anal. Chim. Acta* **2013**, *762*, 68–75.

(12)   Thomas, M. C.; Mitchell, T. W.; Harman, D. G.; Deeley, J. M.; Murphy, R. C.; Blanksby, S. J. Elucidation of Double Bond Position in Unsaturated Lipids by Ozone Electrospray Ionization Mass Spectrometry. *Anal. Chem.* **2007**, *79* (13), 5013–5022.

(13)   Sun, C.; Black, B. A.; Zhao, Y. Y.; Gänzle, M. G.; Curtis, J. M. Identification of Conjugated Linoleic Acid (CLA) Isomers by Silver Ion-Liquid Chromatography/In-Line Ozonolysis/Mass Spectrometry (Ag +-LC/O3-MS). *Anal. Chem.* **2013**, *85* (15), 7345–7352.

(14)   Thomas, M. C.; Mitchell, T. W.; Harman, D. G.; Deeley, J. M.; Nealon, J. R.; Blanksby, S. J. Ozone-Induced Dissociation: Elucidation of Double Bond Position within Mass-Selected Lipid Ions. *Anal. Chem.* **2008**, *80* (1), 303–311.

(15) Poad, B. L. J.; Pham, H. T.; Thomas, M. C.; Nealon, J. R.; Campbell, J. L.; Mitchell, T. W.; Blanksby, S. J. Ozone-Induced Dissociation on a Modified Tandem Linear Ion-Trap: Observations of Different Reactivity for Isomeric Lipids. *J. Am. Soc. Mass Spectrom.* **2010**, *21* (12), 1989–1999.

(16) Marshall, D. L.; Pham, H. T.; Bhujel, M.; Chin, J. S. R.; Yew, J. Y.; Mori, K.; Mitchell, T. W.; Blanksby, S. J. Sequential Collision- and Ozone-Induced Dissociation Enables Assignment of Relative Acyl Chain Position in Triacylglycerols. *Anal. Chem.* **2016**, *88* (5), 2685–2692.

(17) Poad, B. L. J.; Green, M. R.; Kirk, J. M.; Tomczyk, N.; Mitchell, T. W.; Blanksby, S. J. High-Pressure Ozone-Induced Dissociation for Lipid Structure Elucidation on Fast Chromatographic Timescales. *Anal. Chem.* **2017**, *89* (7), 4223–4229.

(18) Ma, X.; Xia, Y. Pinpointing Double Bonds in Lipids by Paternò-Büchi Reactions and Mass Spectrometry. *Angew. Chemie - Int. Ed.* **2014**, *53* (10), 2592–2596.

(19) Ma, X.; Chong, L.; Tian, R.; Shi, R.; Hu, T. Y.; Ouyang, Z.; Xia, Y. Identification and Quantitation of Lipid C=C Location Isomers: A Shotgun Lipidomics Approach Enabled by Photochemical Reaction. *Proc. Natl. Acad. Sci.* **2016**, *113* (10), 2573–2578.

(20) Ma, X.; Zhao, X.; Li, J.; Zhang, W.; Cheng, J. X.; Ouyang, Z.; Xia, Y. Photochemical Tagging for Quantitation of Unsaturated Fatty Acids by Mass Spectrometry. *Anal. Chem.* **2016**, *88* (18), 8931–8935.

(21) Stinson, C. A.; Xia, Y. A Method of Coupling the Paternò–Büchi Reaction with Direct Infusion ESI-MS/MS for Locating the C=C Bond in Glycerophospholipids. *Analyst* **2016**, *141* (12), 3696–3704.

(22) Murphy, R. C.; Okuno, T.; Johnson, C. A.; Barkley, R. M. Determination of Double Bond Positions in Polyunsaturated Fatty Acids Using the Photochemical Paternò-Büchi Reaction with Acetone and Tandem Mass Spectrometry. *Anal. Chem.* **2017**, *89* (16), 8545–8553.

(23) Kliman, M.; May, J. C.; McLean, J. A. Lipid Analysis and Lipidomics by Structurally Selective Ion Mobility-Mass Spectrometry. *Biochim. Biophys. Acta - Mol. Cell Biol. Lipids* **2011**, *1811* (11), 935–945.

(24) Paglia, G.; Kliman, M.; Claude, E.; Geromanos, S.; Astarita, G. Applications of Ion-Mobility Mass Spectrometry for Lipid Analysis. *Anal. Bioanal. Chem.* **2015**, *407* (17), 4995–5007.

(25) Groessl, M.; Graf, S.; Knochenmuss, R. High Resolution Ion Mobility-Mass Spectrometry for Separation and Identification of Isomeric Lipids. *Analyst* **2015**, *140* (20), 6904–6911.

(26) Kyle, J. E.; Zhang, X.; Weitz, K. K.; Monroe, M. E.; Ibrahim, Y. M.; Moore, R. J.; Cha, J.; Sun, X.; Lovelace, E. S.; Wagoner, J.; et al. Uncovering Biologically Significant Lipid Isomers with Liquid Chromatography, Ion Mobility Spectrometry and Mass Spectrometry. *Analyst* **2016**, *141* (5), 1649–1659.

(27)   Dodds, J. N.; May, J. C.; McLean, J. A. Investigation of the Complete Suite of the Leucine and Isoleucine Isomers: Toward Prediction of Ion Mobility Separation Capabilities. *Anal. Chem.* **2017**, *89* (1), 952–959.

(28)   Poad, B. L. J.; Zheng, X.; Mitchell, T. W.; Smith, R. D.; Baker, E. S.; Blanksby, S. J. Online Ozonolysis Combined with Ion Mobility- Mass Spectrometry Provides a New Platform for Lipid Isomer Analyses. *Anal. Chem.* **2018**, *90* (2), 1292-1300.

(29)   Stinson, C. A.; Zhang, W.; Xia, Y. UV Lamp as a Facile Ozone Source for Structural Analysis of Unsaturated Lipids via Electrospray Ionization-Mass Spectrometry. *J. Am. Soc. Mass Spectrom.* **2018***, 29,* 481-489.

(30)   May, J. C.; Goodwin, C. R.; Lareau, N. M.; Leaptrot, K. L.; Morris, C. B.; Kurulugama, R. T.; Mordehai, A.; Klein, C.; Barry, W.; Darland, E.; et al. Conformational Ordering of Biomolecules in the Gas Phase: Nitrogen Collision Cross Sections Measured on a Prototype High Resolution Drift Tube Ion Mobility-Mass Spectrometer. *Anal. Chem.* **2014**, *86* (4), 2107–2116.

(31)   May, J. C.; Dodds, J. N.; Kurulugama, R. T.; Stafford, G. C.; Fjeldsted, J. C.; McLean, J. a. Broadscale Resolving Power Performance of a High Precision Uniform Field Ion Mobility-Mass Spectrometer. *Analyst* **2015**, *140* (20), 6824–6833.

(32)   Cruickshank-Quinn, C.; Quinn, K. D.; Powell, R.; Yang, Y.; Armstrong, M.; Mahaffey, S.; Reisdorph, R.; Reisdorph, N. Multi-Step Preparation Technique to Recover Multiple Metabolite Compound Classes for In-Depth and Informative Metabolomic Analysis. *J. Vis. Exp.* **2014**, No. 89, 1–12.

(33)   Zoschke, K.; Börnick, H.; Worch, E. Vacuum-UV Radiation at 185 Nm in Water Treatment – A Review. *Water Res.* **2014**, *52* (0), 131–145.

(34)   Stinson, C. A. *UV-Induced Online Photochemical Reactions for Enhanced Biomolecule Structural Characterization on an ESI MS/MS Platform*. Ph. D. Dissertation, Purdue University: West Layfayette, IN, 2015.

(35)   Criegee, R. Mechanism of Ozonolysis. *Angew. Chemie Int. Ed. English* **1975**, *14* (11), 745–752.

(36)   Santrock, J.; Gorski, R. a; O'Gara, J. F. Products and Mechanism of the Reaction of Ozone with Phospholipids in Unilamellar Phospholipid Vesicles. *Chem. Res. Toxicol.* **1992**, *5* (1), 134–141.

(37)   Sun, C.; Zhao, Y. Y.; Curtis, J. M. A Study of the Ozonolysis of Model Lipids by Electrospray Ionization Mass Spectrometry. *Rapid Commun. Mass Spectrom.* **2012**, *26* (8), 921−930.

(38)   Klutsch, G.; Fliszár, S. Quantitative Investigation of the Ozonolysis Reaction. XVII. Relative Reaction Rates for the Ozone Attack on Phenylethylenesl. *Can. J. Chem.* **1972**, *50*, 2841–2844.

(39)   Pryor, W. A.; Giamalva, D.; Church, D. F. Kinetics of Ozonation. 3. Substituent Effects on the Rates of Reaction of Alkenes. *J. Am. Chem. Soc.* **1985**, *107* (9), 2793–2797.

(40)   Fisher, T. J.; Dussault, P. H. Alkene Ozonolysis. *Tetrahedron* **2017**, *73* (30), 4233–4258.

(41)   Kim, H. I.; Kim, H.; Pang, E. S.; Ryu, E. K.; Beegle, L. W.; Loo, J. A.; Goddard, W. A.; Kanik, I. Structural Characterization of Unsaturated Phosphatidylcholines Using Traveling Wave Ion Mobility Spectrometry. *Anal. Chem.* **2009**, *81* (20), 8289–8297.

(42)   Paglia, G.; Angel, P.; Williams, J. P.; Richardson, K.; Olivos, H. J.; Thompson, J. W.; Menikarachchi, L.; Lai, S.; Walsh, C.; Moseley, A.; et al. Ion Mobility-Derived Collision Cross Section as an Additional Measure for Lipid Fingerprinting and Identification. *Anal. Chem.* **2015**, *87* (2), 1137–1144.

(43)   Leaptrot, K. L.; May, J. C.; Dodds, J. N.; Mclean, J. A. Conformational Atlas of Sphingolipids and Glycerophospholipids Mapped by Uniform Field Ion-Mobility Mass Spectrometry. *Prep.*

(44)   May, J. C.; Morris, C. B.; McLean, J. A. Ion Mobility Collision Cross Section Compendium. *Anal. Chem.* **2017**, *89* (2), 1032–1044.

(45)   Stow, S. M.; Causon, T. J.; Zheng, X.; Kurulugama, R. T.; Mairinger, T.; May, J. C.; Rennie, E. E.; Baker, E. S.; Smith, R. D.; McLean, J. A.; et al. An Interlaboratory Evaluation of Drift Tube Ion Mobility-Mass Spectrometry Collision Cross Section Measurements. *Anal. Chem.* **2017**, *89* (17), 9048–9055.

CHAPTER 3

EVALUATION OF SURFACE INDUCED DISSOCIATION IN CONJUNCTION WITH

ION MOBILITY-MASS SPECTROMETRY FOR LIPID STRUCTURAL

CHARACTERIZATION

3.1   Introduction

The critical roles that lipids fulfill in both healthy and diseased biological systems have

motivated the development of novel analytical strategies for lipid identification and quantitation.[1–3] However, the sheer quantity of unique lipids present in the lipidome, which is estimated to

number in the tens of thousands,[4,5] along with their inherent structural diversity has historically

made the task of analyzing lipids arising from biological samples daunting. Multiple review

articles have recently been published discussing the current state of lipidomic research and the

challenges that persist in the field.[6–8] While mass spectrometry (MS) continues to be the driving

analytical technology for lipidomics, scientists have increasingly recognized the need to include

additional analytical techniques with MS that provide a greater level of structural fidelity beyond

what traditional MS-based fragmentation approaches like collision induced dissociation (CID) can

provide.[9,10] To that end, a plethora of alternative fragmentation strategies for lipid structural

characterization have been developed over the years, including both more generalized approaches

that fragment the lipid analyte indiscriminately and more pinpointed approaches that target a

specific lipid substructure or chemical bond. Examples of the former include high energy CID

(HCD)[11,12] and radical-based fragmentation strategies such as radical-directed dissociation

(RDD),[13,14] electron-impact excitation of ions from organics (EIEIO),[15,16] and ultraviolet

photodissociation (UVPD).[17,18] Radical-based techniques, in particular, provide unique structural information due to their ability to induce fragmentation along the fatty acid chain. However, nontargeted mechanisms such as these often lead to very complex fragmentation spectra and low signal-to-noise for diagnostic fragments, hampering their utility for analysis of complex samples. Targeted approaches, on the other hand, involve specific ion-molecule reactions that target a particular region of the lipid, often the double bond position of the fatty acid chains. The two main techniques of this type commonly used for lipid analysis include ozone-induced dissociation (Oz-ID)[19–21] and the Paterno-Büchi reaction (PB),[22–24] both of which ultimately induce fragmentation specifically at the lipid double bond. Each of the aforementioned fragmentation techniques have distinct advantages and disadvantages when applied to lipids, especially in the context of more complex biological samples. Thus far, no single analytical technique has been able to rapidly identify a given lipid to the highest level of structural specificity (i.e. headgroup class, acyl chain composition, *sn*-orientation, double bond position, and chirality), which indicates that novel, highly structurally specific fragmentation technologies are still needed. Moreover, an analytical platform combining multiple complementary techniques for lipid analysis will likely be necessary for the full structural characterization of lipids in biological samples.

Surface induced dissociation (SID) is a fragmentation technique originally developed by the Cooks lab in the 1980's for analysis of small molecules in sector mass spectrometers.[25–28] In contrast to traditional CID fragmentation approaches, which occur via sequential collisions of the precursor molecule with a neutral background gas, SID imparts a large quantity of energy to the precursor through a single collision with a solid surface. Therefore, SID occurs on a faster reaction timescale compared to CID and results in the dissociation proceeding under kinetic control, rather than under thermodynamic control as seen in CID.[29,30] Thus, SID is potentially able to access

fragmentation pathways unavailable to CID. Historically, the hardware implementation of SID was challenging due the requirement that ions be directed onto a solid surface, which required either extensive instrument modification or the design of new instrumental configurations for the explicit purpose of conducting SID experiments.[28,31–35] However, more recently the Wysocki group at the Ohio State University have developed an SID device that can be incorporated inline into a commercial Waters Synapt G2 for experiments that combine SID and ion mobility-mass spectrometry (IM-MS) analysis.[36] The Wysocki group has primarily used the combination of SID and IM-MS to investigate the fragmentation of protein supramolecular complexes, and have demonstrated that SID fragmentation of protein complexes sprayed under native-like conditions preserves the native topology of the subunits and allows for the determination of protein quaternary structure.[37–39] This stands in contrast to CID, in which collisional activation typically leads to protein unfolding and the ejection of highly charged monomers.[30] Interestingly, the SID device was designed such that it could be incorporated either before or after the ion mobility cell of the Synapt instrument, which allows for the greater flexibility in designing experiments. Incorporation of IM before SID allows for the separation of different isobaric ions (e.g., conformers or isomers) prior to fragmentation, whereas when IM is utilized after SID, the gas-phase collision cross sections of the SID product ions can be measured, which provides information on the molecule's dissociation pathways.

In this work, we have developed a methodology for tuning and operating the SID device in the SID-IM configuration for small molecule analysis, in contrast to the large proteins and protein complexes typically studied with this device. Lipids were selected for this small molecule SID evaluation due to the challenges that persist in lipid structural characterization. Here, we explore the utility of SID for the generation of unique, diagnostic fragments indicative of specific

lipid structural features in order to aid identification efforts in lipidomic workflows. To investigate the application of SID to this molecular class, seven lipid species across four lipid subclasses were analyzed via SID-IM-MS. Energy-resolved ion breakdown curves (ERIBC) and IM-MS spectra were utilized to examine lipid dissociation pathways and the structures of fragments generated.

3.2   Experimental Methods

3.2.1   Sample Preparation

Lipid standards 1- hexadecanoyl-2-(9Z-octadecenoyl)-sn-glycero-3-phosphocholine (PC 16:0/18:1(9Z)),   1-hexadecanoyl-2-(9Z-octadecenoyl)-sn-glycero-3-phosphoethanolamine   (PE 16:0/18:1(9Z)), 1-hexadecanoyl-2-(9Z-octadecenoyl)-sn-glycero-3-phosphoserine (PS 16:0/18:1), 1-hexadecanoyl-2-(9Z-octadecenoyl)-sn-glycero-3-phosphoglycerol (PG 16:0/18:1), 1',3'-Bis-[1,2-di-(9Z-octadecenoyl)-sn-glycero-3-phospho]-sn-glycerol   (CL 18:1(9Z)/18:1(9Z)/18:1(9Z)/18:1(9Z)),   methyl (9Z)-octadecenoate (FA 18:1 (9Z)), and corticosterone (ST) were purchased from Avanti Polar Lipids and Cayman Chemical. Prior to analysis, individually infused samples were diluted to working concentrations ranging from 10 to 30 µM in 7/3 acetonitrile/water (Optima LC/MS grade, Fisher Scientific). Formic acid (0.1%, Optima grade, Fisher Scientific) was added to PC, PE, PS, PG, FA, and ST samples, 1 mM NaI (Fisher Scientific) was added to the PG sample, and 10 mM NH_4COOH (HPLC grade, Fluka, Honeywell) was added to the CL sample to promote formation of $[M+H]^+$, $[M+Na]^+$, and $[M+NH_4]^+$ ion species, respectively. For mass calibration, 2 mg/mL NaI (Fisher Scientific) in 50/50 isopropyl alcohol/water (Optima LC/MS grade, Fisher) was utilized following Waters recommended calibration protocols.

3.2.2   Instrumentation and Tuning the SID Device

All experiments were performed on a Synapt G2 IM-MS instrument (Waters Corporation), modified with a custom SID device located between the trapping and mobility regions of the instrument (i.e., SID-IM-MS) as described previously (Figure 3.1(A)).[36,38] In order to accommodate the device, the Trapping TriWave Ion Guide (TWIG) was exchanged for a truncated Trap TWIG. Collision with the fluorinated self-assembled monolayer (FSAM) on gold surface was enabled by tuning each of the deflector lenses to optimize SID ion activation. When not utilizing SID, a "flythrough" tuning strategy was used that allowed transmission of the ion beam through the SID device without surface collision (Figure 3.1(B)). In this mode, a gentle voltage gradient was optimized for signal transmission from the trap, through the device, and into the helium cell and TWIMS cell with minimal activation; the voltages utilized for this tune permitted transmission of multiple small molecule lipid species, with the exception of the cardiolipin sample, which required its own separate "flythrough" tune due to its larger mass. It should be noted that due to the fact that switching between TOF only and IMTOF modes of the Synapt G2 raises the Trap Bias of the instrument by approximately ~43 V, three primary small molecule "flythrough" tunes were developed and utilized, with the TOF only mode used solely to mass calibrate the instrument and the IMTOF modes (small molecule and cardiolipin tunes, respectively) used for all experiments.

Tuning the SID device in surface collision mode (Figure 3.1(C)) was significantly more complex and required optimization of the lenses for the fragmentation of each compound analyzed. Generally, collision mode tune files utilized much larger magnitudes of voltages applied to the deflector lenses in comparison with respective "flythrough" tune files in order to steer the ion beam into collision with the surface and extract the resulting fragment ions. The collision energy for SID
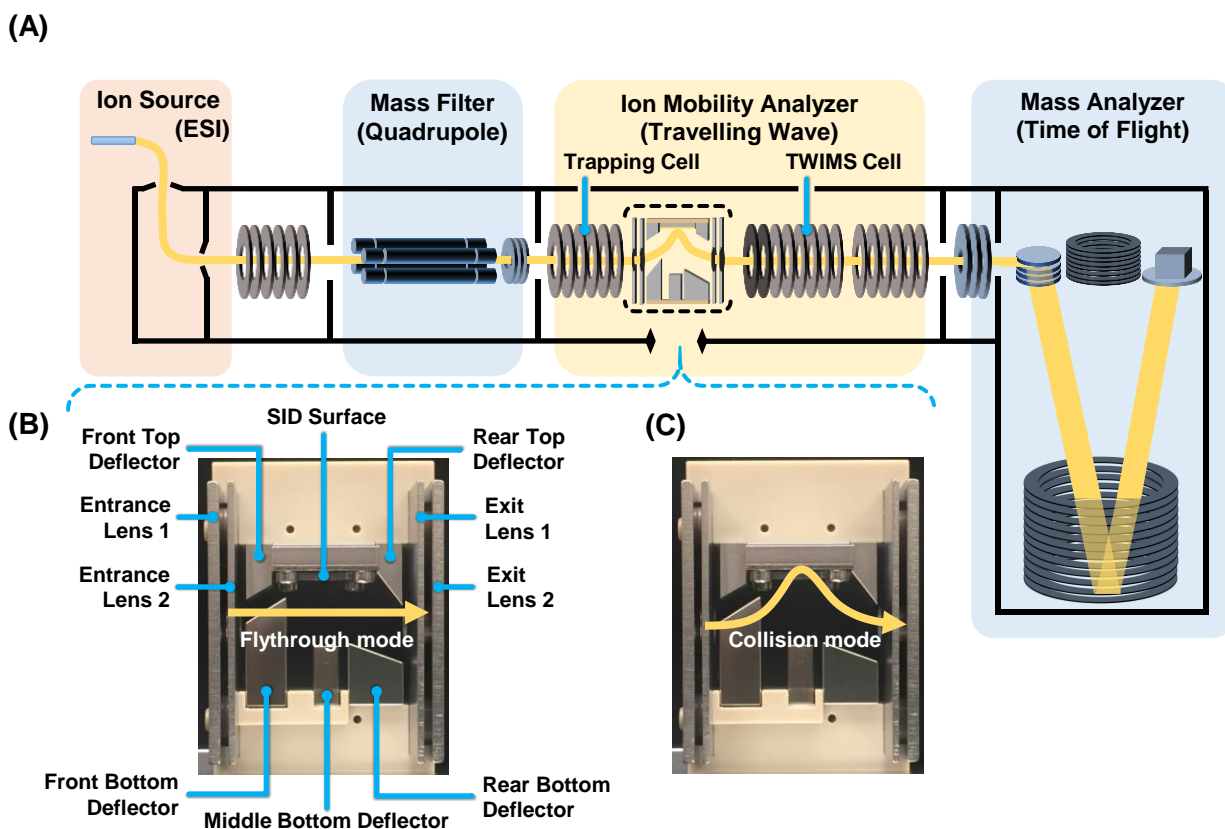
Figure 3.1 A schematic representation of the instrumentation used in this study. (**A**) A commercial Synapt G2 IM-MS was modified as described previously with a custom SID device installed in-line between the Trapping Cell and the TWIMS Cell. The SID device is controlled by adjusting the voltages on ten ion optical lenses and can be operated in (**B**) "Flythrough mode" in which lenses are tuned to pass ions through the device without collision with the surface and (**C**) "Collision mode" in which the lenses are tuned to direct the ion beam towards the SID surface and resulting fragment ions are drawn through the exit slits of the device and directed into the ion mobility stage of the instrument.

is determined by the potential difference between the trap cell exit and the SID surface. Therefore, to perform SID across a range of collision energies, the Trap Bias parameter was increased to increase the potential difference between the trap exit and the surface, and concurrently the Entrance 1 and Front Bottom Deflector lenses were increased by the same magnitude as the Trap Bias to maintain ion transmission through the device. Nominally, all of the SID optics would be readjusted at each SID collision energy to maximize ion transmission, however, satisfactory transmission could be achieved by only adjusting two optics (Entrance 1 and Front Bottom Deflector) in the device, in addition to the instrumental Trap Bias parameter. As a consequence of altering only two of the device lenses when changing the SID collision energy, the further from the initial SID tune file the collision energy is raised (or lowered), the signal transmission becomes increasingly unoptimized, resulting in faster signal depletion than what is observed at equivalent CID collision energies. In these experiments, SID collision tune files were optimized at a collision energy of 30 V, with the exception of FA, which was optimized at 10 V due to its low mass. Tuning the device optics under these intermediate collision energies at which total signal abundance was the largest was found to minimize the ion transmission losses observed at the lowest and highest collision energies surveyed.

To date, the majority of published work using this particular instrument configuration and SID device has involved the analysis of proteins and large supramolecular complexes. As the IM-MS instrument utilizes buffer gases to improve ion transmission through the TWIG stages, for small molecule analysis, it is important to minimize excess ion activation via CID when transmitting ions from the source to the detector, as high ion transmission conditions can also lead to ion heating. In this study, it was observed that activation via incidental CID primarily occurred as a result of the post-SID injection energy into the TWIMS stage, defined as the potential

difference between the SID surface and the Helium Cell. It was determined that ion activation occurred for IM injection energies of 20 V or higher for the lipids analyzed in this study (Supplementary Figure C.1). By retuning the instrumental and SID device optics at 0 V collision energy, total fragment ion signal was reduced to less than 3% relative abundance of the precursor ion signal, with the exception of particularly labile lipids (PE, PS, CL, and FA) where fragment ion signal was minimized to less than 10%, which was necessary to maintain sufficient ion signal for the precursor (>10,000 counts) to conduct SID fragmentation studies.

3.2.3   *Experimental Parameters and Operation of the Modified Instrument*

All experiments were performed with the Synapt G2 operating in IMTOF Sensitivity mode, in which the protonated precursor of PC 16:0/18:1 (m/z 760.6) when isolated in the quadruple, had a measured mass resolving power of approximately 25,000. The SID device was operated using an external power supply and software. All samples were directly infused and source conditions were individually optimized for each lipid. Analyte ions were mass-isolated by the quadrupole prior to either SID or CID. Both SID and CID fragmentation spectra were collected over a range of collision energies with post IM-MS analysis. IM travelling wave conditions utilized the default settings (wave height of 40 V and wave velocity of 650 m/s) for all lipids with the exception of ST (wave height of 35 V and wave velocity of 1000 m/s) which required different settings to disperse the fragment ions more broadly across the drift time space. The helium cell of the Synapt G2 serves to kinetically cool the ion beam prior to IM separation, allowing for increased nitrogen pressure in the TWIMS cell which improves ion mobility resolution.[40] Therefore, the helium cell was set at its maximal value of 200 mL/min for all samples except CL, in which the helium flow rate was lowered to 120 mL/min for more optimal signal transmission. Increasing the argon gas flow rate

in the trapping cell and the nitrogen gas flow rate in the TWIMS mobility cell was observed to increase the abundance of fragment ions arising from incidental CID. Therefore, these settings were decreased from their default settings to 0.4 mL/min argon and 60 mL/min nitrogen for all samples except CL which instead had 1 mL/min argon and 4o mL/min nitrogen. For comparison with SID fragmentation spectra, CID was also performed at laboratory frame collision energies equivalent to those used in SID. All fragmentation experiments were performed in triplicate. Collision energies were stepped in increments of 10 V for all lipids except PC and FA which were stepped in 5 V increments, and collision voltages were increased until the total ion signal was fully depleted. The collision energy ranges for each lipid were as follows: PC 0-150 V, PE 0-120 V, PS 0-100 V, PG 0-100 V, FA 0-25 V, CL 0-100V, and ST 0-50 V. More detailed descriptions of experimental parameters can be found in the Supplemental material.

3.2.4   Data Analysis

All mass spectra were first processed in MassLynx v4.1 and Driftscope v2.5. Due to the large quantity of data generated (approximately 420 total data files) a custom C++ program was written to automate the data processing in MassLynx and subsequent exporting of each spectra into Excel as a peak list at each collision energy. First, the direct infusion total ion chromatogram corresponding to each fragmentation energy was summed to produce an integrated mass spectrum. Next, the bottom 70% of signal was omitted to remove background ions, and the remaining profile spectrum was smoothed and centered to produce the final MS/MS spectrum. The default smoothing and centering settings in MassLynx were used, and centering was performed as a function of height rather than area. Then, the peak list and corresponding intensities were copied to Excel where the spectra were further processed using custom VBA macros to remove all peaks

above the mass of the precursor, remove centering artifact apodes, and convert the signal to relative intensity. Finally, an additional VBA macro was used to automatically generate energy-resolved ion breakdown curves for the CID and SID fragmentation experiments of each lipid. The energy-resolved ion breakdown curves plot the decomposition products observed as a function of lab frame collision energy in terms of relative abundance normalized to the most abundant ion at each individual collision energy, rather than abundance of the precursor ion.

3.3   Results and Discussion

3.3.1   Direct Comparison of CID and SID Fragmentation Spectra

To facilitate initial characterization efforts, the commonly studied phosphatidylcholine standard, PC 16:0/18:1 (9Z), was utilized for tuning the SID device for small molecule fragmentation. The structure of this lipid is depicted in Figure 3.2(A), with observed cleavage sites and resulting fragment ion m/z annotated. Once a suitable SID tune was developed, the protonated lipid precursor at m/z 760.6 was isolated in the quadrupole and then subjected to SID activation at 30 V (Figure 3.2(B)). For comparison, the lipid was also fragmented via CID at an equivalent lab frame energy (Figure 3.2(C)). It was observed that the fragment ions were largely identical between the two fragmentation spectra, indicating that for a collision energy of 30 V, SID does not access any fragmentation pathways unavailable to CID. The dominant product ion in both spectra is the expected loss of the phosphocholine headgroup at m/z 184.1, while other low abundance fragments include other headgroup fragments and the loss of the sn2 acyl chain at m/z 496.3. The major difference between the two fragmentation spectra is reflected in the differences in relative abundance of both the precursor ion and some of the low mass headgroup fragment ions. The precursor ion at m/z 760.6 is more substantially depleted in the SID fragmentation

Figure 3.2 Comparison of the SID (**B**) and CID (**C**) fragmentation spectra of the lipid PC 16:0/18:1 at equivalent lab frame collision energies. Selected product ions and their cleavage sites are annotated on the precursor molecule (**A**). Observed fragment ions are largely identical between the two fragmentation modalities, with the phosphocholine headgroup loss (m/z 184.1) serving as the dominant product ion arising from both ion activation modes.

spectra, and the headgroup fragments at m/z 86.1, m/z 99.0, and m/z 125.0 are also increased in the SID fragmentation spectra relative to the CID fragmentation spectra. These observations are indicative of the fact that SID imparts more energy to the target molecule than CID does at an equivalent lab frame energy, which is consistent with the literature and indicates the validity of the current SID tuning methodology.

3.3.2   Validation of Lipid Fragments using IM-MS Spectra and Kendrick Mass Defect Analysis

In an effort to identify lipid fragments unique to SID, and therefore generated via dissociation mechanisms unavailable to CID, SID and CID were performed over a range of collision energies for each of the lipid samples. Surveying a broad range of collision energies corrects for the fact that SID imparts more energy to the target molecule and allows for an interrogation of the entire chemical space of product ions that may be generated by each fragmentation mechanism. The fragmentation of glycerophospholipids has been detailed thoroughly in the literature, particularly their dissociation via CID.[9,41] Therefore, elucidation of novel fragmentation mechanisms such as those potentially accessed via SID requires careful study of low abundance fragment ions, as well as those which appear at low m/z. Examination of IM-MS product ion spectra allows for facile inspection of low intensity fragments by filtering out chemical noise for improved signal-to-noise, as well as enabling the identification of ions which fall within the same mobility-mass correlation region as other known fragments of the precursor within the spectrum. Figure 3.3 depicts a comparison of SID (A) and CID (B) IM-MS fragmentation spectra for the PC 16:0/18:1 standard at a collision energy of 50 V. As previously observed at a collision energy of 30 V in Figure 3.2, the majority of detected fragment ions, particularly those of significant signal intensity, are conserved between the two fragmentation
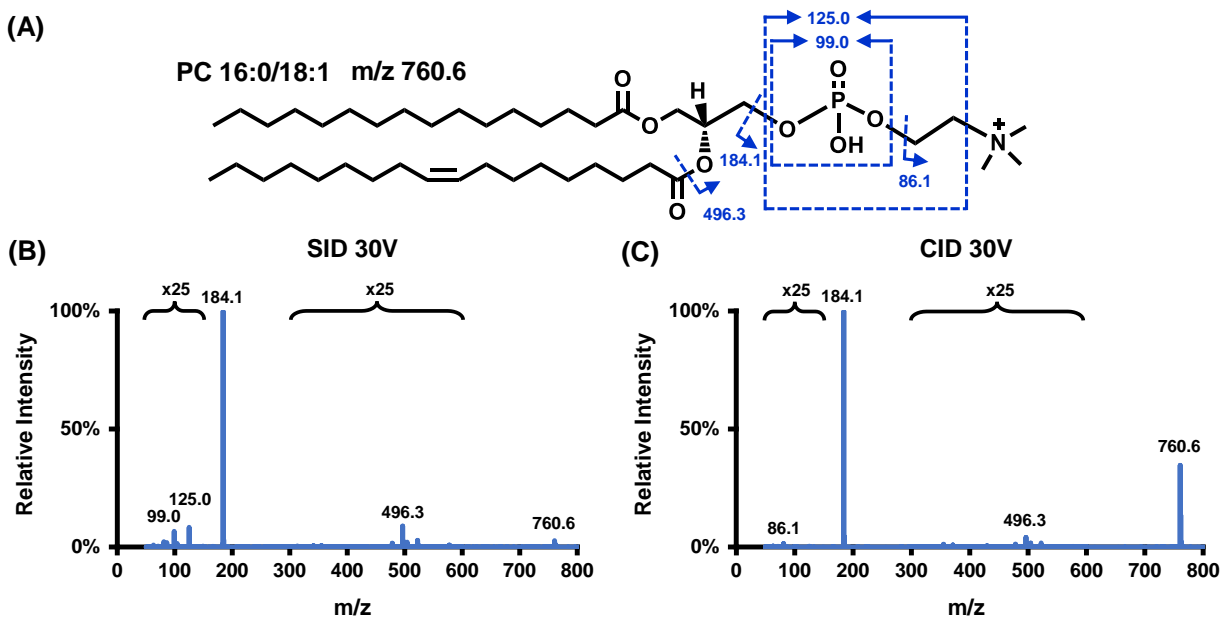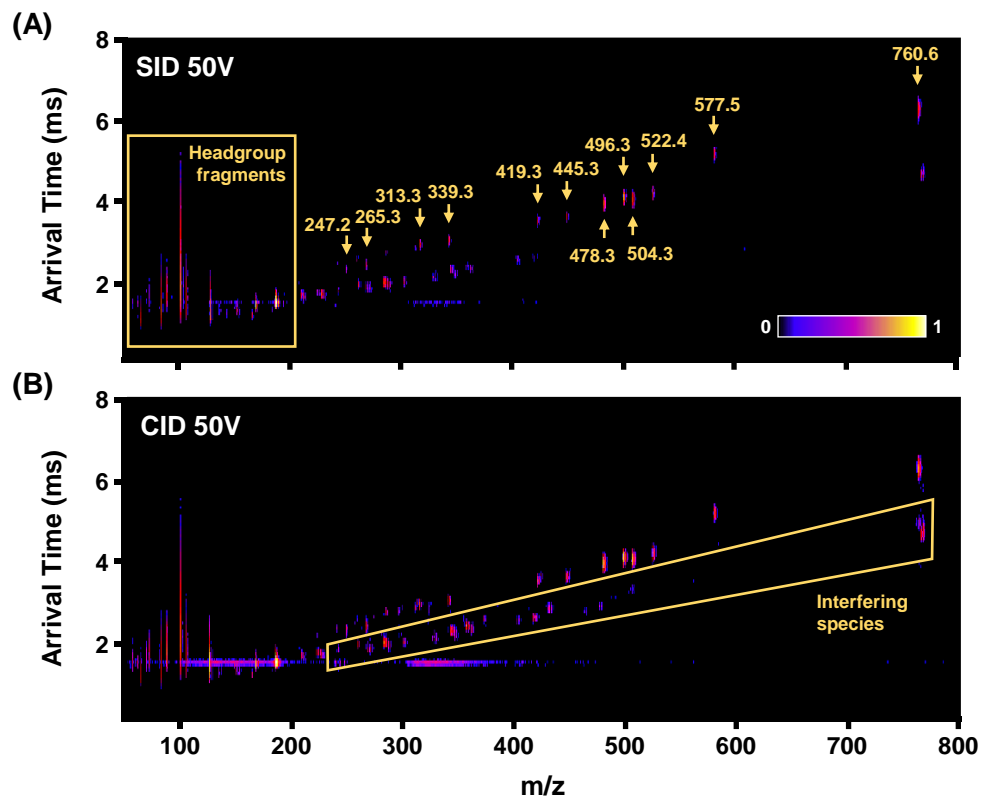
Figure 3.3 Comparison of the SID (**A**) and CID (**B**) IM-MS fragmentation spectra of the lipid PC 16:0/18:1 at equivalent lab frame collision energies. As similarly observed in the MS fragmentation spectra in Figure 2, detected fragment ions are largely identical between the two fragmentation modalities. The IM analysis in both ion activation modes reveals the presence of a series of interfering species which resulted from transmission of multiple precursor ions within the quadrupole isolation window, but these interferents partition in a distinct region of IM-MS space which is removed from the ions of interest.

modalities. These fragment ions, which are labeled in Figure 3.3A, correspond well with established fragmentation mechanisms for PC lipids. However, closer inspection of the IM-MS fragment ion spectra reveals additional details about the nature of the structure of the product ions. For example, the vertical "streaking" which appears at low m/z corresponds to ions which are formed during the TWIMS analysis, such as those generated through metastable decay, and this uncorrelated ion mobility signal is observed in both the SID and CID mobility spectra for several low mass headgroup fragments, such as m/z 86.1, m/z 99.0, and m/z 125.0. More importantly, when IM separation occurs post-fragmentation, the mobility-mass correlations can be used to link product ions to their precursor(s). These relationships, commonly referred to as trendlines in the IM literature, serves two crucial purposes: (1) they allow for the isolation of product-specific mass and mobility spectra and thus improves the signal-to-noise ratio for the ions of interest,[42] which is especially useful for the analysis of low abundance signals originating from complex spectra, and (2) these correlations validate whether a given fragment ion results from the fragmentation of a specific precursor. For example, the SID and CID IM-MS fragmentation spectra depicted in Figure 3.3(A) and Figure 3.3(B) appear to have minor differences in the appearance of some of the lower abundance fragments. However, these low abundance fragment ions do not lie along the mobility-mass correlation for the protonated precursor ion (m/z 760.6) of PC 16:0/18:1. Rather, these ions are fragment ions resulting from the dissociation of a higher charge-state interfering species that was isolated in the quadrupole along with m/z 760.6. This is evidenced by the fact that these species have an overall lower arrival time distribution than known fragments ions originating from m/z 760.6. In this case, ion mobility provides utility via an extra dimension for product ion discrimination, and prevents misattribution of fragment ions to the incorrect precursor.

The assignment of SID product ions can be reinforced using Kendrick mass defect (KMD) analysis. Represented by the decimal mass number following the nominal mass, the mass defect refers to the change in mass due to the binding energy of nucleons and thus is intrinsically related to the chemical composition of the analyte.[43,44] The Kendrick scale, which rescales the mass axis based on the mass of a CH_2 group (14 Da) has been shown to demonstrate utility for the relational analysis of molecules distinguished by their CH_2 groups, such as petroleum-based hydrocarbons and lipids.[45–47] In this case, KMD analysis was applied to the 50 V SID fragmentation spectra of PC 16:0/18:1. The KMD was determined for each of the fragment ions by subtracting the Kendrick-scaled mass from the nominal Kendrick mass, and the resulting KMD was then plotted as a function of exact mass, as shown in Figure 4A. Projecting the data in this manner resulted in two distinct trendlines of fragment ions, highlighted in blue and yellow on the figure, and a cluster of fragment ions at low m/z which are lipid headgroup fragments that do not undergo mobility-selective separation in the TWIMS (that is, ions which are transmitted under "ion surfing" conditions).[48] These two trendlines were reminiscent of the fragment ion mobility-mass correlations observed in Figure 3.3(A), and plotting the IM arrival times as a function of mass resulted in Figure 3.4(B). Comparing the two plots in Figure 3.4 led to the conclusion that the two trendlines in the KMD analysis represented fragment ions from two separate precursor ions, the precursor of interest at m/z 760.6 and one or more interfering ions described previously. The KMD analysis, like the IM-MS spectra, aligned chemically similar fragment ions into distinct regions of space. The chemical structures of the majority of product ions resulting from SID of PC 16:0/18:1 were deduced from the precursor structure, all of which are denoted by a yellow marker in Figure 3.4(A) and Figure 3.4(B). It should be noted that the blue ions that appear on the yellow trendlines of Figure 3.4(A) and Figure 3.4(B) are not interferents, but rather isotopes of other yellow ion
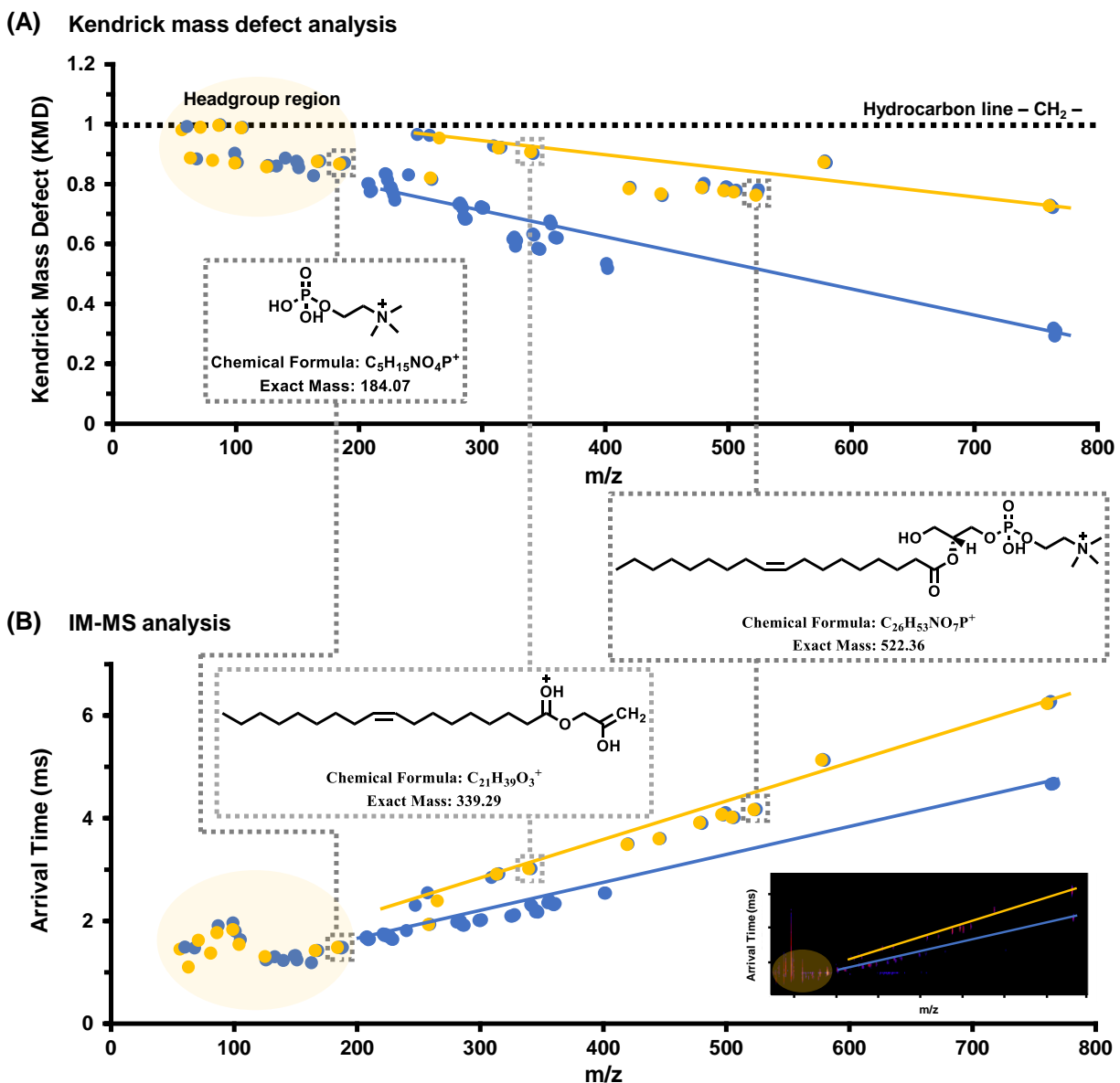
Figure 3.4 Kendrick mass defect analysis **(A)** of the fragment ions resulting from SID of PC 16:0/18:1 at 50 V displays similar trends as a function of m/z as the fragment ions' ion mobility arrival times **(B)**. The yellow trendline represents fragment ions resulting from the dissociation of the PC 16:0/18:1 precursor at m/z 760.6, with yellow markers representing fragment ions with chemical formulas and structures verified to result from known PC fragmentation pathways. As previously observed in **Figure 3.3**, the blue trendline represents fragment ions resulting from an interfering species isolated by the quadrupole alongside m/z 760.6 and the interferent's resulting fragment ions which are separated out in both IM space and KMD space from the fragment ions of interest. The region at lower m/z are ions arising from post-mobility dissociation as well as ions which are not observed to mobility separate under the TW conditions used.

structures. Here, utilization of both the IM-MS data and KMD analysis was critical for the assignment of fragment ions to the correct precursor and subsequent validation of SID product ion structures.

As a second example demonstrating the utility of combined IM-MS and KMD analysis, several unique fragment ions of PG 16:0/18:1 were observed at high SID collision energies (> 70 V) which were not detected in the complementary CID spectra (Supplementary Figure C.2). Analysis of the SID IM-MS product ions spectra suggested that the fragments in question (m/z 284.3, m/z 340.4, and m/z 368.4) might be fragment ions of the PG lipid, as their signals grouped in a region of mobility-mass space in proximity to known fragment ions for PG 16:0/18:1 (Supplementary Figures C.2 and C.3). Nevertheless, KMD analysis revealed that the ions in question did not correlate in KMD space with other known fragments, indicating that they likely did not result from SID of the sodiated PG 16:0/18:1 precursor at m/z 771.51 (Supplementary Figure C.3). Moreover, all three of the ions of interest (m/z 284.3, m/z 340.4, and m/z 368.4) possessed KMD values which were very close to the hydrocarbon limit of 1 (0.987, 0.987, and 0.988, respectively) which indicated that theses ions were potentially hydrocarbon interferents released from the surface at high SID collision energies. This example highlights how orthogonal strategies such as ion mobility and mass defect analyses contribute additional molecular information and aid in fragment ion identification and validation.

3.3.3   Comparison of Energy-Resolved CID and SID

Once the product ions were verified via IM-MS and KMD analyses, the relative intensities of the most abundant fragment ions were plotted as a function of collision energy to generate energy-resolved ion breakdown curves (ERIBC). Energy-resolved measurements provide insight

on the major decomposition mechanisms an analyte undergoes as the collision energy increases. These energy-resolved plots were constructed for each of the seven lipids analyzed in this study. Three of these lipids have their respective CID and SID ERIBC depicted in Figure 3.5, with corticosterone (ST), PC 16:0/18:1, CL (18:1)$_4$ represented in panels A, B, and C, respectively. In general across all of the lipids analyzed, it was observed that as the mass of the lipid precursor increased, the energy required to induce fragmentation also increased, which is a feature common to collision-based fragmentation techniques. Additionally, as observed previously in the fragmentation spectra comparisons in Figure 3.1 and the IM-MS spectra comparisons in Figure 3.2, the most abundant product ions are identical between SID and CID fragmentation mechanisms for all three lipids depicted in Figure 3.5, as well as in the ERIBC for the other four lipids, which can be viewed in the Supplementary material. However, the collision energies in which each fragment ion appears is lower in SID versus CID. In other words, the transitions from one dominant species in the mass spectra to another (annotated as shaded regions in the figure, preceding from white, to light gray, to dark gray, to represent the transition from the precursor, first-generation fragments, and second-generation fragments) occur at lower collision energies in SID relative to CID.

The largest differences between SID and CID energy-resolved ion breakdown curves occurred at the highest collision energies surveyed. For example, SID was observed to deplete the signal of the headgroup of PC 16:0/18:1 at m/z 184.1 into successively smaller secondary fragments, such as m/z 99.0, a process which was not fully observed for CID at the maximum collision energy accessible by this instrument. The other glycerophospholipids surveyed behaved similarly to PC 16:0/18:1, with high energy SID leading to the production of small headgroup fragments only minimally detected via CID fragmentation. Additionally, the CL fragment m/z

73
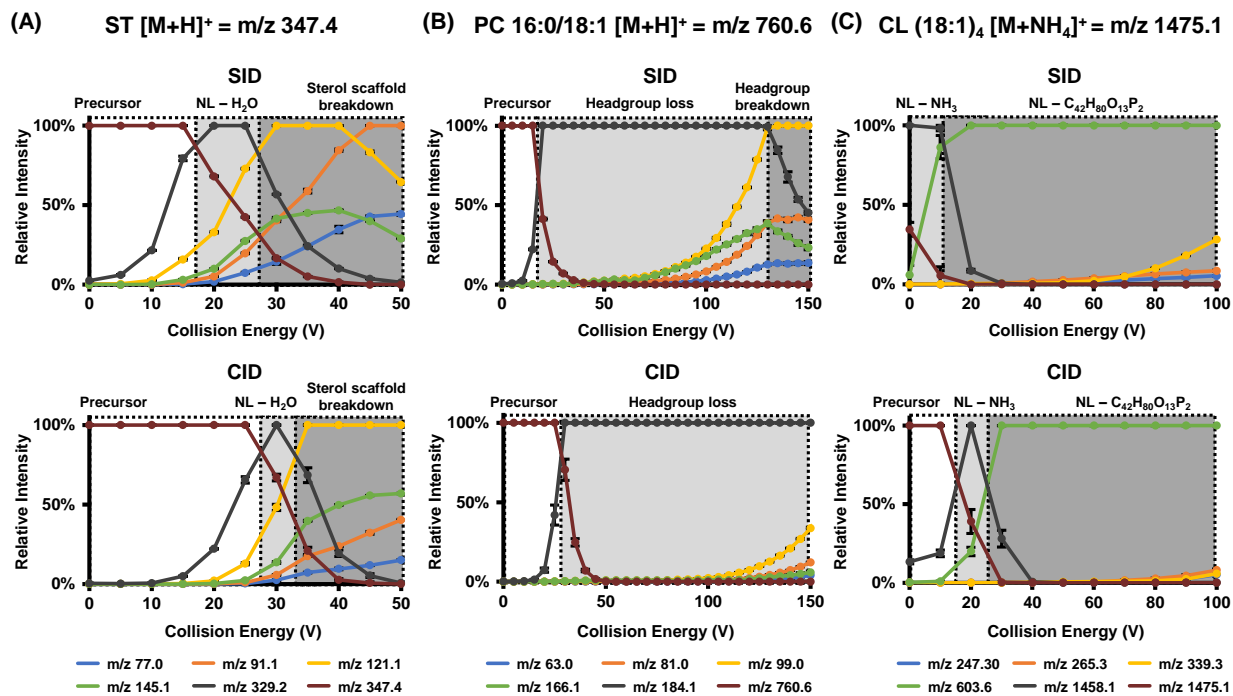
Figure 3.5 Relative ion intensity of precursor and predominant fragment ions as a function of lab frame collision energy for corticosterone ST **(A)**, PC 16:0/18:1 **(B)**, and CL(18:1)4 **(C)** for both SID (**top**) and CID (**bottom**). Shaded areas of each energy-resolved ion breakdown curve correspond to the precursor species (**white**), the first-generation fragments (**light gray**), and second-generation fragments (**dark gray**). Because SID is a higher energy fragmentation technique, onset of precursor fragmentation and further structural decomposition occur at lower collision energies relative to CID.

603.6 begins to break down into smaller structures (m/z 247.3, m/z 265.3, and m/z 339.3) at approximately 70 V via SID, while only minimal fragmentation of the same ion is observed at 100 V when performing CID. To summarize the comparison of the two fragmentation mechanisms for the lipids analyzed, the ΔU_{50}, or the collision energy at which 50% of a species has been depleted, was determined for the precursor and the first product ion of each of the lipids for both SID and CID. This information is collected in Table 1, and complements the energy-resolved plots. The ΔU_{50} for both precursor and product ion were always lower for SID relative to CID for the lipids analyzed, indicating that SID is a more efficient fragmentation mechanism. Together, these observations provide additional support that SID deposits greater energy to the analyte molecule than does CID in the current instrumental configuration, which as stated previously is supported by theory and prior results in the literature.[25,29,49]

Aside from the differences in fragment ion appearance and depletion energies between the two dissociation mechanisms, only minor differences were observed for the ERIBC of the lipids. For example, the formation of m/z 166.1 is preferred over the formation of m/z 81.0 in the fragmentation of PC 16:0/18:1 for SID relative to CID (see Supplementary Figure C.4 for a clearer representation of this observation), but otherwise no fragment ions unique to SID were detected for this lipid, or the other lipids analyzed in this study. These observations suggest that although SID imparts greater energy to the analyte in the dissociation process, smaller molecules such as lipids may not possess additional higher energy fragmentation pathways that are otherwise inaccessible to CID. In contrast to small molecules, larger analytes such as proteins and protein complexes benefit more from the shortened timescale of SID fragmentation whereby the precursor is less able to vibrationally redistribute the energy imparted across its chemical bonds. In other words, SID fragmentation is more ergodic for small molecules than larger molecules because small

molecules take less time to distribute the collision energy across their normal modes due to having fewer chemical bonds and overall degrees of freedom. For these reasons, the lack of unique SID fragments in these small molecule experiments is justifiable. For the lipids in this study, most of the differences between SID and CID in the ERIBC occurred at very high collision energies, with very small headgroup fragments (< 100 m/z) that are not particularly useful for structural identification, however other classes of molecules could still potentially benefit from the large energy deposition provided by SID. Although SID was not found to generate novel fragment ions or fragmentation pathways for the lipids analyzed in this study, it remains a useful technique due to its high fragmentation efficiency and ability to generate fragments from higher energy dissociation pathways at lower lab frame collision energies.

3.4   Conclusions

Surface induced dissociation (SID) was used to fragment seven different lipid molecules representing four different lipid subclasses to investigate the utility of the technique for lipid structural analysis. For the small molecule lipids analyzed in this study, SID was found to produce comparable fragmentation spectra to traditional CID fragmentation. However, SID promoted more fragmentation at the same lab frame energy, which provided in-depth structural information, particularly regarding the lipid headgroup of glycerophospholipids. The use of IM separation following SID fragmentation provided additional structural information for the generated product ions, and mobility-mass trends combined with mass defect analysis aided in the assignment of product ions to the correct precursor species. Finally, energy-resolved ion breakdown curves verified initial assessments based on individual fragmentation spectra that SID deposits a greater quantity of energy to the target molecule in comparison to CID, which was supported by the

observation that fragment ion appearance energies are lower in SID than CID. Taken together, SID serves as another important analytical technique in the toolkit for lipid structural analysis, particularly when combined with orthogonal techniques such as ion mobility and mass defect analysis.

3.5   Acknowledgements

3.6   References

(1)   Wenk, M. R. The Emerging Field of Lipidomics. *Nat. Rev. Drug Discov.* **2005**, *4* (7), 594–610.

(2)   Blanksby, S. J.; Mitchell, T. W. Advances in Mass Spectrometry for Lipidomics. *Annu. Rev. Anal. Chem.* **2010**, *3* (1), 433–465.

(3)   Rolim, A. E. H.; Henrique-Araújo, R.; Ferraz, E. G.; de Araújo Alves Dultra, F. K.; Fernandez, L. G. Lipidomics in the Study of Lipid Metabolism: Current Perspectives in the Omic Sciences. *Gene* **2015**, *554* (2), 131–139.

(4)   Schuster, S.; Fichtner, M.; Sasso, S. Use of Fibonacci Numbers in Lipidomics –
        Enumerating Various Classes of Fatty Acids. *Nat. Publ. Gr.* **2017**, No. January, 1–9.

(5)   Wishart, D. S.; Feunang, Y. D.; Marcu, A.; Guo, A. C.; Liang, K.; Rosa, V.; Sajed, T.;
        Johnson, D.; Li, C.; Karu, N.; et al. HMDB 4 . 0 : The Human Metabolome Database for
        2018. *Nucleic Acids Res.* **2018**, *46* (D1), 608–617.

(6)   Harris, R. A.; Leaptrot, K. L.; May, J. C.; McLean, J. A. New Frontiers in Lipidomics
        Analyses Using Structurally Selective Ion Mobility-Mass Spectrometry. *TrAC - Trends
        Anal. Chem.* **2019**, *116*, 316–323.

(7)   Hancock, S. E.; Poad, B. L. J.; Batarseh, A.; Abbott, S. K.; Mitchell, T. W. Advances and
        Unresolved Challenges in the Structural Characterization of Isomeric Lipids. *Anal.
        Biochem.* **2017**, *524*, 45–55.

(8)   Zheng, X.; Smith, R. D.; Baker, E. S. Recent Advances in Lipid Separations and Structural
        Elucidation Using Mass Spectrometry Combined with Ion Mobility Spectrometry, Ion-
        Molecule Reactions and Fragmentation Approaches. *Curr. Opin. Chem. Biol.* **2018**, *42*,
        111–118.

(9)   Pulfer, M.; Murphy, R. C. Electrospray Mass Spectrometry of Phospholipids. *Mass
        Spectrom. Rev.* **2003**, *22* (5), 332–364.

(10)   Ivanova, P. T.; Milne, S. B.; Byrne, M. O.; Xiang, Y.; Brown, H. A. Glycerophospholipid
        Identification and Quantitation by Electrospray Ionization Mass Spectrometry. *Methods
        Enzymol.* **2007**, *432* (07), 21–57.

(11)   Pittenauer, E.; Allmaier, G. The Renaissance of High-Energy CID for Structural Elucidation
        of Complex Lipids : MALDI-TOF/RTOF-MS of Alkali Cationized Triacylglycerols. *J. Am.
        Soc. Mass Spectrom.* **2009**, *20*, 1037–1047.

(12)   Bird, S. S.; Marur, V. R.; Sniatynski, M. J.; Greenberg, H. K.; Bruce, S. Serum Lipidomics
        Profiling Using LC-MS and High Energy Collisional Dissociation Fragmentation: Focus on
        Triglyceride Detection and Characterization. *Anal Chem* **2012**, *83* (17), 6648–6657.

(13)   Pham, H. T.; Ly, T.; Trevitt, A. J.; Mitchell, T. W.; Blanksby, S. J. Differentiation of
        Complex Lipid Isomers by Radical-Directed Dissociation Mass Spectrometry. *Anal. Chem.*
        2012, *84* (17), 7525–7532.

(14)   Pham, H. T.; Julian, R. R. Radical Delivery and Fragmentation for Structural Analysis of
        Glycerophospholipids. *Int. J. Mass Spectrom.* **2014**, *370*, 58–65.

(15)   Campbell, J. L.; Baba, T. Near-Complete Structural Characterization of
        Phosphatidylcholines Using Electron Impact Excitation of Ions from Organics. *Anal. Chem.*
        2015, *87* (11), 5837–5845.

(16)   Baba, T.; Campbell, J. L.; Blanc, J. C. Y. Le; Baker, P. R. S. Quantitative Structural
        Multiclass Lipidomics Using Differential Mobility : Electron Impact Excitation of Ions

from Organics (EIEIO) Mass Spectrometry. *J. Lipid Res.* **2018**, *59*, 910–919.

(17)   Klein, D. R.; Brodbelt, J. S. Structural Characterization of Phosphatidylcholines Using 193 Nm Ultraviolet Photodissociation Mass Spectrometry. *Anal. Chem.* **2017**, *89* (3), 1516–1522.

(18)   Ryan, E.; Quynh, C.; Nguyen, N.; Shiea, C.; Reid, G. E. Detailed Structural Characterization of Sphingolipids via 193 Nm Ultraviolet Photodissociation and Ultra High Resolution Tandem Mass Spectrometry. *J. Am. Soc. Mass Spectrom.* **2017**, *28* (7), 1406–1419.

(19)   Thomas, M. C.; Mitchell, T. W.; Harman, D. G.; Deeley, J. M.; Nealon, J. R.; Blanksby, S. J. Ozone-Induced Dissociation: Elucidation of Double Bond Position within Mass-Selected Lipid Ions. *Anal. Chem.* **2008**, *80* (1), 303–311.

(20)   Kozlowski, R. L.; Campbell, J. L.; Mitchell, T. W.; Blanksby, S. J. Combining Liquid Chromatography with Ozone-Induced Dissociation for the Separation and Identification of Phosphatidylcholine Double Bond Isomers. *Anal. Bioanal. Chem.* **2015**, *407* (17), 5053–5064.

(21)   Marshall, D. L.; Pham, H. T.; Bhujel, M.; Chin, J. S. R.; Yew, J. Y.; Mori, K.; Mitchell, T. W.; Blanksby, S. J. Sequential Collision- and Ozone-Induced Dissociation Enables Assignment of Relative Acyl Chain Position in Triacylglycerols. *Anal. Chem.* **2016**, *88* (5), 2685–2692.

(22)   Ma, X.; Xia, Y. Pinpointing Double Bonds in Lipids by Paternò-Büchi Reactions and Mass Spectrometry. *Angew. Chemie - Int. Ed.* **2014**, *53* (10), 2592–2596.

(23)   Ma, X.; Zhao, X.; Li, J.; Zhang, W.; Cheng, J. X.; Ouyang, Z.; Xia, Y. Photochemical Tagging for Quantitation of Unsaturated Fatty Acids by Mass Spectrometry. *Anal. Chem.* **2016**, *88* (18), 8931–8935.

(24)   Zhang, W.; Zhang, D.; Chen, Q.; Wu, J.; Ouyang, Z.; Xia, Y. Online Photochemical Derivatization Enables Comprehensive Mass Spectrometric Analysis of Unsaturated Phospholipid Isomers. *Nat. Commun.* **2019**, *10* (1), 1–9.

(25)   Mabud, M. a.; Dekrey, M. J.; Graham Cooks, R. Surface-Induced Dissociation of Molecular Ions. *Int. J. Mass Spectrom. Ion Process.* **1985**, *67* (3), 285–294.

(26)   Cooks, R. G.; Ast, T.; Lafayette, W. COLLISIONS OF POLYATOMIC IONS WITH SURFACES. *Int. J. Mass Spectrom. Ion Process.* **1990**, *100*, 209–265.

(27)   Hayward, M. J.; Mabud, M. A.; Cooks, R. G. Ion / Surface Collisions for Distinction of Isomeric [C6H6]+ and [C6H6]2+ Ions. *J. Am. Chem. Soc.* **1988**, *110* (5), 1343–1346.

(28)   Grill, V.; Shen, J.; Evans, C.; Cooks, R. G. Collisions of Ions with Surfaces at Chemically Relevant Energies: Instrumentation and Phenomena. *Rev. Sci. Instrum.* **2001**, *72* (8), 3149–3179.

(29)   Wysocki, V. H.; Joyce, K. E.; Jones, C. M.; Beardsley, R. L. Surface-Induced Dissociation of Small Molecules, Peptides, and Non-Covalent Protein Complexes. *J. Am. Soc. Mass Spectrom.* **2008**, *19* (2), 190–208.

(30)   Zhou, M.; Wysocki, V. H. Surface Induced Dissociation: Dissecting Noncovalent Protein Complexes in the Gas Phase. *Acc. Chem. Res.* **2014**, *47*, 1010–1018.

(31)   Schey, K. L.; Durkin, D. A.; Thornburg, K. R. Design and Performance of an In-Line Surface-Induced Dissociation Device in a Four-Sector Mass Spectrometer. *J. Am. Soc. Mass Spectrom.* **1995**, *6* (4), 257–263.

(32)   Bier, M. E.; Schwartz, J. C.; Schey, K. L.; Cooks, R. G. Tandem Mass Spectrometry Using an In-Line Ion-Surface Collision Device. *Int. J. Mass Spectrom. Ion Process.* **1990**, *103*, 1–19.

(33)   Wysocki, V. H.; Ding, J. M.; Jones, J. L.; Callahan, J. H.; King, F. L. Surface-Induced Dissociation in Tandem Quadrupole Mass Spectrometers: A Comparison of Three Designs. *J. Am. Soc. Mass Spectrom.* **1992**, *3* (1), 27–32.

(34)   Sun, W.; May, J. C.; Russell, D. H. A Novel Surface-Induced Dissociation Instrument for Ion Mobility-Time-of-Flight Mass Spectrometry. *Int. J. Mass Spectrom.* **2007**, *259* (1–3), 79–86.

(35)   Sun, W.; May, J. C.; Gillig, K. J.; Russell, D. H. A Dual Time-of-Flight Apparatus for an Ion Mobility-Surface-Induced Dissociation-Mass Spectrometer for High-Throughput Peptide Sequencing. *Int. J. Mass Spectrom.* **2009**, *287* (1–3), 39–45.

(36)   Zhou, M.; Huang, C.; Wysocki, V. H. Surface-Induced Dissociation of Ion Mobility-Separated Noncovalent Complexes in a Quadrupole/Time-of-Flight Mass Spectrometer. *Anal. Chem.* **2012**, *84* (14), 6016–6023.

(37)   Zhou, M.; Jones, C. M.; Wysocki, V. H. Dissecting the Large Noncovalent Protein Complex GroEL with Surface-Induced Dissociation and Ion Mobility-Mass Spectrometry. *Anal. Chem.* **2013**, *85* (17), 8262–8267.

(38)   Zhou, M.; Dagan, S.; Wysocki, V. H. Impact of Charge State on Gas-Phase Behaviors of Noncovalent Protein Complexes in Collision Induced Dissociation and Surface Induced Dissociation. *Analyst* **2013**, *138* (5), 1353–1362.

(39)   Song, Y.; Nelp, M. T.; Bandarian, V.; Wysocki, V. H. Refining the Structural Model of a Heterohexameric Protein Complex: Surface Induced Dissociation and Ion Mobility Provide Key Connectivity and Topology Information. *ACS Cent. Sci.* **2015**, *1* (9), 477–487.

(40)   Giles, K.; Williams, J. P.; Campuzano, I. Enhancements in Travelling Wave Ion Mobility Resolution. *Rapid Commun. Mass Spectrom.* **2011**, *25* (11), 1559–1566.

(41)   Murphy, R. C.; Axelsen, P. H. Mass Spectrometric Analysis of Long-Chain Lipids. *Mass Spectrom. Rev.* **2011**, *30* (4), 579–599.

(42)   Harris, R. A.; May, J. C.; Stinson, C. A.; Xia, Y.; McLean, J. A. Determining Double Bond Position in Lipids Using Online Ozonolysis Coupled to Liquid Chromatography and Ion Mobility-Mass Spectrometry. *Anal. Chem.* **2018**, *90* (3), 1915–1924.

(43)   May, J. C.; McLean, J. A. Advanced Multidimensional Separations in Mass Spectrometry: Navigating the Big Data Deluge. *Annu. Rev. Anal. Chem.* **2016**, *9* (1), 387–409.

(44)   Sleno, L. The Use of Mass Defect in Modern Mass Spectrometry. *J. Mass Spectrom.* **2012**, *47* (2), 226–236.

(45)   Kendrick, E. A Mass Scale Based on CH2 = 14.0000 for High Resolution Mass Spectrometry of Organic Compounds. *Anal. Chem.* **1963**, *35* (13), 2146–2154.

(46)   Hughey, C. A.; Hendrickson, C. L.; Rodgers, R. P.; Marshall, A. G. Kendrick Mass Defect Spectrum : A Compact Visual Analysis for Ultrahigh-Resolution Broadband Mass Spectra. *Anal. Chem.* **2001**, *73* (19), 4676–4681.

(47)   Lerno, L. A.; German, J. B.; Lebrilla, C. B. Method for the Identification of Lipid Classes Based on Referenced Kendrick Mass Analysis. *Anal. Chem.* **2010**, *82* (10), 4236–4245.

(48)   May, J. C.; McLean, J. A. The Influence of Drift Gas Composition on the Separation Mechanism in Traveling Wave Ion Mobility Spectrometry: Insight from Electrodynamic Simulations. *Int. J. Ion Mobil. Spectrom.* **2013**, *16* (2), 85–94.

(49)   McCormack, A. L.; Jones, J. L.; Wysocki, V. H. Surface-Induced Dissociation of Multiply Protonated Peptides. *J. Am. Soc. Mass Spectrom.* **1992**, *3* (8), 859–862.

CHAPTER 4

MASS SPECTROMETRY AND ION MOBILITY STUDY OF POLY(ETHYLENE

GLYCOL)-BASED POLYURETHANE OLIGOMERS[‡]

4.1   Introduction

Polyurethanes (PURs) are multi-block copolymers having alternating sequences of soft and hard blocks. The soft blocks are typically polyester or polyether polyols of varying molecular weight. Methylene diphenyl diisocyanate (MDI) is a common hard block component that readily forms urethane linkages when reacted with polyols or short chain diols, the latter known as chain extenders. PURs can be extremely complex and structural characterization can be challenging because of intrinsic distribution variations, cross-linking, and structural heterogeneity.

One specific limitation to characterizing PURs, and copolymers in general, is the inability to determine the exact sequence of units in oligomer chains. Consider, for example, an oligomer consisting of one MDI unit (M) and two polyols (PEG) of differing molecular weights, $(PEG)_n$, where n is the number of polyol repeat units. A peak in the mass spectrum corresponding to oligomers formed from one M and eight PEGs (polyols) could be combinations of $(PEG)_1$-M-$(PEG)_7$, $(PEG)_2$-M-$(PEG)_6$, $(PEG)_3$-M-$(PEG)_5$, or $(PEG)_4$-M-$(PEG)_4$. All will have the same elemental composition and exact mass. However, the differences in their structural sequences can potentially be elucidated through fragmentation (MS/MS) and ion mobility (IM-MS) studies.

Tandem mass spectrometry (MS/MS) and ion mobility–mass spectrometry (IM-MS) work reported on PEG-PURs has not been extensive. Our group has published a CID-MS and IM-MS study of poly(butylene adipate)-based PURs.[1] Synthesis and characterization of sequence coded PURs have been reported by the Charles-Lutz collaboration as part of their effort to produce molecular bar codes that can be read by MS/MS.[2,3] Other workers have studied polymer species distribution within various PUR chains. For example, Aou, et al. used MALDI-MS to determine the distributions of hard segment lengths in PUR foams by "soft" hydrolysis.[4] Pasch et al. obtained sequence analysis of toluene diisocyanate-MDI oligomers from a cross-linked PUR using the combination of hydrolysis, MALDI-MS and MS/MS.[5] Yontz and Hsu reported a MALDI study of poly(urea-urethanes) to determine the hard segment chain-length distribution and its relationship to water content.[6] Gies et al. published a MALDI MS/MS study of carbodiimide branching reactions[7] and used MALDI and MS/MS to identify the cause of increased viscosity observed in processing of poly-MDI.[8] Lastly, Lattimer et al. combined MALDI with pyrolysis to study the structure of segmented PURs formed from MDI and poly(butylene adipate).[9] Nearly all of the aforementioned work has used fragmentation as the primary method of PUR structure characterization. A few groups have used IM-MS to characterize non-PUR based synthetic polymers as well as biomolecular polymers.[10-12] While all these studies represent important contributions to the understanding of PUR chain distributions, the characterization of PEG-PURs via tandem mass spectrometry fragmentation (MS/MS) and ion mobility analysis remains undone.

The present communication is a preliminary report of the synthesis, MS/MS, and IM-MS of three isomeric PUR oligomers formed from MDI and PEG having one MDI (M) and 12 polyols (PEGs). One is the symmetrical $(PEG)_6$-M-$(PEG)_6$ oligomer (6-M-6); and the other two are $(PEG)_4$-M-$(PEG)_8$ (4-M-8) and $(PEG)_2$-M-$(PEG)_{10}$ (2-M-10). The major fragmentation products

observed are resultant of the 1,3-and 1,5-hydrogen shift reactions. Distinct IM-MS trends are observed for the oligomers where the differences in drift times between the doubly charged isomeric species are greater than what is observed for the singly charged isomers.

4.2   Experimental

4.2.1   Materials and Instrumentation

Methanol (MeOH), water (H_2O), and formic acid of Optima grade purity were purchased from Fisher Scientific (Fair Lawn, NJ). A mixture of fluoroalkyl phosphazenes, tris(fluoroalkyl)triazines, betaine, and trifluoracetic acid reference standards were purchased as a commercially available mixture (Tune Mix, G1969-85000) from Agilent Technologies (Santa Clara, CA). In this manuscript, flow-injection ion mobility-mass spectrometry (IM-MS) and tandem mass spectrometry (MS/MS) data was acquired using a 1260 Infinity LC system and a 6560 IM-QTOF MS (Agilent).

4.2.2   Oligomer Synthesis

The symmetrical 6-M-6 oligomer, compound IDT747 (Figure 4.1(A)), was synthesized by the addition of methylene diphenyl diisocyanate (MDI) to a 10-fold excess of monodisperse hexa-polyethylene glycol in toluene containing a catalytic amount of triethylamine and purified by column chromatography on silica gel.[13] Hexa-PEG was synthesized using the procedure outlined by Gothard and Grybowski[14] as reported in the supplemental section.

Synthesis of the asymmetric 4-M-8, compound IDT764 (Figure 4.1(B)), was achieved by the addition of mono-tritylated tetra-polyethylene glycol to a 3-fold excess of MDI followed by the addition of the mono-carbamate to an excess of octa-polyethylene glycol. The resultant intermediate was semi-purified by column chromatography. Next, the trityl protecting group was

(A) **IDT747 6-M-6** m = 5, n = 5
(B) **IDT764 4-M-8** m = 3, n =7
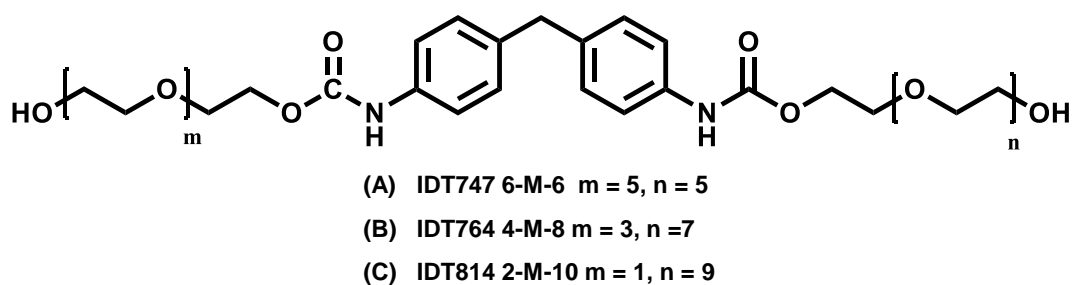(C) **IDT814 2-M-10** m = 1, n = 9

Figure 4.1 PEG-PUR oligomers used in this study. The three synthesized oligomers are isomeric, each consisting of a single MDI hard block and twelve total PEG soft blocks, in which m and n represent the number of soft block units on each side of the MDI hard block.

removed under acidic conditions and further purification by column chromatography gave the desired asymmetric oligomer. A pure sample of 2-M-10, compound IDT814 (Figure 4.1(C)), was synthesized in a similar manner by first mixing mono-tritylated deca-PEG with a 5-fold excess of MDI, stirring at ambient temperature for 1 hour and then adding the resultant crude mixture to 220 equivalents of diethylene glycol and stirring again at ambient temperature for 18 hours. The mono-tritylated MDI intermediate was purified by column chromatography and deprotected under acidic conditions, giving IDT814 following a second column purification step. A detailed description of the synthesis of both the symmetric and the asymmetric PURs is outlined in the supplemental section.

4.2.3   Data Acquisition and Analysis Procedures

Measurement values within this manuscript were acquired using an IM-MS workflow. Briefly, each polymer was prepared at an analytical concentration of 0.1 µM in MeOH. 5 µL of each sample was injected via an autosampler using a previously described flow injection method.[15] An isocratic 1.5 min gradient of 50:50 MeOH:H_2O at 100 µL•min^{-1} flow rate was used to introduce the samples into the IM-MS instrument. Analytes were ionized using a thermally assisted electrospray ionization source (Dual JetStream, Agilent) at 325 °C and an ion transfer capillary voltage (VCap) of 4000 V. The ion source gas was nitrogen operated with a drying gas flow rate of 13 L•min^{-1}, and a sheath gas flow rate of 12 L•min^{-1}. Ion mobility separations were performed using a uniform field drift tube operated with high-purity nitrogen drift gas at 3.95 Torr and room temperature (~298 K). A single drift field analysis at 17.26 V•cm^{-1} was performed on a standardized calibrant mixture (Agilent Tune Mix) to normalize sample drift times and perform the conversion to collision cross section (CCS), as previously described.[16] The time-of-flight

Table 4.1 Major observed fragment ions for each of the three isomeric PEG-PUR oligomers. The fragmentation mechanism leading to the formation of each ion is labelled.

4-M-8			6-M-6			2-M-12		
		m/z			m/z			m/z
	[M+Na]$^+$	837.4		[M+Na]$^+$	837.4		[M+Na]$^+$	837.4
Fragmentation Mechanism	1,3 H-shift	643.3	**Fragmentation Mechanism**	1,3 H-shift	555.2	**Fragmentation Mechanism**	1,3 H-shift	731.3
	1,3 H-shift	467.2		1,3 H-shift	305.2		1,3 H-shift	481.3
	1,3 H-shift	393.2		1,3 H-shift	261.1		1,3 H-shift	437.2
	1,3 H-shift	217.1		1,5 H-shift	573.2		1,5 H-shift	749.4
	1,5 H-shift	661.3		1,5 H-shift + CO$_2$ loss	529.2		1,5 H-shift + CO$_2$ loss	705.4
	1,5 H-shift + CO$_2$ loss	617.3		1,5 H-shift	287.1		1,5 H-shift	463.2
	1,5 H-shift	485.2						
	1,5 H-shift + CO$_2$ loss	441.2						
	1,5 H-shift	375.2						

acquisition mass range was set at m/z 100 to m/z 1700. For fragmentation studies, individual m/z values were quadrupole isolated using an isolation width of approximately 4 m/z units. These isolated masses underwent collision induced dissociation (CID) using the following series of collision energies (CE, laboratory frame): 0 V, 30 V, 40 V, 50 V, 60 V, 70 V, and 80 V. A 1 min post-acquisition gradient of 50:50 MeOH:H_2O at 100 µL•min^{-1} was used to flush the LC lines between samples. Data analysis was performed using MassHunter IM-MS Browser (vB.08.00, Agilent) and MassHunter Qualitative Analysis (vB.08.00, Agilent).

4.2.4   Computational Methods

Insight into the gas-phase conformation of IM-MS results were supplemented with computational studies. Computation modeling included a two-step approach: (1) sampling conformational space and (2) obtaining CCS values for the generated conformations. A geometry optimization at the Hartree-Fock level with 6-31G* basis set was performed with Gaussian 09 for each of the PEG-PUR oligomers separately.[17] Partial charges were derived from ab initio electrostatic potential calculations using a 6-31G* basis set. Sodium ions were added post-optimization and partial charge computations with tLeap. Conformational sampling for optimized PEG-PUR oligomers with sodium ions were acquired using a simulated annealing protocol implemented in AMBER.[18] Sodium ions were restricted to 20 Å distance from a central carbon the entirety of the simulation. For each polymer, a molecular dynamic (MD) simulation began by heating the molecule from 0 K to 650 K over 250 ps, followed by a maintained temperature of 800 K for 9,000 ps. With continuous temperature at 800 K, a structural snapshot was saved every 16,667 steps, and a total of 3,000 structural snapshots were saved. These 3,000 high-energy structures were then cooled to 300 K during a 15 ps MD simulation.
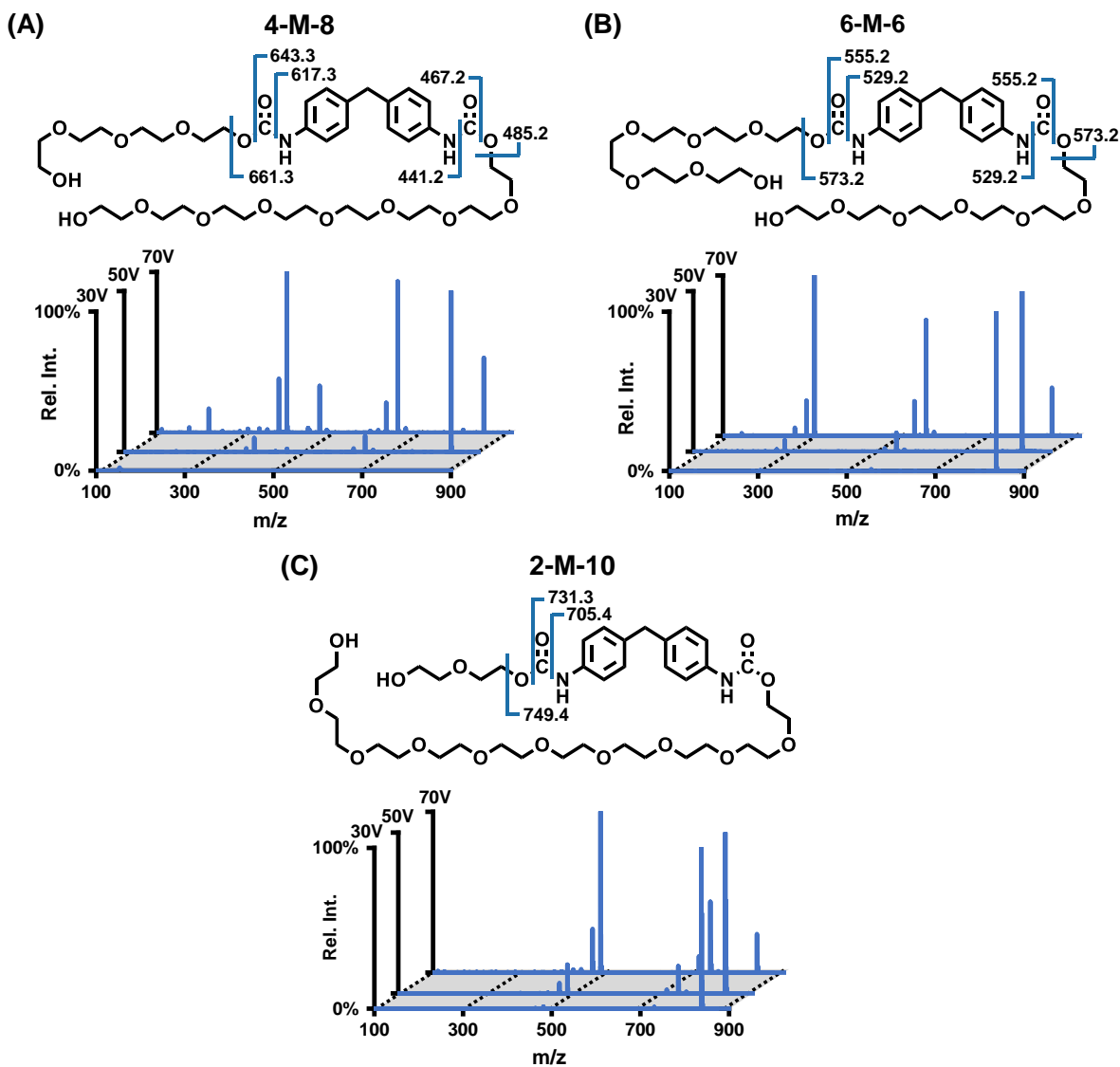
Figure 4.2 IM-MS/MS analysis of three isomeric PEG-PUR oligomers $(PEG)_4$-M-$(PEG)_8$ (4-M-8) (**A**), $(PEG)_6$-M-$(PEG)_6$ (6-M-6) (**B**), and $(PEG)_2$-M-$(PEG)_{10}$ (2-M-10) (**C**). The structures of the precursors are shown, annotated by selected fragment ions at cleavage sites. Representative MS/MS spectra are depicted at fragmentation energies of 30V, 50V, and 70V, with diagnostic fragment ions and their requisite mechanisms labelled in the table below for each isomer.

Theoretical CCS for the resulting 3,000 conformations was determined using MOBCAL software. Projection approximation (PA) was used to generate helium CCS values.[19-21] Nitrogen PA CCS values were determined for a set of confirmations spanning the entire CCS range using superposition projection approximation. These values were used to create a linear trend and obtain Nitrogen CCS values for the remaining conformations.[22-25]

4.3   Results and Discussion

4.3.1   *Fragmentation Schemes of Isomeric PEG-PUR Oligomers*

Synthesized 4-M-8, 6-M-6, and 2-M-10, PUR oligomers were individually analyzed via IM-MS/MS. The intact $[M+Na]^+$ species of *m/z* 837.4 was mass-selected and subjected to a range of CEs from 0 to 80 V. The resulting fragmentation spectrum contained multiple masses unique to each isomeric species. Specifically, the 6-M-6 and 2-M-10 isomers each contained six primary diagnostic peaks, and the 4-M-8 fragmentation spectrum contained nine diagnostic peaks as summarized in Table 1. Fragmentation spectra for each isomer are shown in the Figure 4.2 for 30 V, 50 V, and 70 V CEs. Here, the IM dimension is used to filter out the background chemical noise, which improves the quality of the MS/MS results. Though each isomeric oligomer has a unique fragmentation spectrum and associated diagnostic fragment ions, all product ions originate from only one of two possible fragmentation mechanisms. Namely, these species are undergoing either a 1,3- or 1,5-hydrogen shift around the carbonyl/amide bond located at the MDI motif. The proposed mechanism of these hydrogen shifts is shown in Figure 4.3(A). Full structures of all observed fragmentation products for the PEG-PURs within this study can be found in the supplemental section (Figures D.4-9). Previous work has shown that other PUR polymer species undergo these same 1,3- and 1,5-H shifts.[1] Specifically, poly(butylene)adipate polyesters (PBA-
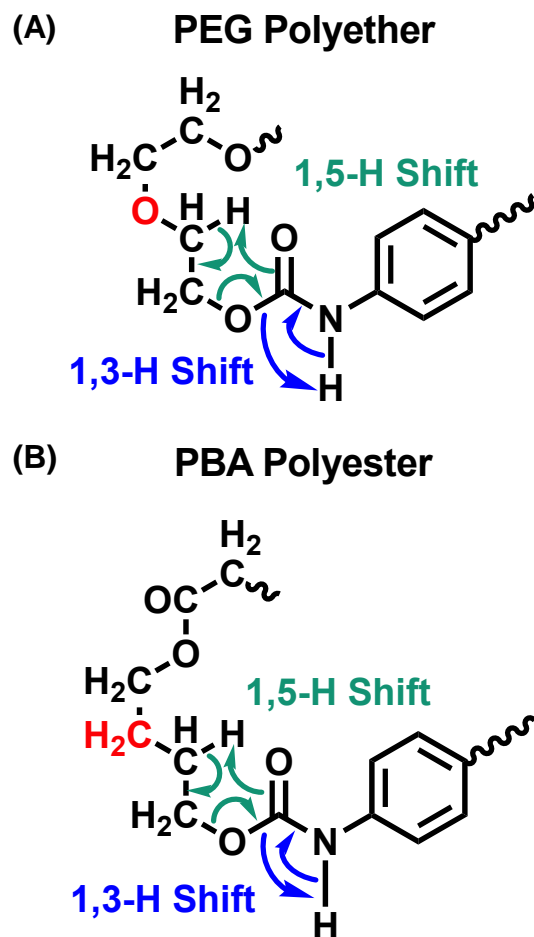
Figure 4.3 Proposed mechanisms for the fragmentation of PEG-polyethers and PBA-polyesters. 1,3-hydrogen shift and 1,5-hydrogen shift fragmentation occurs similarly in PEG-polyethers **(A)** and PBA-polyesters **(B)**. However, the ratio of 1,3-hydrogen shift to 1,5-hydrogen shift products differs between PEG-PURs and PBA-PURs.

PURs, Figure 4.3(B)), have a similar reaction mechanism. However, it was observed that the 1,3-H shift is preferred by PEG PURs whereas the 1,5-H shift dominated the fragmentation results of PBA-PURs. This result is unexpected given that the proposed transition state structures for fragment-ion formation (Figure 4.3) are nearly identical for polyesters and polyethers. One possible explanation regarding this observation is that PEG-PUR soft blocks contain an electron-withdrawing oxygen, indicated in red (Figure 4.3(A)), which could influence electron movement in that locale during fragmentation reactions. Alternatively, PBA-PUR soft blocks contain a CH_2 motif in the same position. Research on this issue is ongoing.

4.3.2 Fragmentation Characterization at Discrete Collision Energies

The fragmentation pattern of each isomeric oligomer was acquired across several collision voltages, namely 0 V, 30 V, 40 V, 50 V, 60 V, 70 V, and 80 V. Primary fragments began forming from the precursor *m/z* 837.4 at 40 V with all diagnostic fragments being observed at 80 V. However, the intact molecule was not fully depleted at 80 V CID. Figure 4.4 depicts the relative intensity of the most abundant diagnostic fragments (relative intensity $\geq 10\%$) at a given collision voltage. Intensities for each fragment ion were normalized relative to the largest peak at each collision energy. As previously mentioned, the 1,3-H shift in all three isomeric species was preferred based on the observation that the peaks generated from a 1,3-H shift which correspond to a diol and isocyanate (retro-polymerization). This phenomenon is corroborated by the observation that the 1,3H shift fragmentation products are the most abundant fragments for all three oligomers as shown in Figure 4.4. Briefly, in 4-M-8 oligomers, the isocyanate fragments are *m/z* 467.2 and *m/z* 643.3, with corresponding diol products at *m/z* 393.2 and *m/z* 217.1. In 6-M-6 oligomers, the isocyanate fragment is *m/z* 555.2 with its corresponding diol at *m/z* 305.2. In 2-M-
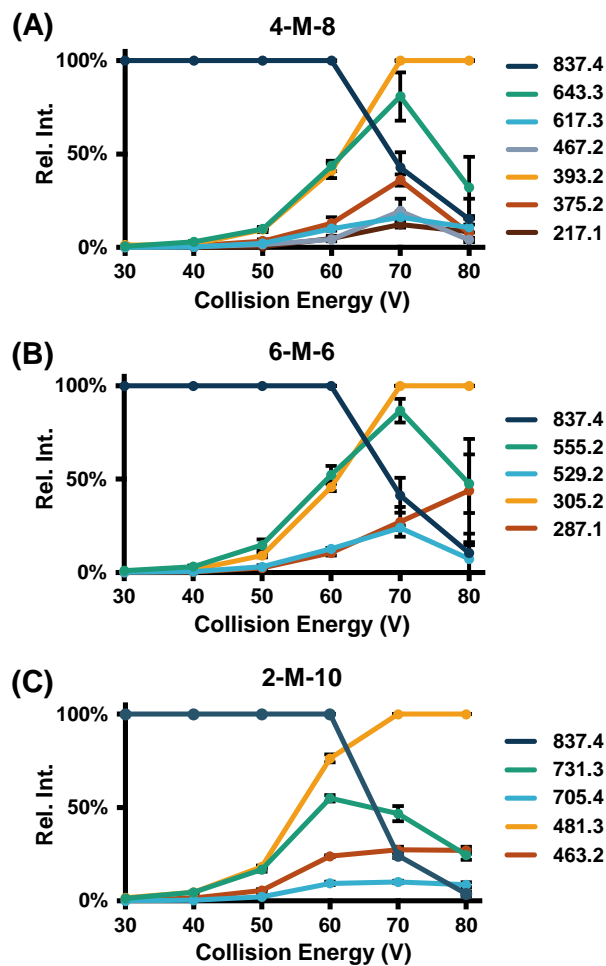
Figure 4.4 Energy-resolved ion breakdown curves were generated for 4-M-8 **(A)**, 6-M-6 **(B)**, and 2-M-10 **(C)** from 30-80V. The relative intensity of selected diagnostic fragment ions outlined in **Figure 4.2** (with relative signal $\geq$ 10% + standard error) were plotted as a function of collision energy.

10 oligomers, the isocyanate fragments are *m/z* 379.1 (unobserved) and *m/z* 731.3 with respective

corresponding diols at *m/z* 481.3 and *m/z* 129.1 (unobserved). For 1,5-H shift mechanism products,

carbamic acid products are generally only observed in very low abundance having been largely

converted to an amine via loss of CO_2 (e.g. *m/z* 573.2 to *m/z* 529.2 for the 6-M-6 oligomer).

Fragments bearing a vinyl end-group were observed to have the greatest abundance among the

1,5-H shift products indicating that these species tended to retain the charge carrier following the

fragmentation reaction. Characterization of all anticipated fragmentation products for each of the

isomeric oligomers can be found in the supplemental section (Figures D.1-3).

4.3.3 Ion Mobility Analysis of PEG-PUR Oligomers

For all three isomeric oligomers, both singly and doubly charged sodium adducted species

were detected in the acquired IM-MS spectra. Figure 4.5(A) depicts an example IM-MS spectrum

for the 4-M-8 oligomer, with the +1 and +2 species having *m/z* of 837.4 and *m/z* 430.2 and drift

times of approximately 36.5 ms and 23.5 ms, respectively. The collision cross section (CCS, $Å^2$),

summarized in Table 4.2, was calculated using the measured drift times as previously reported[16,26]

for both charge states of all three oligomers. It was observed that, for the +1 oligomer ions, the 6-

M-6 species has the smallest CCS and exited the drift tube first, followed by the 2-M-10 species,

and lastly the 4-M-8 species (Figure 4.5(B)). However, given that the difference in CCS between

the three species is less than 1%, these ions are unlikely to have baseline separation in a mixture.[27]

For the +2 oligomer ions, a shift in the drift time of the 2-M-10 species was observed such that

this oligomer has the smallest CCS and exited from the drift tube first, rather than the 6-M-6

oligomer as was observed for the +1 species (Figure 4.5(C)). In this case, the differences in CCS

between the three species (> 3%) are sufficient such that all three oligomers should be separated

Table 4.2 Averaged CCS values and their standard deviations (N=3) for both the +1 and +2 species of each of the isomeric oligomers based on the drift profiles shown in **Figure 4.5(B)** and **(C)**.

		CCS of each species (Å^2)		
		4-M-8	**6-M-6**	**2-M-10**
Charge State	**+1**	270.8 ± 0.0	268.2 ± 0.1	269.8 ± 0.2
	+2	349.6 ± 0.1	340.1 ± 0.1	313.6 ± 0.7

in a mixture.[27] The source of this shift in drift time for the +2 2-M-10 species is currently unknown. However, it is hypothesized that the flexible 10-PEG tail of the molecule could potentially wrap around the rest of the structure, thereby decreasing the CCS of this structure relative to the others. Ongoing work involves the use of molecular modeling to provide additional structural insight into this observed effect.[28,29]

4.3.4 Preliminary Computational Modeling Results

Computational models have been used to provide structural insight to the gas phase conformations of polymeric species observed in experimental CCS measurements.[19,20] MD simulations are used to compute theoretical structures representing the energy profile, or the conformational landscape, of a given molecule. The calculated CCS values of the generated conformations provide insight on the structure of the observed local energy minima of an ion within experimental IM measurements. To compare the gas phase structure of doubly sodium adducted PEG-PUR oligomers, which displayed an interesting shift in drift time for the 2-M-10 species, the number of conformations were calculated as shown in Figure 4.6(B). Theoretical CCS values obtained were within a 5% difference of the experimental measurement, and there is good agreement between experimental and theoretical distributions (Figure 4.6(A, B)). Theoretical CCS calculations show the lowest conformational density for the doubly sodium adducted 2-M-10 oligomer, followed by the 6-M-6, and then the 4-M-8 oligomers. Structural analyses suggest that 2-M-10 coordinates both sodium cations on the larger polymeric arm with 10 monomers, which could be the cause of the observed more compact gas phase conformation, as shown in supplemental section (Figure D.10). The larger CCS density of the 6-M-6 and 4-M-8 species is attributed to each arm of the polymer coordinating a sodium cation yielding a more extended
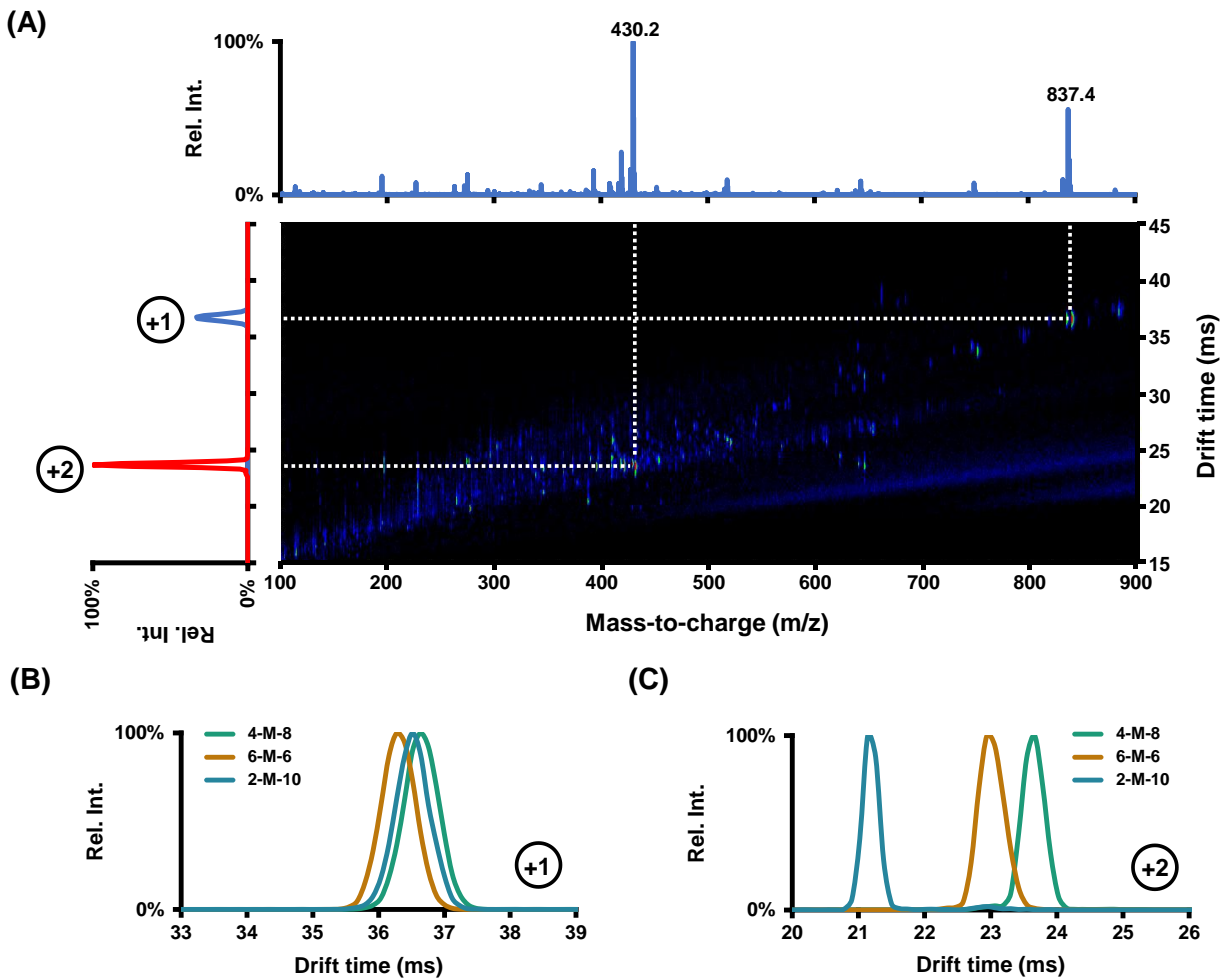
96

Figure 4.5 (A) Representative IM-MS spectrum of the 4-M-8 oligomer. Both +1 and +2 sodium adducted species were detected. **(B)** Drift time separation of the +1 ions for each of the isomeric oligomers. **(C)** Drift time separation of the +2 ions for each of the isomeric oligomers.

structure. The conformational density from tentative CCS values reflects the observed size separation from experimental measurements.

4.4   Conclusions

Three isomeric PEG-PUR oligomers were synthesized and analyzed via IM-MS/MS. These include the symmetric 6-M-6, the 4-M-8, and 2-M-10. This preliminary investigation has determined diagnostic fragment ions for each of the isomeric oligomers and identified the mechanisms that lead to their formation, namely, a 1,3-hydrogen shift and a 1,5-hydrogen shift. Energy-resolved ion breakdown curves from 30-80 V revealed that 1,3-hydrogen shift products were the most abundant fragment ions detected. Although the oligomers can be distinguished via their diagnostic MS/MS fragmentation, these three isomeric species can also be separated via IM. These observations indicate those within the polymer chemistry field have the option to use an MS/MS or IM-MS instrument to characterize these oligomers.

CCS values were determined for both +1 and +2 species for all three oligomers. The separation and difference in CCS values were more pronounced for the +2 sodium adducted species. Additionally, there was a shift in drift tube elution order between the +1 and +2 species. While the 2-M-10 oligomer had a longer drift time than the 6-M-6 oligomer for the +1 species, it has a shorter drift time for the +2 species. The source of this behavior is a topic for future investigation, although preliminary computational results corroborate the experimental measurements.
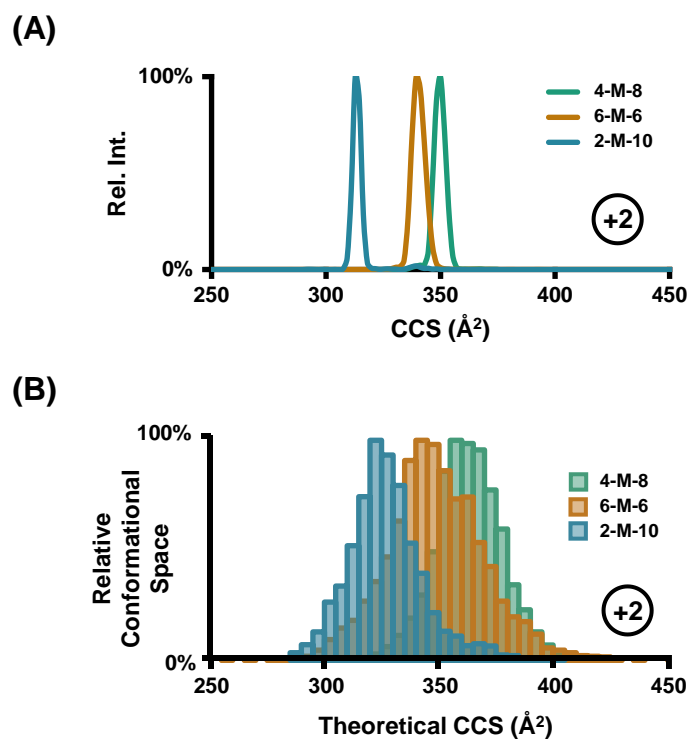
Figure 4.6 (A) Measured arrival time distributions for the +2 cations for each of the isomeric oligomers were converted to CCS space using established protocols. **(B)** Distribution of theoretical structures of PEG-PUR oligomers match experimental trends across calculated CCS values for the +2 cations.

4.5 Acknowledgements

4.6 References

(1) Gies, A. P.; Hercules, D. M. Collision Induced Dissociation Study of Ester-Based Polyurethane Fragmentation Reactions. *Anal. Chim. Acta* **2014**, *808*, 199–219.

(2) Karamessini, D.; Petit, B. E.; Bouquey, M.; Charles, L. Identification-Tagging of Methacrylate-Based Intraocular Implants Using Sequence Defined Polyurethane Barcodes. **2017**.

(3) Gunay, U. S.; Petit, B. E.; Karamessini, D.; Al Ouahabi, A.; Amalian, J.-A.; Chendo, C.; Bouquey, M.; Gigmes, D.; Charles, L.; Lutz, J.-F. Chemoselective Synthesis of Uniform Sequence-Coded Polyurethanes and Their Use as Molecular Tags. *Chem* **2016**, *1* (1), 114–126.

(4) Aou, K.; Schrock, A. K.; Ginzburg, V. V; Price, P. C. Characterization of Polyurethane Hard Segment Length Distribution Using Soft Hydrolysis / MALDI and Monte Carlo Simulation. *Polymer (Guildf).* **2013**, *54* (18), 5005–5015.

(5) Mass, V.; Schrepp, W.; von Vacano, B.; Pasch, H. Sequence Analysis of an Isocyanate Oligomer by MALDI-TOF Mass Spectrometry Using Collision Induced Dissociation. *Macromol. Chem. Phys.* **2009**, *210* (22), 1957–1965.

(6) Yontz, D. J.; Hsu, S. L. A Mass Spectrometry Analysis of Hard Segment Length Distribution in Polyurethanes. *Macromolecules* **2000**, *33* (22), 8415–8420.

(7) Gies, A. P.; Heath, W. H.; Keaton, R. J.; Jimenez, J. J.; Zupancic, J. J. MALDI–TOF/TOF CID Study of Polycarbodiimide Branching Reactions. *Macromolecules* **2013**, *46* (19), 7616–7637.

(8)   Gies, A. P.; Stefanov, Z.; Rau, N. J.; Chakraborty, D.; Boopalachandran, P.; Chauvel, J. P. Iron(III)-Catalyzed Chain Growth Reactions of Polymeric Methylene Diphenyl Diisocyanate. *Macromolecules* **2016**, *49* (4), 1201–1221.

(9)   Lattimer, R. P.; Polce, M. J.; Wesdemiotis, C. MALDI-MS Analysis of Pyrolysis Products from a Segmented Polyurethane. *J. Anal. Appl. Pyrolysis* **1998**, *48* (1), 1–15.

(10)   Amalian, J. A.; Cavallo, G.; Al Ouahabi, A.; Lutz, J. F.; Charles, L. Revealing Data Encrypted in Sequence-Controlled Poly(Alkoxyamine Phosphodiester)s by Combining Ion Mobility with Tandem Mass Spectrometry. *Anal. Chem.* **2019**, *91* (11), 7266–7272.

(11)   Alalwiat, A.; Tang, W.; Gerişlioğlu, S.; Becker, M. L.; Wesdemiotis, C. Mass Spectrometry and Ion Mobility Characterization of Bioactive Peptide-Synthetic Polymer Conjugates. *Anal. Chem.* **2017**, *89* (2), 1170–1177.

(12)   Clemmer, D. E.; Jarrold, M. F. Ion Mobility Measurements and Their Applications to Clusters and Biomolecules. *J. Mass Spectrom.* **1997**, *32* (6), 577–592.

(13)   Houton, K. A.; Burslem, G. M.; Wilson, A. J. Development of Solvent-Free Synthesis of Hydrogen-Bonded Supramolecular Polyurethanes. *Chem. Sci.* **2015**, *6* (4), 2382–2388.

(14)   Gothard, C. M.; Grzybowski, B. A. A Cost-Effective, Column-Free Route to Ethylene Glycol Oligomers EG_6, EG_{10}, and EG_{12}. *Synthesis (Stuttg).* **2012**, *44* (5), 717–722.

(15)   Nichols, C. M.; May, J. C.; Sherrod, S. D.; McLean, J. A. Automated Flow Injection Method for the High Precision Determination of Drift Tube Ion Mobility Collision Cross Sections. *Analyst* **2018**, *143* (7), 1556–1559.

(16)   Stow, S. M.; Causon, T. J.; Zheng, X.; Kurulugama, R. T.; Mairinger, T.; May, J. C.; Rennie, E. E.; Baker, E. S.; Smith, R. D.; McLean, J. A.; et al. An Interlaboratory Evaluation of Drift Tube Ion Mobility–Mass Spectrometry Collision Cross Section Measurements. *Anal. Chem.* **2017**, *89* (17), 9048–9055.

(17)   Frisch, M. J.; Trucks, G. W.; Schlegal, H. B.; Scuseria, G. E.; Robb, M. A.; Cheeseman, J. R.; Scalmani, G.; Barone, V.; Petersson, G. A.; Nakatsuji, H.; et al. Gaussian 09, Revision A.02. Gaussian, Inc.: Wallingford, CT 2009.

(18)   Case, D. A.; Babin, V.; Berryman, J. T.; Betz, R. M.; Cai, Q.; Cerutti, D. S.; Cheatham, T. E. I.; Darden, T. A.; Duke, R. E.; Gohlke, H.; et al. AMBER 2014. University of California: San Francisco, CA 2014.

(19)   Mesleh, M. F.; Hunter, J. M.; Shvartsburg, A. A.; Schatz, G. C.; Jarrold, M. F. Structural Information from Ion Mobility Measurements: Effects of the Long-Range Potential. *J. Phys. Chem.* **1996**, *100* (40), 16082–16086.

(20)   Shvartsburg, A. A.; Jarrold, M. F. An Exact Hard-Spheres Scattering Model for the Mobilities of Polyatomic Ions. *Chem. Phys. Lett.* **1996**, *261* (1–2), 86–91.

(21) Campuzano, I.; Bush, M. F.; Robinson, C. V.; Beaumont, C.; Richardson, K.; Kim, H.; Kim, H. I. Structural Characterization of Drug-like Compounds by Ion Mobility Mass Spectrometry: Comparison of Theoretical and Experimentally Derived Nitrogen Collision Cross Sections. *Anal. Chem.* **2012**, *84* (2), 1026–1033.

(22) Bleiholder, C.; Wyttenbach, T.; Bowers, M. T. A Novel Projection Approximation Algorithm for the Fast and Accurate Computation of Molecular Collision Cross Sections (I). Method. *Int. J. Mass Spectrom.* **2011**, *308* (1), 1–10.

(23) Anderson, S. E.; Bleiholder, C.; Brocker, E. R.; Stang, P. J.; Bowers, M. T. A Novel Projection Approximation Algorithm for the Fast and Accurate Computation of Molecular Collision Cross Sections (III): Application to Supramolecular Coordination-Driven Assemblies with Complex Shapes. *Int. J. Mass Spectrom.* **2012**, *330–332* (2012), 78–84.

(24) Bleiholder, C.; Contreras, S.; Do, T. D.; Bowers, M. T. A Novel Projection Approximation Algorithm for the Fast and Accurate Computation of Molecular Collision Cross Sections (II). Model Parameterization and Definition of Empirical Shape Factors for Proteins. *Int. J. Mass Spectrom.* **2013**, *345–347*, 89–96.

(25) Bleiholder, C.; Contreras, S.; Bowers, M. T. A Novel Projection Approximation Algorithm for the Fast and Accurate Computation of Molecular Collision Cross Sections (IV). Application to Polypeptides. *Int. J. Mass Spectrom.* **2013**, *354–355*, 275–280.

(26) Picache, J. A.; Rose, B. S.; Balinski, A.; Leaptrot, K. L.; Sherrod, S. D.; May, J. C.; McLean, J. A. Collision Cross Section Compendium to Annotate and Predict Multi-Omic Compound Identities. *Chem. Sci.* **2019**, *10* (4), 983–993.

(27) Dodds, J. N.; May, J. C.; McLean, J. A. Correlating Resolving Power, Resolution, and Collision Cross Section: Unifying Cross-Platform Assessment of Separation Efficiency in Ion Mobility Spectrometry. *Anal. Chem.* **2017**, *89* (22), 12176–12184.

(28) Forsythe, J. G.; Stow, S. M.; Nefzger, H.; Kwiecien, N. W.; May, J. C.; McLean, J. A.; Hercules, D. M. Structural Characterization of Methylenedianiline Regioisomers by Ion Mobility-Mass Spectrometry, Tandem Mass Spectrometry, and Computational Strategies: I. Electrospray Spectra of 2-Ring Isomers. *Anal. Chem.* **2014**, *86* (9), 4362–4370.

(29) Stow, S. M.; Onifer, T. M.; Forsythe, J. G.; Nefzger, H.; Kwiecien, N. W.; May, J. C.; McLean, J. A.; Hercules, D. M. Structural Characterization of Methylenedianiline Regioisomers by Ion Mobility-Mass Spectrometry, Tandem Mass Spectrometry, and Computational Strategies. 2. Electrospray Spectra of 3-Ring and 4-Ring Isomers. *Anal. Chem.* **2015**, *87* (12), 6288–6296.

CHAPTER 5

CONCLUSIONS AND FUTURE DIRECTIONS FOR ION MOBILITY-MASS

SPECTROMETRY FOR THE STRUCTURAL ANALYSIS OF LIPIDS AND OTHER

MOLECULES

5.1   Summary

Mass spectrometry is an analytical technique well-suited to the characterization of complex samples due to its unique combination of high sensitivity, specificity, and throughput. However, a fundamental limitation of the technique involves its inability to distinguish the presence of isomers, preventing complete characterization of a sample. Oftentimes, these isomeric species are of relevance to the experimenter: in lipidomics, only cis fatty acids are produced naturally in the body by humans and other animals, while trans fatty acids are usually acquired via diet. Additionally, certain double bond position lipid isomers have been observed to differ in their binding affinities with membrane proteins such as Cytochrome *c* Oxidase.[1,2] Isomerism is also important in the analysis of synthetic polymers; the physical properties of a polyurethane polymer sample are determined by several factors, one of which is the number of and sequence of "hard" and "soft" blocks the polymer oligomer contains.[3,4] Many sequence isomers may exist in a given polyurethane sample at each oligomer length, but mass spectrometry alone is blind to this particular form of structural complexity. However, mass spectrometry can be combined with additional analytical techniques to overcome these limitations, and different techniques can be utilized in conjunction with mass spectrometry to characterize the multiples types of structural heterogeneity that may be present in a sample.

Improving the analytical characterization via mass spectrometry of structurally complex samples, especially those containing isomers, motivates the present work. To that end, ion mobility is utilized in conjunction with mass spectrometry, providing an orthogonal dimension of separation based on molecular size and shape in the gas phase.[5] Although ion mobility has only been incorporated into commercial mass spectrometry platforms in the last decade or so, the separation technique has quickly found broad application in the analysis of complex biological samples and synthetic polymer samples alike due to its speed and structural sensitivity. It has been demonstrated that ion mobility can be used to separate certain types of isomers, such as lipid *cis* and *trans* isomers.[6,7] However, current instrument platforms lack the necessary resolving power to separate compounds differing in CCS by less than about 2%, such as enantiomers, or in the case of lipids, double bond position isomers.[8-10] Thus, even with IM-MS, alternative strategies are necessary for honing in on fine structural details and increasing the information content gained in a single experiment.

Several strategies have been explored to address the limitations discussed above and reduce the isomer problem. In Chapter 2, an online ozonolysis device was developed for the elucidation of bond position in lipids. The device, which could be utilized with IM-MS alone or integrated with LC for LC-Oz-IM-MS, uses UV light to induce formation of ozone in solution.[11] Ozone subsequently reacts in a site-specific manner with the lipid double bond, resulting in bond cleavage; mass spectral detection of the products allows for the determination of double bond location in the precursor. The combination of LC, IM, ozonolysis, and mass spectrometry in a single platform enables the discrimination of multiple types of lipid isomers including *cis/trans*, double bond position isomers, and potentially *sn*-regiosomers. However, several features of the ozonolysis device still require slight refinement, as the flow cell-based design suffers from low

reaction conversion efficiency at LC flow rates, which prevents analysis of low abundance species in complex samples. Addressing these limitations is a subject for further research.

Chapter 3 developed an alternative approach for the structural characterization of lipids. In this study, SID was utilized in combination with IM-MS to determine whether the fragmentation technique, which has been demonstrated to impart greater energy to the target molecule than traditional CID approaches,[12,13] generates unique, structurally informative fragment ions not observed using other fragmentation mechanisms. A custom-machined SID device[14] was installed between the trapping and mobility cells on a Waters Synapt G2 IM-MS instrument in an SID-IM-MS configuration, such that SID product ions are separated via IM post-fragmentation. Although SID was not observed to generate novel fragment ions for the seven lipid species characterized, it did promote greater fragmentation at a lower lab frame collision energy. Additionally, the utilization of IM post-SID gave rise to mobility-mass correlations between the product ions and their precursor, a structural relationship that aided in the correct assignment of products to their precursors and diminishing chemical noise. Other data visualizations strategies were also investigated in this work, including energy-resolved ion breakdown curves (ERIBC) and Kendrick mass defect, to fully characterize the mechanisms involved in the fragmentation of the lipid samples by SID.

Building on several of the analytical strategies developed in the preceding sections for lipid analysis, Chapter 4 applied IM-MS/MS for the characterization of synthetic polyurethane samples, specifically a system of three isomeric PEG-polyurethane oligomers. Each of the oligomers contained a single hard block and twelve soft block segments, but the soft blocks were differentially arranged around the hard block to give three sequence isomers. It was demonstrated that, although the compounds could not be distinguished via mass spectrometry, their +1 charge

states differed in their fragmentation spectra, wherein the primary fragmentation mechanisms observed were 1,3-hydrogen shifts and 1,5-hydrogen shifts around the urethane linkage. The differences in CCS for the singly-sodium adducted oligomers were too small for them to separate via IM on the current instrument platform; however, CCS differences were large enough to distinguish between the doubly-sodium adducted species, again underscoring the importance of utilizing multiple analytical techniques when characterizing samples containing isomeric compounds.

Overall, the analytical tools developed in this dissertation work help to overcome the isomer problem endemic to complex samples such as lipids and polymers. As has been emphasized throughout, the structural heterogeneity present in complex samples often requires multiple techniques utilized in tandem to discriminate features that initially seem hidden in the mass spectrum. Increasing the structural information content that can be gained in a single experiment will aid in both untargeted 'omics workflows, wherein previously unidentified features may possess important biological relevance, and the characterization of polymer samples, such that polymers with specific properties can be more readily synthesized.

5.2   Future Directions

5.2.1   Application of Online Ozonolysis to Untargeted Lipidomic Workflows

The work in Chapter 2 demonstrates a proof-of-concept LC separation of a mixture of three isomeric PC lipid standards, illustrating how the ozonolysis device when integrated in a LC-oz-IM-MS platform allows for the discrimination of both *cis/trans* isomers (via LC and IM) and double bond position isomers (via ozonolysis). However, the analytical trade-off between flow rate and reaction conversion efficiency inherent in a flow cell-based design leads to diminished

ozonolysis product signal in complex samples and complicates the correlation of ozonolysis precursor and product ions. Several slight modifications intended to increase ozonolysis conversion at LC-compatible flow rates have already been made, including adding a second low-pressure mercury lamp for increased irradiation of the sample volume and swapping out the inflexible "windowed" polyimide-coated fused silica line with UV-transparent fluorinated ethylene-propylene (FEP) tubing which can be wrapped around the lamps multiple times for a larger reaction volume. However, one caveat of increasing the reaction volume is that the device can no longer be rapidly switched "on" and "off" over the course of a single LC peak. Instead, separate "on" and "off" LC separations must be performed and later stitched back together manually via retention time. Nevertheless, the increased conversion efficiency gained due to the increased reaction volume is necessary for optimizing the device for application in untargeted lipidomic experiments.

Another factor that merits further analysis prior to incorporating the device into an untargeted lipidomic workflow is how the reaction conversion efficiency changes as a function of solvent composition, which is directly relevant to the development of an effective LC gradient for use with the device. A simple experiment could be performed utilizing flow injection prior to oz-IM-MS in which different solvent compositions are chosen to simulate the composition at points along an LC gradient, monitoring the conversion (in terms of peak area of the ozonolysis product versus the peak area of the precursor ion, as a percentage out of 100%) of a lipid standard containing a single double bond at each of these points (Figure 5.1). Prior work from the Xia group optimizing a similar mercury lamp-mediated reaction, the Paternò-Büchi reaction, has indicated that the solution-phase reaction yields are highest in water, slightly lower in methanol and acetonitrile, and significantly reduced in isopropanol.[15] If this is also the case for ozonolysis, it is
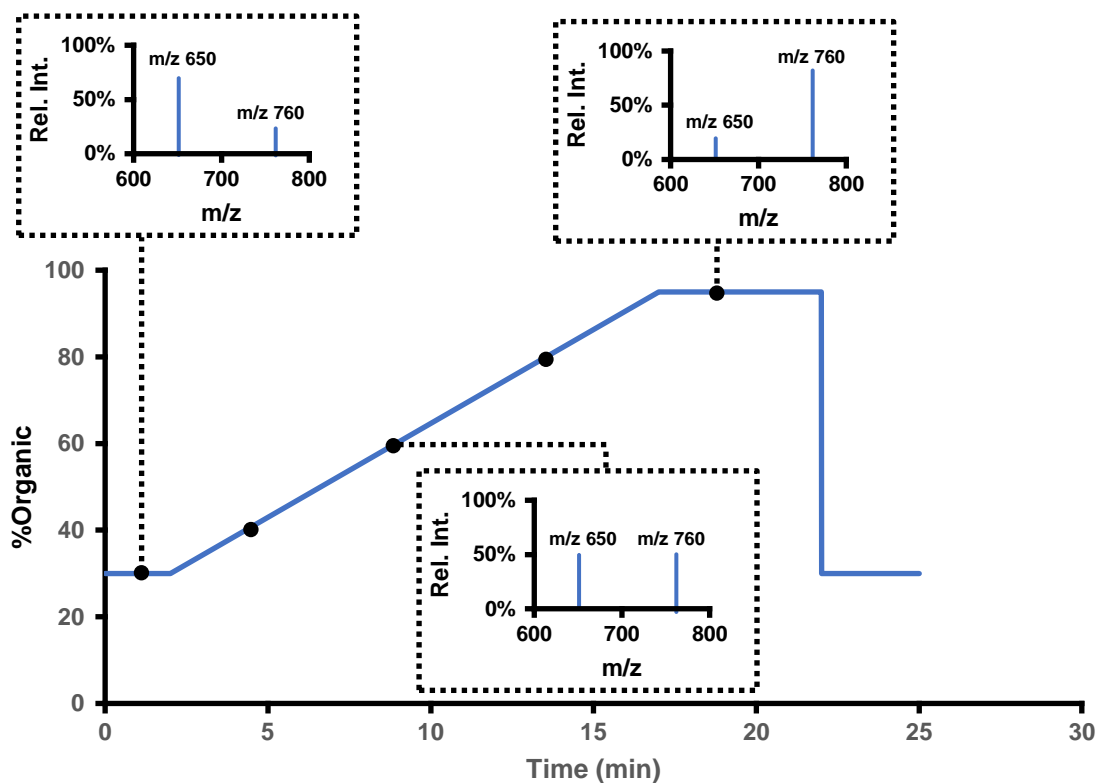
Figure 5.1 Suggested future experiment in which the conversion of a lipid standard (PC 16:0/18:1) is monitored at different solvent compositions along a potential LC gradient. The conversion efficiency is expected to decrease as the percentage of organic solvent increases. This experiment will be utilized to optimize a LC-Oz-IM-MS gradient.

expected that the reaction yield would likely diminish over the course of a reversed-phase LC gradient. Once an LC gradient that promotes sufficient conversion has been developed, the next step would be to perform the LC-Oz-IM-MS workflow on a mixture of lipid standards from a variety of classes, such as the SPLASH® mix or the Differential Ion Mobility System Suitability mix, both from Avanti Polar Lipids. This experiment would further indicate the relative conversion rates for different classes of lipid molecules and whether the current implementation of the device provides sufficient yields necessary for full coverage of the lipidome.

Some final considerations for future work on this project include removing the need to bypass the LC degasser manifold in the LC-Oz-IM-MS workflow, which impacts the reproducibility of the chromatographic separation. Because the solution-phase ozonolysis reaction relies on dissolved oxygen gas, all experiments up to this point have had the degasser bypassed; however, for adoption of the methodology into untargeted lipidomics workflows, this limitation needs to be addressed. An air-pressurized reaction chamber containing the original device and gas-permeable tubing could potentially be utilized to reintroduce dissolved gas to the solvent post-LC. However, it is not known at this time how such a set-up would impact the chromatographic separation, if at all. Finally, once the device has been fully optimized for integration with LC and performing these kinds of analyses becomes routine, informatics approaches will be necessary for automating the correlation of ozonolysis precursors and products based on retention times. Other groups that perform similar experiments have already developed software to perform these tasks that could be used as a guide.[16,17]

5.2.2 *Next Generation Ion Mobility Instrumentation for Improved Separation of Isomers*

Throughout this dissertation, the importance of combining the benefits of multiple analytical techniques for the characterization of complex samples, particularly those containing

isomers, has been emphasized. However, for some extremely similar molecular structures, such as enantiomers or diastereomers, the resolving power of ion mobility-mass spectrometry on current instrument platforms is not enough to separate them, and their fragmentation patterns are likewise identical.[8] In this case, the development of next-generation instrumentation is necessary for resolving increasingly structurally similar compounds. It has been suggested that resolving powers (R_p) of over 300 (CCS/ΔCCS) are necessary for separating compounds that differ in CCS by less than 5%, which is far greater than the resolving power of current commercial instruments, which have been observed to have resolving powers around ~40-60 (CCS/ΔCCS).[9,10,] However, prototype instruments such as the Waters Cyclic IMS and the MOBILion Structures for Lossless Ion Manipulation (SLIM)-based IM-MS instrument have recently been developed with resolving powers that exceed 300 (CCS/ΔCCS).[18-21] Both of these instruments utilize longer pathlengths to achieve greater separation capabilities and have been demonstrated to separate isomeric compounds indistinguishable on current-gen platforms.[20,21] SLIM technology, which was developed by Dr. Richard D. Smith at Pacific Northwest National Laboratory, is particularly intriguing due to its ease of fabrication and experimental flexibility.[22] In addition to its uses in mobility-based separations, SLIM ion trapping and storage regions have been designed, among other complex means of ion manipulation.[23,24] In theory, a SLIM ozonolysis reaction cell could potentially be developed, such that mobility separations could be performed both pre- and post-ozonolysis. In such a configuration, IM could be used to align ozonolysis precursors and products rather than LC, and the CCS of ozonolysis products could be measured and utilized in databases much like fragmentation spectra are now for improved lipid fingerprinting. Higher resolving power instrumentation would also be useful for the analysis of complex polymer samples. For example, it would be interesting to determine how the number of isomers and conformers in a polymer

sample scale with increasing molecular weight distribution with increasingly longer oligomer chain lengths. Molecular modeling experiments have suggested that large polymer structures exist as "beads on a string" in which long stretches of the molecule wrap around cations before extending length-ward again.[25] Separation via SLIM or Cyclic IMS could potentially delineate where these conformational changes occur in the molecule. Preliminary data from the MOBILion instrument indicates that even smaller polymer oligomers below 2000 Da potentially contain multiple conformers not observed on a current drift tube instrument (Figure 5.2), so analysis of much larger polymers could yield interesting results.

5.3   Concluding Remarks

As the field of ion-mobility mass spectrometry has matured over time, the ability to analyze increasingly complex samples has improved tremendously. Complex samples, whether biological in origin or the result of synthetic reactions, have necessitated the development of more sophisticated analytical strategies in order to fully characterize the structural heterogeneity. This dissertation work has focused in particular on the presence of isomerism in both lipid and polymer samples, the presence of which is particularly challenging due to the fact that mass spectrometry alone cannot discriminate between isomers. Several experimental approaches have been explored for distinguishing isomers in this work, but a unifying theme emerges that a combination of multiple structurally-selective analytical techniques are necessary for delineating all the forms of isomerism that may be present in a sample. The development of novel IM-MS instrumentation with improved resolving power will continue to increase the field's capacity for reducing isomerism, characterizing complex samples, and enable important discoveries in applications research.
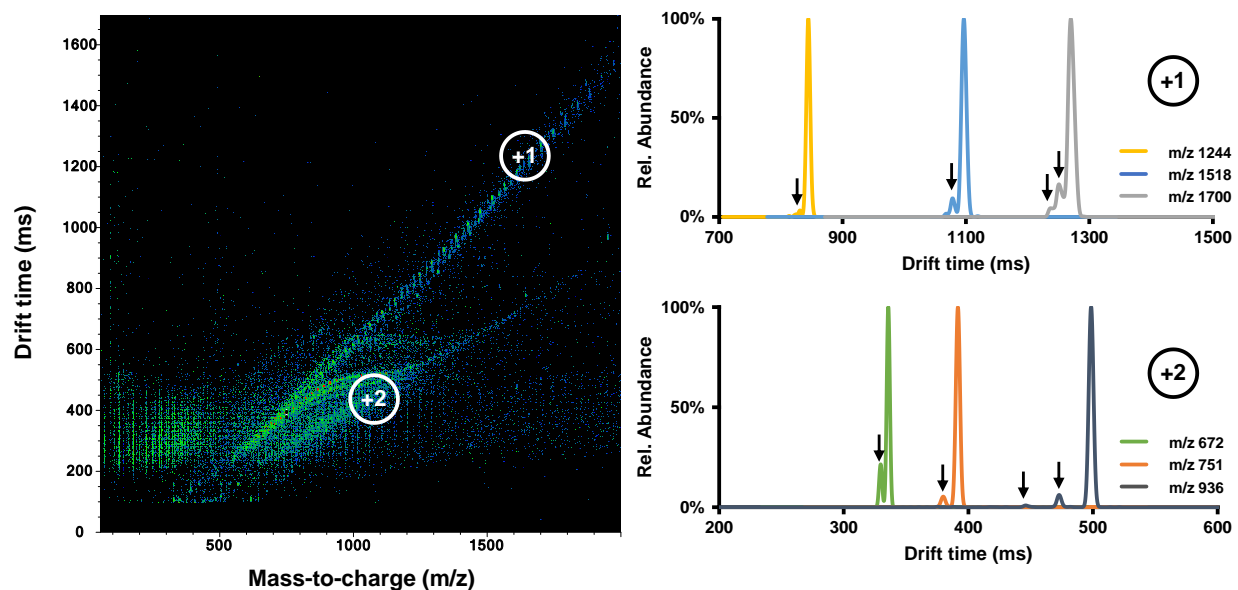
Figure 5.2 Preliminary data acquired on a prototype SLIM IM-MS instrument for a PEG sample with an average molecular weight of 1500. Two or more conformers are observed are observed in the arrival time distributions of the highlighted oligomers.

5.4   References

(1)   Brown, S. H. J.; Mitchell, T. W.; Blanksby, S. J. Analysis of Unsaturated Lipids by Ozone-Induced Dissociation. *Biochim. Biophys. Acta - Mol. Cell Biol. Lipids* **2011**, *1811* (11), 807–817.

(2)   Brown, S. H. J.; Mitchell, T. W.; Oakley, A. J.; Pham, H. T.; Blanksby, S. J. Time to Face the Fats: What Can Mass Spectrometry Reveal about the Structure of Lipids and Their Interactions with Proteins? *J. Am. Soc. Mass Spectrom.* **2012**, *23* (9), 1441–1449.

(3)   Gies, A. P.; Hercules, D. M. Collision Induced Dissociation Study of Ester-Based Polyurethane Fragmentation Reactions. *Anal. Chim. Acta* **2014**, *808*, 199–219.

(4)   Crescentini, T. M.; May, J. C.; McLean, J. A.; Hercules, D. M. Mass Spectrometry of Polyurethanes. *Polymer* **2019**, *181* (3), 121624.

(5)   May, J. C.; McLean, J. A. Ion Mobility-Mass Spectrometry: Time-Dispersive Instrumentation. *Anal. Chem.* **2015**, *87* (3), 1422–1436.

(6)   Groessl, M.; Graf, S.; Knochenmuss, R. High Resolution Ion Mobility-Mass Spectrometry for Separation and Identification of Isomeric Lipids. *Analyst* **2015**, *140* (20), 6904–6911.

(7)   Kyle, J. E.; Zhang, X.; Weitz, K. K.; Monroe, M. E.; Ibrahim, Y. M.; Moore, R. J.; Cha, J.; Sun, X.; Lovelace, E. S.; Wagoner, J.; et al. Uncovering Biologically Significant Lipid Isomers with Liquid Chromatography, Ion Mobility Spectrometry and Mass Spectrometry. *Analyst* **2016**, *141* (5), 1649–1659.

(8)   Dodds, J. N.; May, J. C.; McLean, J. A. Investigation of the Complete Suite of the Leucine and Isoleucine Isomers: Toward Prediction of Ion Mobility Separation Capabilities. *Anal. Chem.* **2017**, *89* (1), 952–959.

(9)   Dodds, J. N.; May, J. C.; McLean, J. A. Correlating Resolving Power, Resolution, and Collision Cross Section: Unifying Cross-Platform Assessment of Separation Efficiency in Ion Mobility Spectrometry. *Anal. Chem.* **2017**, *89* (22), 12176–12184.

(10)   Nichols, C. M.; Dodds, J. N.; Rose, B. S.; Picache, J. A.; Morris, C. B.; Codreanu, S. G.; May, J. C.; Sherrod, S. D.; McLean, J. A. Untargeted Molecular Discovery in Primary Metabolism: Collision Cross Section as a Molecular Descriptor in Ion Mobility-Mass Spectrometry. *Anal. Chem.* **2018**, *90* (24), 14484–14492.

(11)   Stinson, C. A.; Zhang, W.; Xia, Y. UV Lamp as a Facile Ozone Source for Structural Analysis of Unsaturated Lipids Via Electrospray Ionization-Mass Spectrometry. *J. Am. Soc. Mass Spectrom.* **2017**.

(12)   Wysocki, V. H.; Joyce, K. E.; Jones, C. M.; Beardsley, R. L. Surface-Induced Dissociation of Small Molecules, Peptides, and Non-Covalent Protein Complexes. *J. Am. Soc. Mass Spectrom.* **2008**, *19* (2), 190–208.

(13)   Zhou, M.; Wysocki, V. H. Surface Induced Dissociation: Dissecting Noncovalent Protein Complexes in the Gas Phase. *Acc. Chem. Res.* **2014**, *47*, 1010–1018.

(14)   Zhou, M.; Huang, C.; Wysocki, V. H. Surface-Induced Dissociation of Ion Mobility-Separated Noncovalent Complexes in a Quadrupole/Time-of-Flight Mass Spectrometer. *Anal. Chem.* **2012**, *84* (14), 6016–6023.

(15)   Stinson, C. A.; Xia, Y. Method of Coupling Paternò-Büchi Reaction with Direct Infusion ESI-MS/MS for Locating C=C Bond in Glycerophospholipids. *Analyst* **2016**, *141*, 3696–3704.

(16)   Batarseh, A. M.; Abbott, S. K.; Duchoslav, E.; Alqarni, A.; Blanksby, S. J.; Mitchell, T. W. Discrimination of Isobaric and Isomeric Lipids in Complex Mixtures by Combining Ultra-High Pressure Liquid Chromatography with Collision and Ozone-Induced Dissociation. *Int. J. Mass Spectrom.* **2018**, *431*, 27–36.

(17)   Zhang, W.; Zhang, D.; Chen, Q.; Wu, J.; Ouyang, Z.; Xia, Y. Online Photochemical Derivatization Enables Comprehensive Mass Spectrometric Analysis of Unsaturated Phospholipid Isomers. *Nat. Commun.* **2019**, *10* (1), 1–9.

(18)   Ibrahim, Y. M.; Hamid, A. M.; Deng, L.; Garimella, S. V. B.; Webb, I. K.; Baker, E. S.; Smith, R. D. New Frontiers for Mass Spectrometry Based upon Structures for Lossless Ion Manipulations. *Analyst* **2017**, *142* (7), 1010–1021.

(19)   Deng, L.; Webb, I. K.; Garimella, S. V. B.; Hamid, A. M.; Zheng, X.; Norheim, R. V.; Prost, S. A.; Anderson, G. A.; Sandoval, J. A.; Baker, E. S.; et al. Serpentine Ultralong Path with Extended Routing (SUPER) High Resolution Traveling Wave Ion Mobility-MS Using Structures for Lossless Ion Manipulations. *Anal. Chem.* **2017**, *89* (8), 4628–4634.

(20)   May, J. C.; Leaptrot, K. L.; Rose, B. S.; Wormwood-Moser, K. L.; Deng, L.; Maxon, L.; DeBord, D.; McLean, J. A. Resolving Power and Collision Cross Section Measurement Accuracy of a Prototype High Resolution Ion Mobility Platform Incorporating Structures for Lossless Ion Manipulation. *In preparation*, **2021**.

(21)   Giles, K.; Ujma, J.; Wildgoose, J.; Pringle, S.; Richardson, K.; Langridge, D.; Green, M. A Cyclic Ion Mobility-Mass Spectrometry System. *Anal. Chem.* **2019**, *91* (13), 8564–8573.

(22)   Garimella, S. V. B.; Ibrahim, Y. M.; Webb, I. K.; Tolmachev, A. V.; Zhang, X.; Prost, S. a.; Anderson, G. a.; Smith, R. D. Simulation of Electric Potentials and Ion Motion in Planar Electrode Structures for Lossless Ion Manipulations (SLIM). *J. Am. Soc. Mass Spectrom.* **2014**, *25* (11), 1890–1896.

(23)   Zhang, X.; Garimella, S. V. B.; Prost, S. A.; Webb, I. K.; Chen, T.-C.; Tang, K.; Tolmachev, A. V.; Norheim, R. V.; Baker, E. S.; Anderson, G. a.; et al. Ion Trapping,

Storage, and Ejection in Structures for Lossless Ion Manipulations. *Anal. Chem.* **2015**, *87* (12), 6010–6016.

(24)   Webb, I. K.; Garimella, S. V. B.; Norheim, R. V.; Baker, E. S.; Ibrahim, Y. M.; Smith, R. D. A Structures for Lossless Ion Manipulations (SLIM) Module for Collision Induced Dissociation. *J. Am. Soc. Mass Spectrom.* **2016**, *27* (7), 1285–1288.

(25)   Larriba, C.; Fernandez De La Mora, J. The Gas Phase Structure of Coulombically Stretched Polyethylene Glycol Ions. *J. Phys. Chem. B* **2012**, *116* (1), 593–598.

APPENDIX A

REFERENCE OF ADAPTION FOR CHAPTERS

Chapter 1. **Rachel A. Harris**, Katrina L. Leaptrot, Jody C. May, John A. McLean, "New Frontiers in Lipidomics Analyses Using Structurally Selective Ion Mobility-Mass Spectrometry," *Trends in Anaytical Chemistry*, **2019**, *116*, 316–323.

Chapter 2. **Rachel A. Harris,** Jody C. May, Craig A. Stinson, Yu Xia, John A. McLean, "Determining Double Bond Position in Lipids Using Online Ozonolysis Coupled to Liquid Chromatography and Ion Mobility-Mass Spectrometry," *Analytical Chemistry*, **2018**, *90* (3), 1915–1924.

Chapter 3. **Rachel A. Harris,** Jody C. May, Sophie R. Harvey, Vicki H. Wysocki, John A. McLean, "Evaluation of Surface Induced Dissociation in Conjunction with Ion Mobility-Mass Spectrometry for Lipid Structural Characterization," In Preparation for *Analytical Chemistry*, **2021**.

Chapter 4. **Rachel A. Harris**[*], Jaqueline A. Picache[*], Ian D. Tomlinson, Emanuel Zlibut, Berkley M. Ellis, Jody C. May, John A. Mclean, David M. Hercules, "Mass Spectrometry and Ion Mobility Study of Poly(Ethylene Glycol)-based Polyurethane Oligomers," *Rapid Communications in Mass Spectrometry,* **2020**, *No. e8662*, 1–8. (*Co -first authors)

SUPPLEMENTARY MATERIALS FOR CHAPTER 2

B.1   Supplemental Materials for Determining Double Bond Position in Lipids
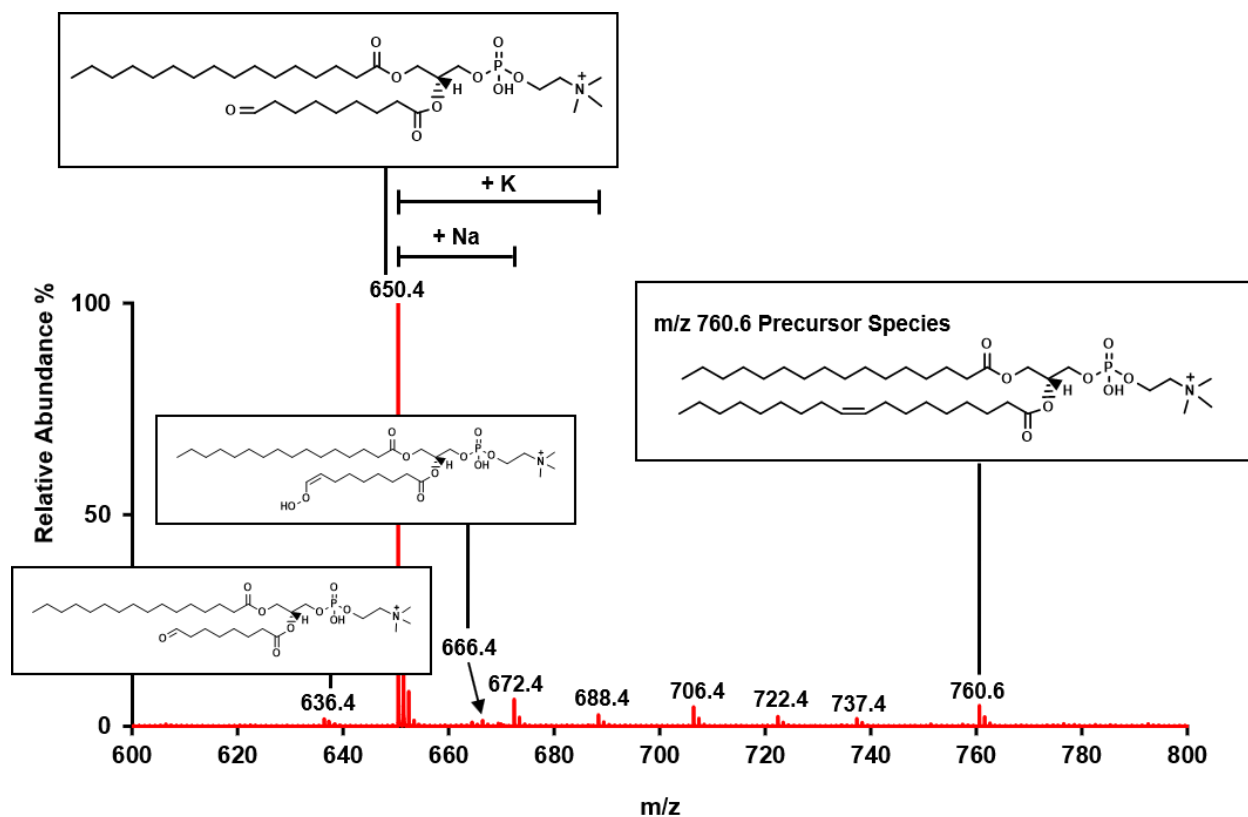
B.1.1   Supplemental Figures

Figure B.1 An expanded version of the PC 16:0/18:1 spectrum following irradiation with the ozonolysis device at 10 µL/min. Observed ions are labeled with their corresponding mass-to-charge, and structures are proposed for several species based on the exact mass measurement (<10 ppm). It should be noted that the ion at *m/z* 737.4 is not likely an ozonolysis product due to its odd-numbered mass and the fact that it does not appear on the same mobility trend line as the other ozonolysis product ions. The diagnostic aldehyde product ion (*m/z* 650.4) indicative of double bond cleavage at the 9th carbon atom in one of the alkyl chains of the precursor (*m/z* 760.6) is the dominant species in the spectrum. Product ions corresponding to sodiated and potassiated forms of the aldehyde product are also observed at *m/z* 672.4 and *m/z* 688.4, respectively. Additionally, the product ion at *m/z* 666.4 is likely a vinyl hydroperoxide or the corresponding carboxylic acid, resulting from rearrangement of the Criegee intermediate.[1,2] Further oxidation of this species at *m/z* 666.4 is thought to result in the formation of the species at *m/z* 636.4 by loss of formaldehyde.[3] Finally, the presence of the ion at *m/z* 706.4 can likely be attributed to solvent adduction of acetonitrile to one of the Criegee ions at *m/z* 666.4. Solvent adduction has previously been reported for solution phase ozonolysis, especially when methanol is used as a solvent.[4]
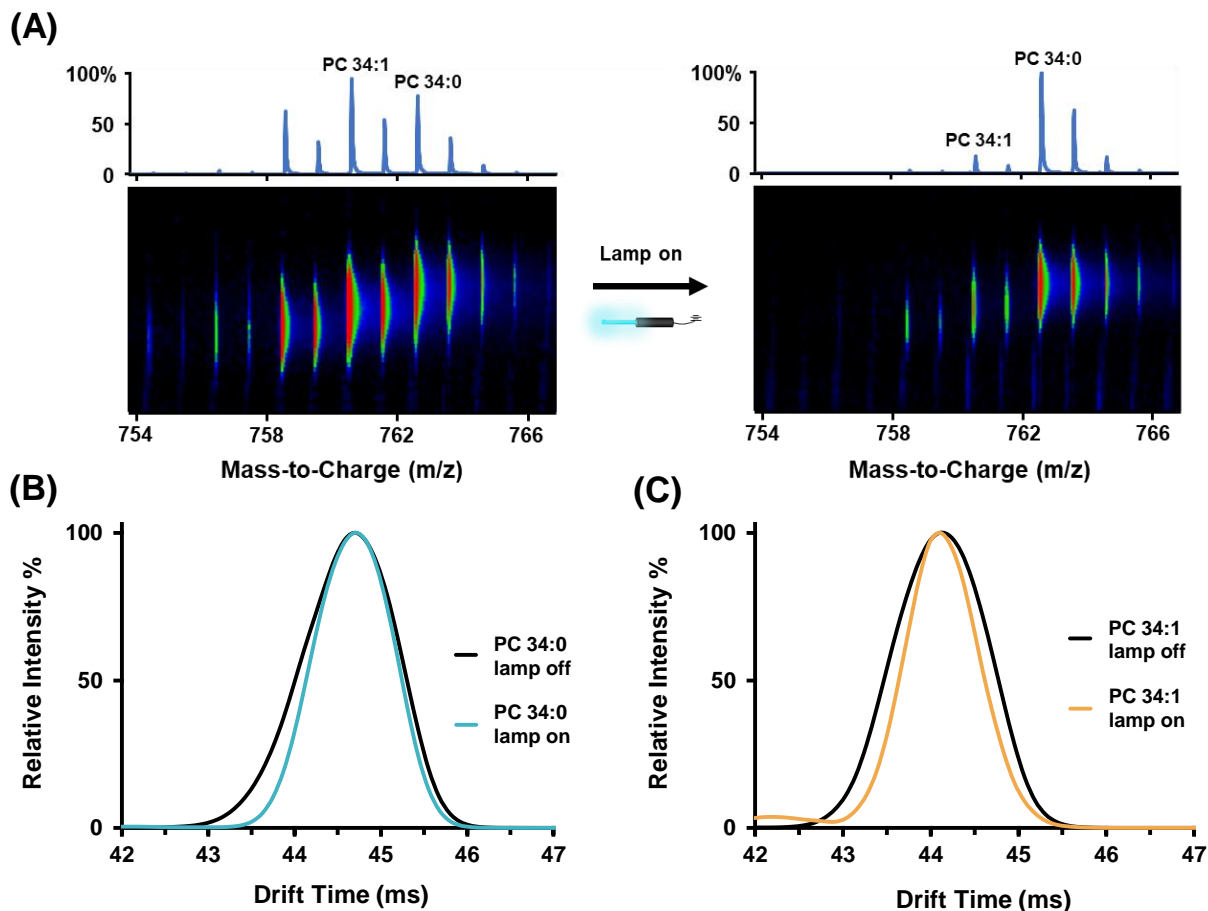
Figure B.2 Comparison of drift time profiles for two lipid species from a PC lipid extract with the ozonolysis device off (black) and on (teal **(B)** or mustard **(C)**). Because lipid species differing in mass by the addition of one double bond to an alkyl chain are spaced 2 Da apart in mass and < 1 ms apart in drift time, the second isotope peak of one species often overlaps with the primary peak of the species containing one fewer double bond **(A)**. As discussed in the primary text, the overlapping of these isotopic envelopes can result in broadened drift profiles and shifts in a given drift profile's measured centroid, both of which can lead to errors in a species' calculated CCS. In the figure above, comparison of two PC lipids with the ozonolysis device turned off and then on reveals the extent of drift profile broadening due to isotopic overlap. Once the lamp is turned on, lipid species containing double bonds are significantly diminished through reaction with ozone so that isotopic overlap is reduced **(A)**. For PC 34:0, the resolving power of the drift peak increased from 35.6 with the lamp off to 41.5 with the lamp on, and PC 34:1 saw a similar increase from a drift peak resolving power of 34.8 to 44.5. Note, however, that neither centroid of the two species were observed to significantly shift upon isotopic subtraction. Nonetheless, the ozonolysis device could aid in direct measurement of the accurate drift profiles of closely related lipid species without need for mathematical corrections due to isotopic overlap, illustrating another potential advantage of this technique.
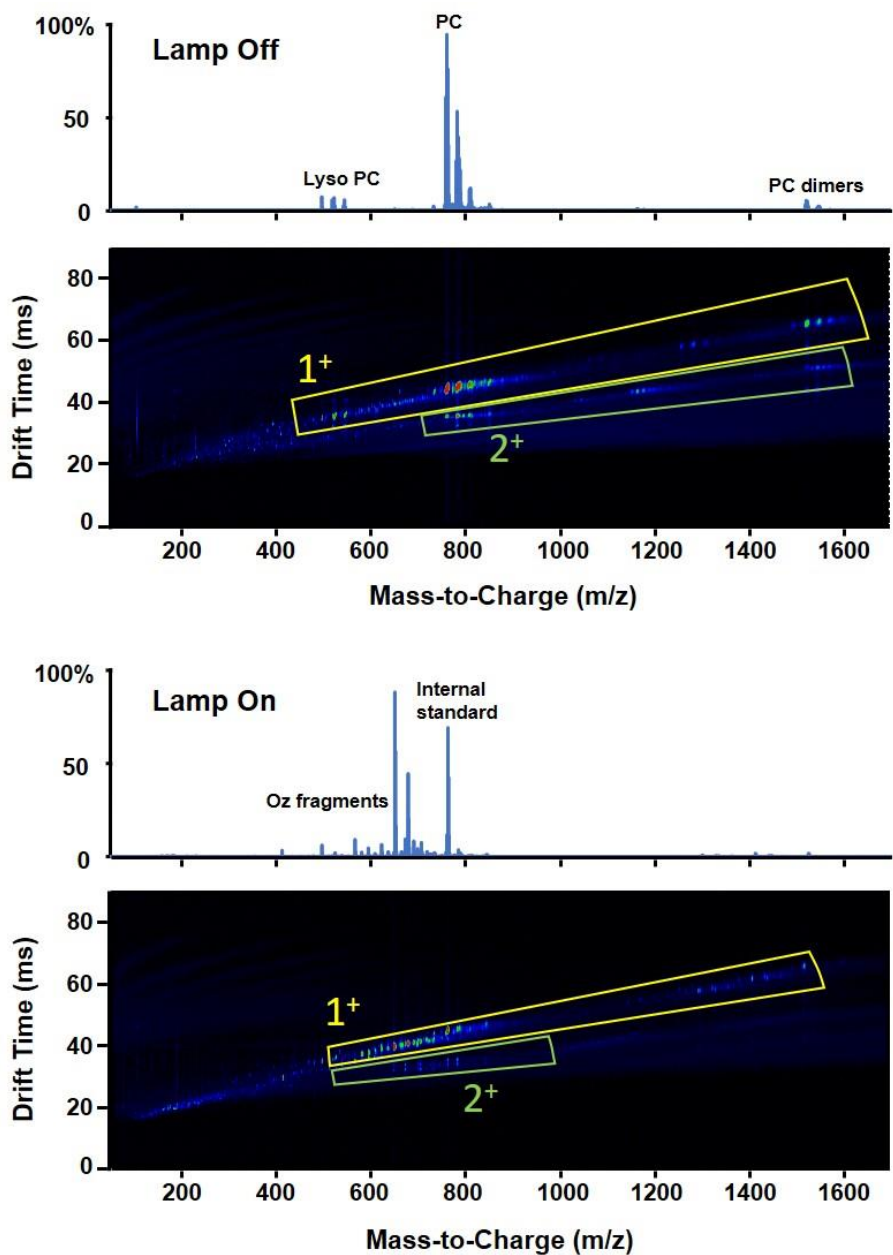
118

Figure B.3 Full IM-MS spectra of the PC lipid extract with the ozonolysis device off (top) and on (bottom). In both spectra, 1+ and 2+ trendline regions are highlighted and relevant features are labeled on the accompanying mass spectra. This work focused solely on the 1+ lipid species. Prior to onset of ozonolysis three main lipid-rich regions of mass-mobility space are observed. These features correspond to lyso PC species (ca. m/z 450 - 600) containing only a single fatty acid tail esterified to the glycerol backbone, PC species containing two fatty acid tails esterified to the glycerol backbone (ca. m/z 700-850), and singly charged dimer species formed from the association of two PC monomers (ca. m/z 1450-1600). Following ozonolysis in the device, any species containing a double bond is significantly depleted such that the lipid-rich regions previously observed are no longer detected, and ozonolysis product ions are observed in the region of m/z 400-750. It can be noted that several species were not observed to deplete upon ozonolysis, most notably m/z 762.6, which corresponds to the fully saturated PC 16:0/18:0 lipid standard that was spiked in as an internal standard, and the 1+ dimer of PC 16:0/18:0 at m/z 1524.2. An additional fully saturated lipid species at m/z 496.3 corresponding to PC 16:0 endogenous to the sample was also detected and not found to diminish in signal upon ozonolysis.
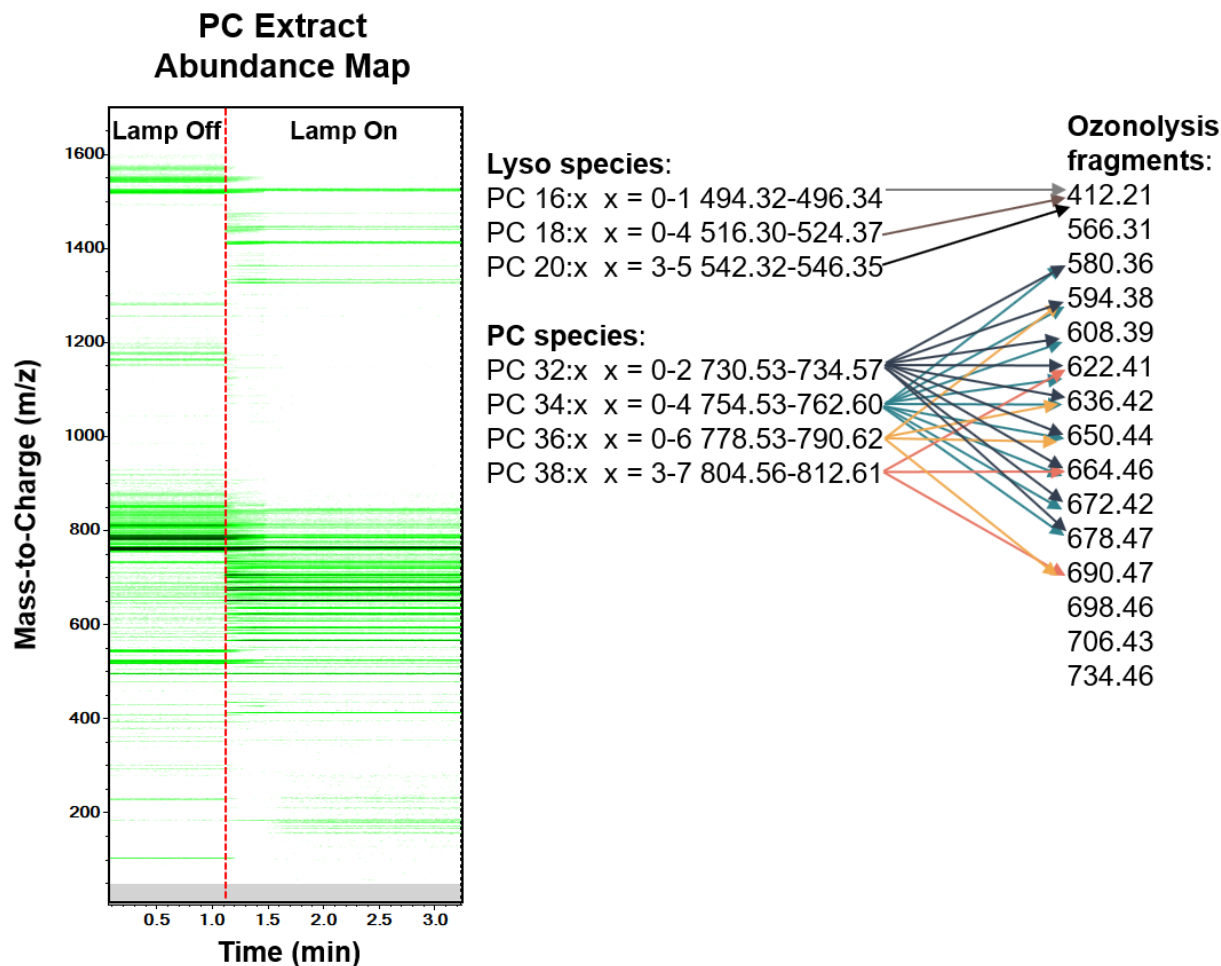
PC Extract Abundance Map

Lamp Off | Lamp On

Mass-to-Charge (m/z)

Time (min)

Lyso species:
PC 16:x x = 0-1 494.32-496.34
PC 18:x x = 0-4 516.30-524.37
PC 20:x x = 3-5 542.32-546.35

PC species:
PC 32:x x = 0-2 730.53-734.57
PC 34:x x = 0-4 754.53-762.60
PC 36:x x = 0-6 778.53-790.62
PC 38:x x = 3-7 804.56-812.61

Ozonolysis fragments:
412.21
566.31
580.36
594.38
608.39
622.41
636.42
650.44
664.46
672.42
678.47
690.47
698.46
706.43
734.46

Figure B.4 The abundance map shown above is another way of visualizing the PC lipid extract data in **Figure B.3**. The intensities for all mass-to-charge signals are plotted as a function of time, clearly delineating how the observed peaks in the spectrum change as a result of ozonolysis. However, as explained in the text, because the ozonolysis reaction occurs prior to source ionization, there is no way to directly correlate observed ozonolysis product ions with their precursors. Possible ozonolysis products were predicted for several lipid species observed in the sample based upon possible precursor structures generated using LIPID MAPS. It was observed that the detected ozonolysis product ions could have been generated by multiple precursors, and that depending on the precursor structure analyzed, multiple possible ozonolysis product ions could also be generated. Thus, the deconvolution the origins of ozonolysis product ions in complex samples is very challenging. However, it was noted that the majority of product ions detected contained no sites of unsaturation in their fatty acid alkyl chains which could indicate that the reaction proceeded to completion even for species containing multiple sites of unsaturation. The peak at *m/z* 690.47 was one of the few exceptions observed, which is thought to contain one unsaturation in its fatty acid chains. This result stands in contrast to those of the fatty acid containing six double bonds that was analyzed (Figure 4 in the text), in which the preferred ozonolysis product occurred as a result of cleavage at the last double bond on the fatty acid tail, which left five unsaturations remaining on the acyl chain. The source of this discrepancy, namely that ozonolysis of a fatty acid standard produced multiply unsaturated product ions while a PC extract produced mainly fully saturated product ions, is unclear at this time. One possible explanation is that the lipid extract predominantly contained lipids with only a single unsaturation in their acyl chains, resulting in the majority of fully saturated ozonolysis product ions. Separation of lipid precursors via chromatography, as suggested in the text, could help to answer this question by correlating lipid precursors directly to their ozonolysis products.
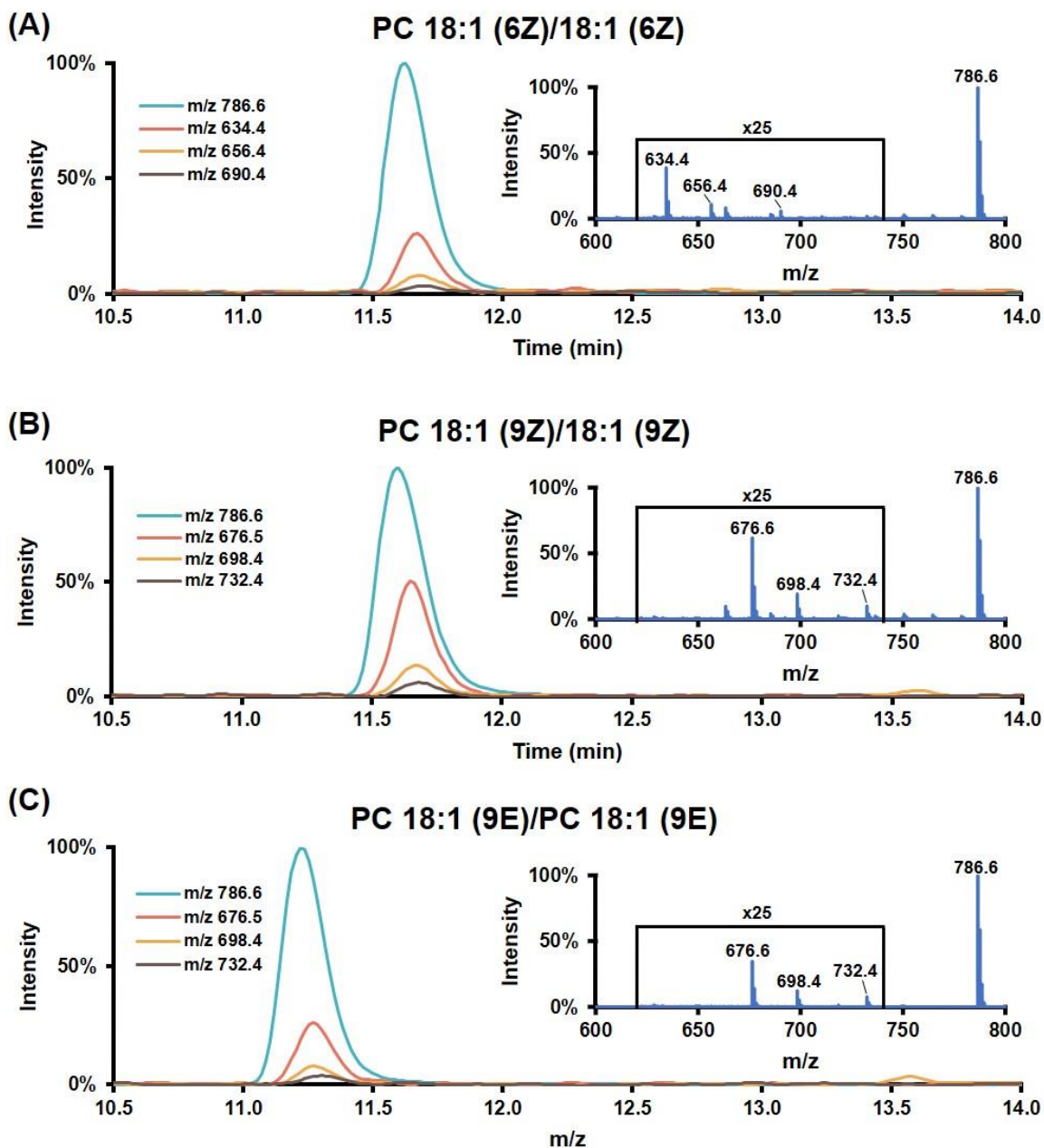
Figure B.5 Comparison of extracted ion chromatograms (EICs) for three PC standards ran separately using the LC-Oz-IM-MS technique, with the ozonolysis device turned on. Analysis of the retention time of the precursor at *m/z* 786 reveals that the *trans* species would elute first in a mixture with a retention time of about 11.24 min, while the two *cis* double bond position isomers would likely elute together with a retention time of about 11.63 min. This elution order is in agreement with the data presented in Figure 6 of the manuscript, in which the three species were combined and run as a mixture. Background subtracted mass spectra taken from each of the peaks give ozonolysis fragments consistent with cleavage at the 9th carbon atom along the acyl chain for both **(B)** and **(C)**, and fragments consistent with cleavage at the 6th carbon atom in the acyl chain for **(A).** The types ozonolysis fragments detected are similar to those observed in **Figure B.1**, and include the diagnostic aldehyde species, a sodiated form of the aldehyde species, and an acetonitrile solvent adducted species like that seen in **Figure B.1** located at a mass approximately 40 Da above the predicted mass of the Criegee ion (*m/z* 692.5).

B.1.2   References

(1)   Santrock, J.; Gorski, R. A; O'Gara, J. F. Products and Mechanism of the Reaction of Ozone with Phospholipids in Unilamellar Phospholipid Vesicles. *Chem. Res. Toxicol*. **1992**, *5* (1), 134–141.

(2)   Brown, S. H. J.; Mitchell, T. W.; Blanksby, S. J. Analysis of Unsaturated Lipids by Ozone-Induced Dissociation. *Biochim. Biophys. Acta - Mol. Cell Biol. Lipids* **2011**, *1811* (11), 807–817.

(3)   Vu, N.; Brown, J.; Giles, K.; Zhang, Q. Ozone-Induced Dissociation on a Traveling Wave High-Resolution Mass Spectrometer for Determination of Double-Bond Position in Lipids. *Rapid Commun. Mass Spectrom.* **2017**, *31* (17), 1415–1423.

(4)   Thomas, M. C.; Mitchell, T. W.; Harman, D. G.; Deeley, J. M.; Murphy, R. C.; Blanksby, S. J. Elucidation of Double Bond Position in Unsaturated Lipids by Ozone Electrospray Ionization Mass Spectrometry. *Anal. Chem.* **2007**, *79* (13), 5013–5022.

APPENDIX C

SUPPLEMENTARY MATERIALS FOR CHAPTER 3

C.1 Supplemental Materials for Evaluation of Surface Induced Dissociation

C.1.1 Example SID Tune Settings for the PC 16:0/18:1 lipid in IMTOF mode

Table C.1 Source settings for PC 16:0/18:1

Capillary (kV)	2.5
Source Temperature (°C)	100
Sampling Cone (V)	40
Extraction Cone (V)	5
Desolvation Temperature (°C)	250
Cone Gas Flow (L/Hr)	0
Desolvation Gas Flow (L/Hr)	700

Table C.2 Gas control settings for PC 16:0/18:1

Source Gas Flow (mL/min)	0
Trap Gas Flow (mL/min)	0.4
Helium Cell Gas Flow (mL/min)	200
IMS Gas Flow (mL/min)	60

Table C.3 DC voltage instrument settings for PC 16:0/18:1

Trap DC		IMS DC		Transfer DC	
Entrance	2.0	IMS Entrance	10.0	Entrance	2.0
Bias	45.0*	Helium Cell DC	35.0	Exit	20.0
Trap DC	-2.0	Helium Exit	-10.0		
Exit	2.0	IMS Exit	0.0		

* Note that the Trap DC Bias is raised to 85.0 V when performing SID 30 V

Table C.4 SID device Tempus settings for PC 16:0/18:1 in "Flythrough mode"

Optics Master	0.0
Exit 2	-46.0
Exit 1	-42.0

Front Top Deflector	-41.0
Front Bottom Deflector	-44.0
Middle Bottom Deflector	-60.0
Surface	-52.0
Rear Top Deflector	-45.0
Rear Bottom Deflector	-47.0
Entrance 2	-50.0
Entrance 1	-46.0

Table C.5 SID device Tempus settings for PC 16:0/18:1 in "Collision mode" at SID 30 V

Optics Master	0.0
Exit 2	-44.0
Exit 1	-65.0
Front Top Deflector	-75.0
Front Bottom Deflector	-14.0
Middle Bottom Deflector	-56.0
Surface	-30.0
Rear Top Deflector	-134.0
Rear Bottom Deflector	-39.0
Entrance 2	-19.0
Entrance 1	-12.0

(A)

SID energy (V) = Trap exit (V) – Surface (V)

Injection energy(V) = Surface (V) – He DC (V)
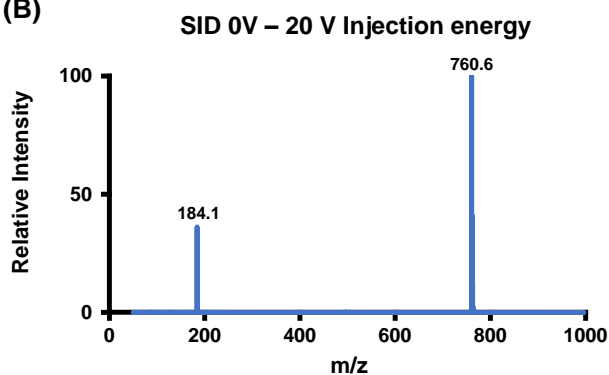
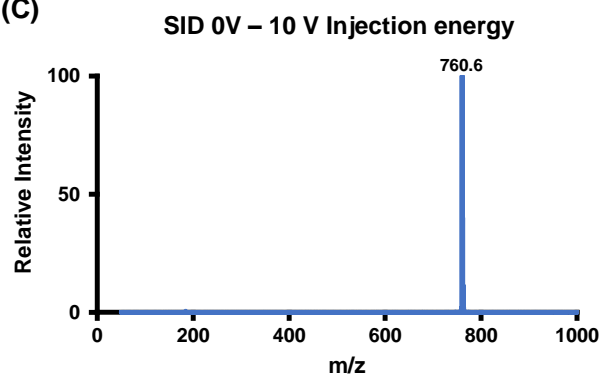**(B)**   **(C)**

Figure C.1 (A) Equations used to determine the energy imparted to analyte ions in collision with the surface and subsequent transmission from the SID cell into the rest of the instrument. Comparison of the fragmentation spectra of the lipid PC 16:0/18:1 with injection energies of 20 V **(B)** and 10 V **(C)** but equivalent SID fragmentation energies. It was observed that lowering the injection energy from 20 V to 10 V eliminated the occurrence of CID fragmentation between the exit lenses of the SID device and the entrance of the Helium Cell. After optimization of the injection energy, the primary fragment ion of PC 16:0/18:1 (m/z 184.1) was reduced to less than 0.25% of the abundance of the precursor (m/z 760.6).
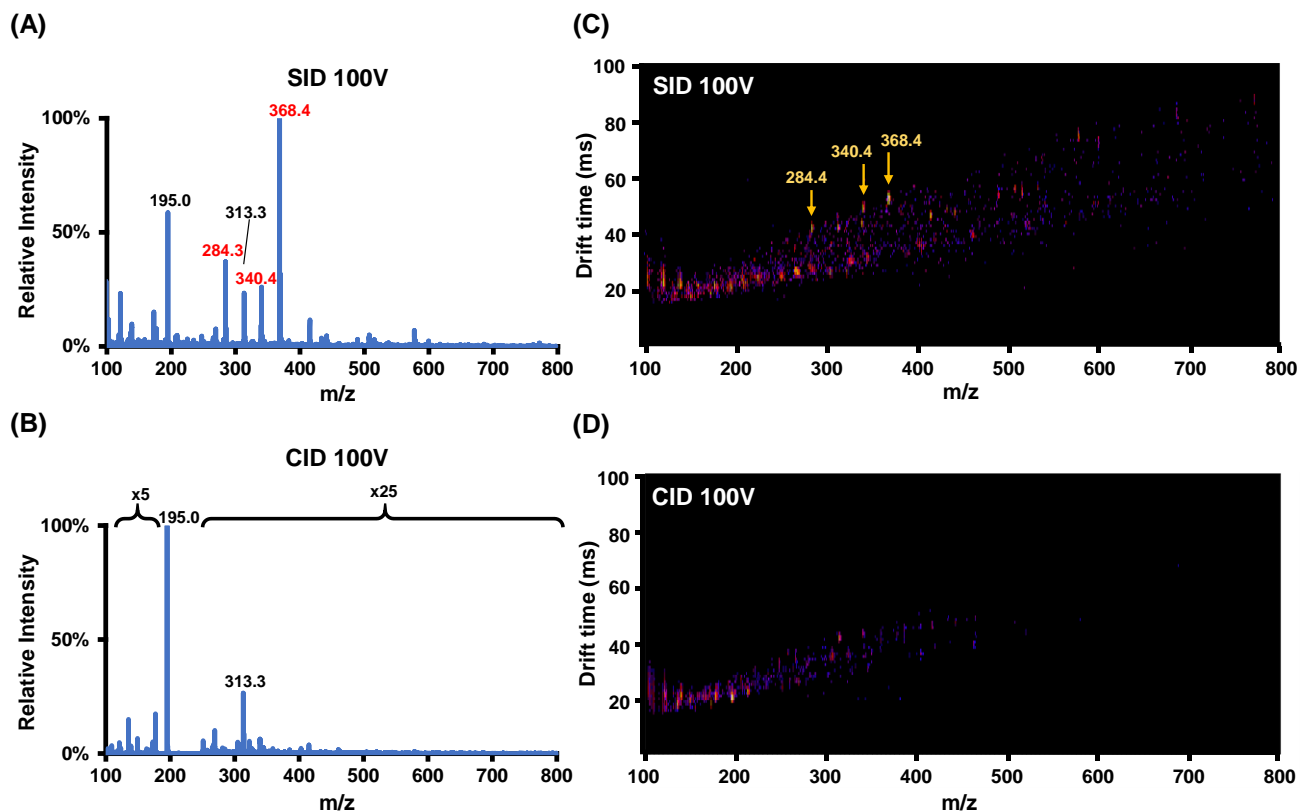
Figure C.2 Comparison of the SID **(A)** and CID **(B)** fragmentation spectra of the lipid PG 16:0/18:1 at a lab frame energy of 100 V. At high collision energies (> 70 V), unique fragment ions (m/z 284.3, m/z 340.4, and m/z 368.4) were observed in SID product ion spectra that were not detected in CID product ion spectra. The unique fragment ions were similarly observed in IM-MS SID fragmentation spectra **(C)** but were not present in IM-MS CID fragmentation spectra **(D)**.

(A) IM-MS analysis
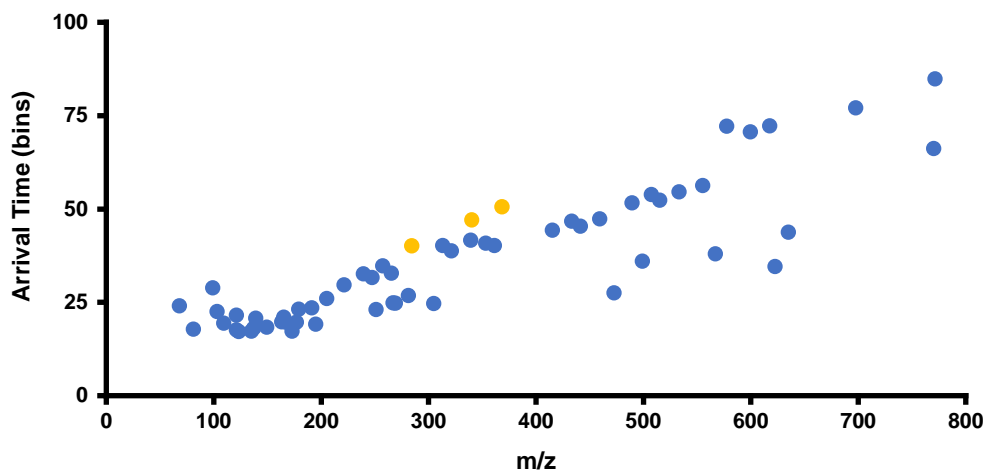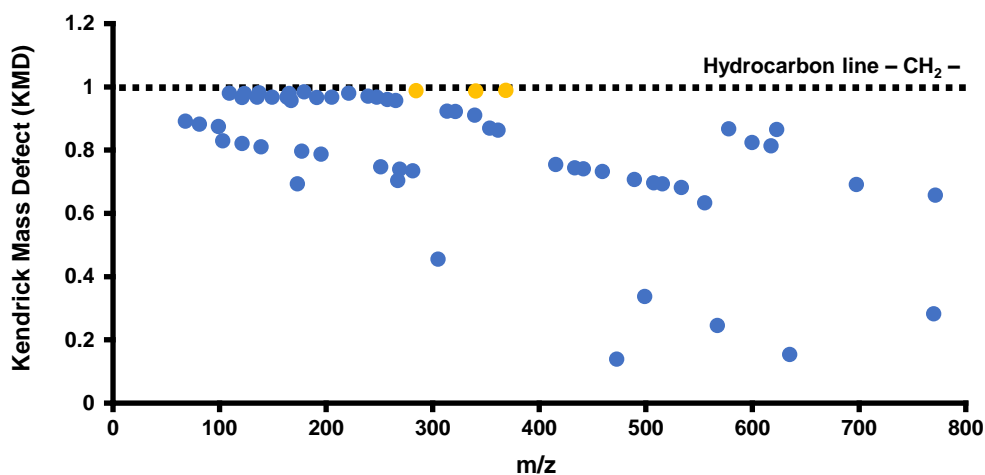

(B) Kendrick mass defect analysis

Figure C.3 (A) The arrival time of detected SID product ions of PG 16:0/18:1 across all collision energies measured is plotted as a function of mass-to-charge. The unique ions observed as a result of SID fragmentation of PG 16:0/18:1 at high collision energies (**Figure S2**), which are depicted with yellow markers, appear to group in a region of mobility-mass space close to known product ions of the precursor. **(B)** Plotting the same fragment ions in terms of their Kendrick mass defect reveals that the unique ions are isolated from other product ion trendlines and thus are not likely to result from SID fragmentation of the precursor. The mass defect of these unique ions (0.987, 0.987, and 0.988) further suggests that these ions are potentially hydrocarbon interferents released from the surface at high SID collision energies.
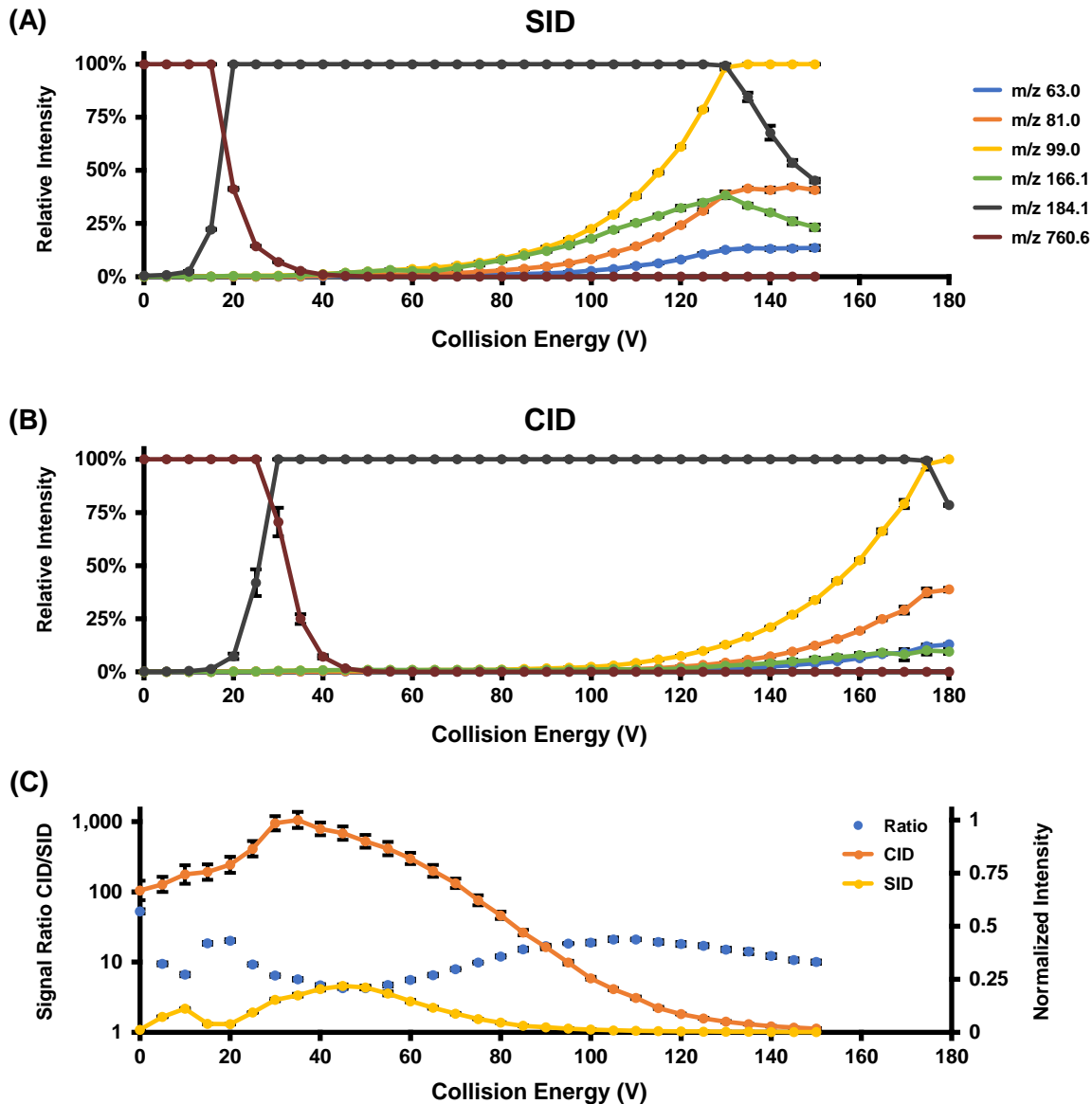
Figure C.4 (A) Relative ion intensity of SID precursor and predominant fragment ions as a function of collision energy for PC 16:0/18:1. **(B)** Relative ion intensity of CID precursor and predominant fragment ions as a function of collision energy for the same precursor ion as **(A)**. **(C)** Comparison of the normalized total ion intensity for CID and SID of PC 16:0/18:1 as a function of collision energy, plotted alongside the ratio of the two normalized signals. In contrast to **Figure 5** as shown in the main text, **(B)** depicts the full range of CID collision energies surveyed for the analyte molecule (0-180 V) which highlights that the fragmentation pathway leading to the formation of m/z 166.1 is increased in SID relative to CID.

Figure C.5 (A) Relative ion intensity of SID precursor and predominant fragment ions as a function of collision energy for PE 16:0/18:1. **(B)** Relative ion intensity of CID precursor and predominant fragment ions as a function of collision energy for the same precursor ion as **(A)**. **(C)** Comparison of the normalized total ion intensity for CID and SID of PE 16:0/18:1 as a function of collision energy, plotted alongside the ratio of the two normalized signals.

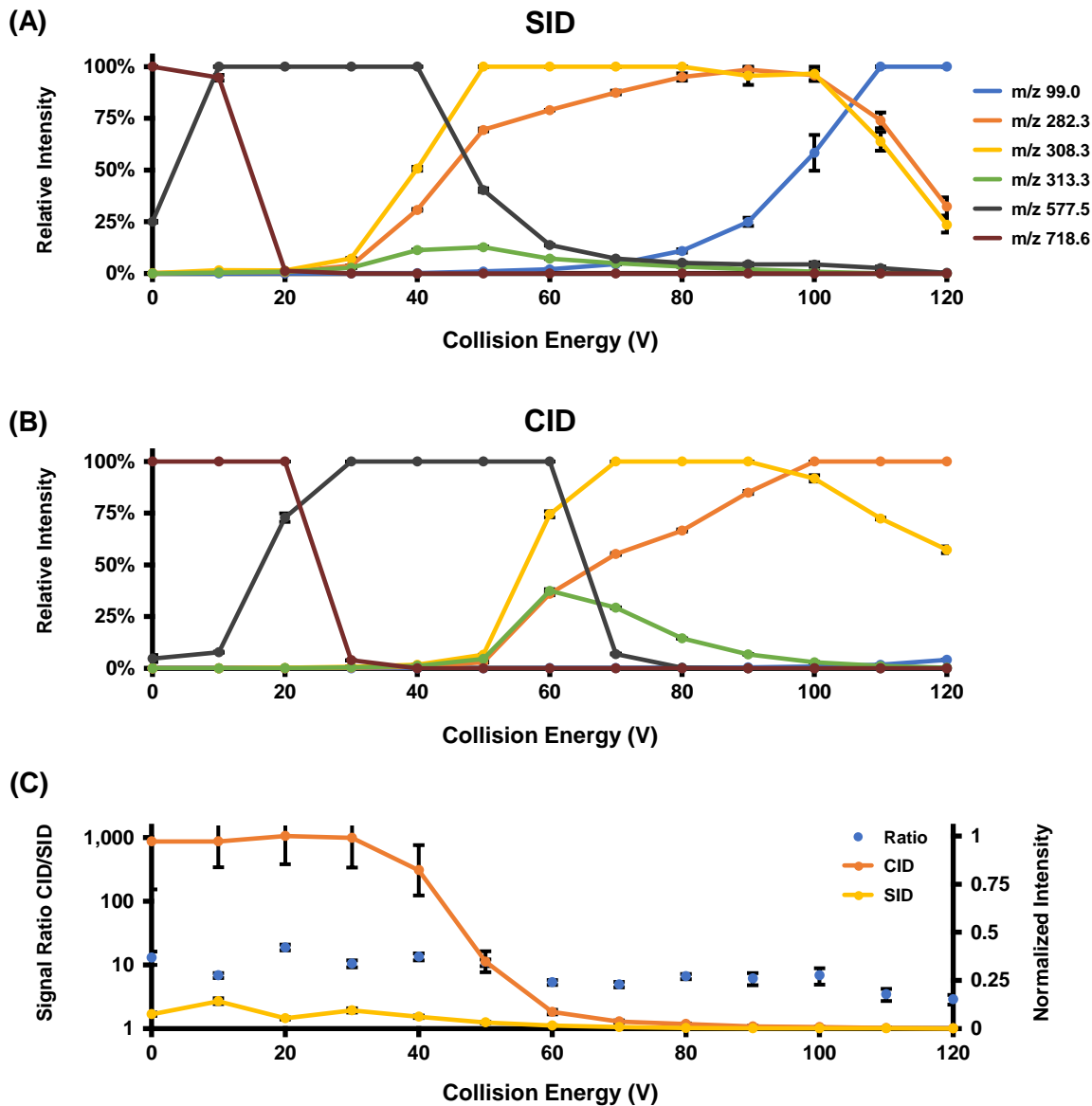**Figure C.6** (**A**) Relative ion intensity of SID precursor and predominant fragment ions as a function of collision energy for PS 16:0/18:1. (**B**) Relative ion intensity of CID precursor and predominant fragment ions as a function of collision energy for the same precursor ion as (**A**). (**C**) Comparison of the normalized total ion intensity for CID and SID of PS 16:0/18:1 as a function of collision energy, plotted alongside the ratio of the two normalized signals

Figure C.7 (A) Relative ion intensity of SID precursor and predominant fragment ions as a function of collision energy for PG 16:0/18:1. **(B)** Relative ion intensity of CID precursor and predominant fragment ions as a function of collision energy for the same precursor ion as **(A)**. **(C)** Comparison of the normalized total ion intensity for CID and SID of PG 16:0/18:1 as a function of collision energy, plotted alongside the ratio of the two normalized signals.
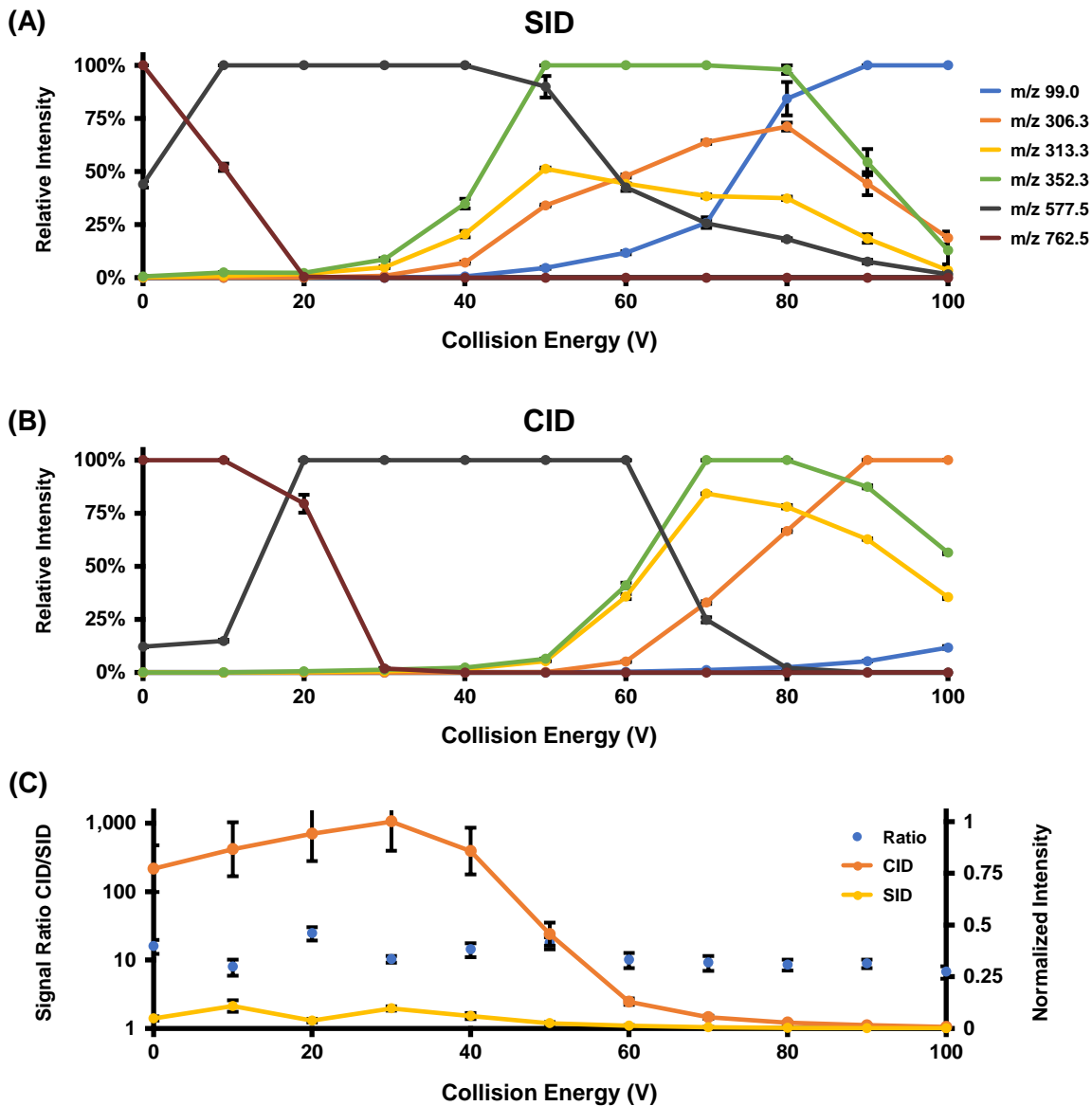
Figure C.8 (A) Relative ion intensity of SID precursor and predominant fragment ions as a function of collision energy for FA 18:1. **(B)** Relative ion intensity of CID precursor and predominant fragment ions as a function of collision energy for the same precursor ion as **(A)**. **(C)** Comparison of the normalized total ion intensity for CID and SID of FA 18:1 as a function of collision energy, plotted alongside the ratio of the two normalized signals.
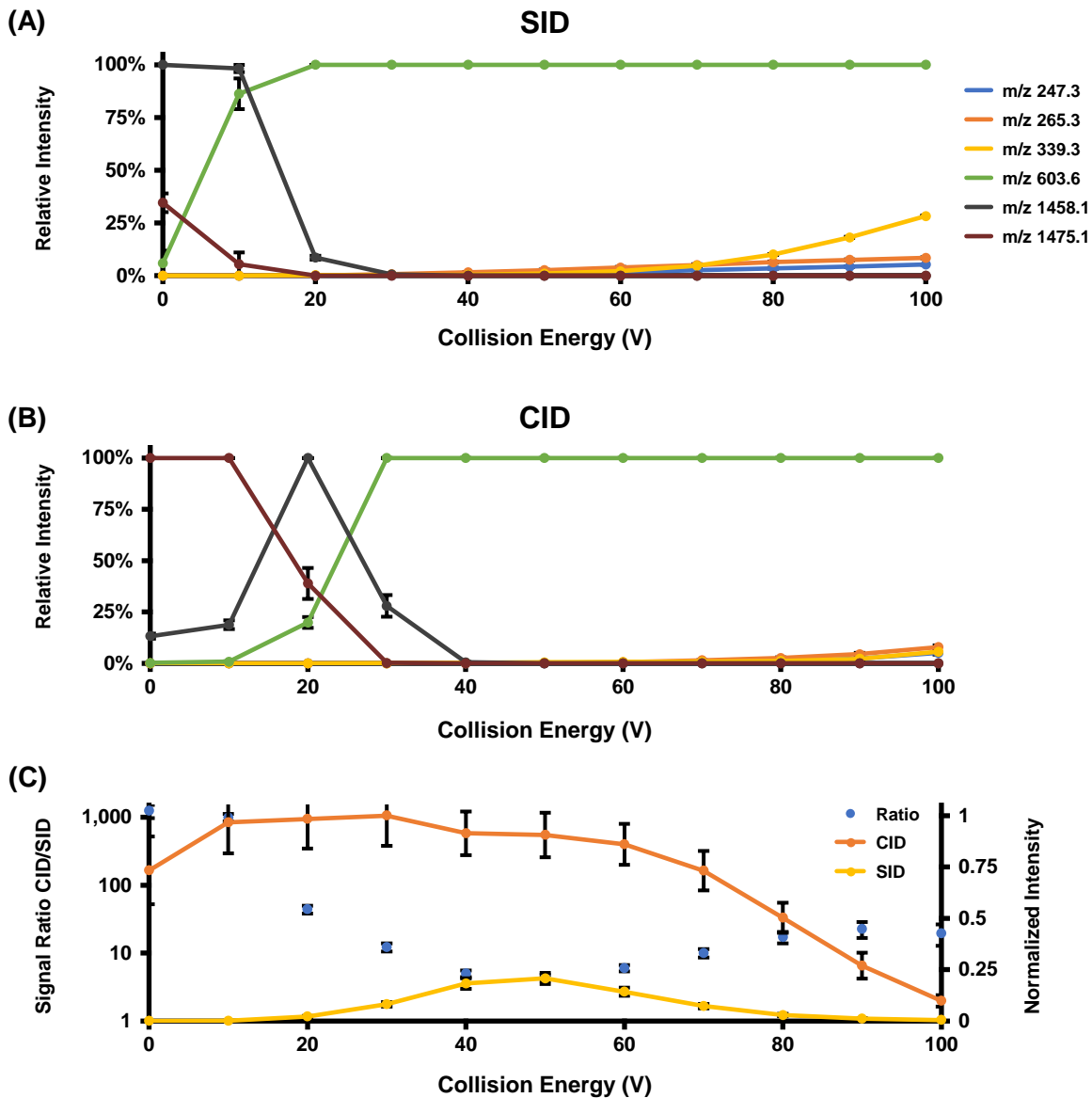
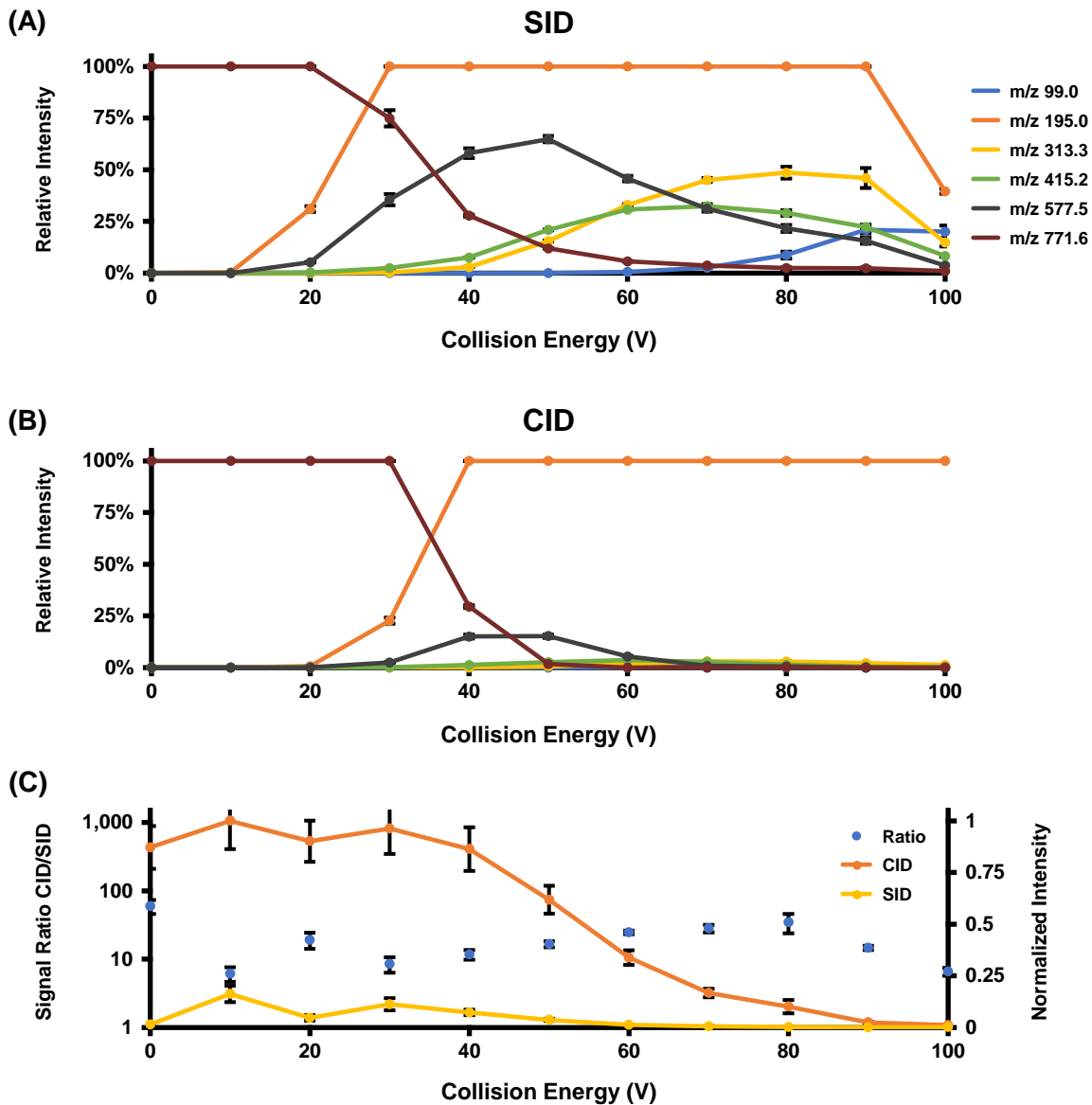**Figure C.9** (**A**) Relative ion intensity of SID precursor and predominant fragment ions as a function of collision energy for CL 18:1. (**B**) Relative ion intensity of CID precursor and predominant fragment ions as a function of collision energy for the same precursor ion as (**A**). (**C**) Comparison of the normalized total ion intensity for CID and SID of CL 18:1 as a function of collision energy, plotted alongside the ratio of the two normalized signals.
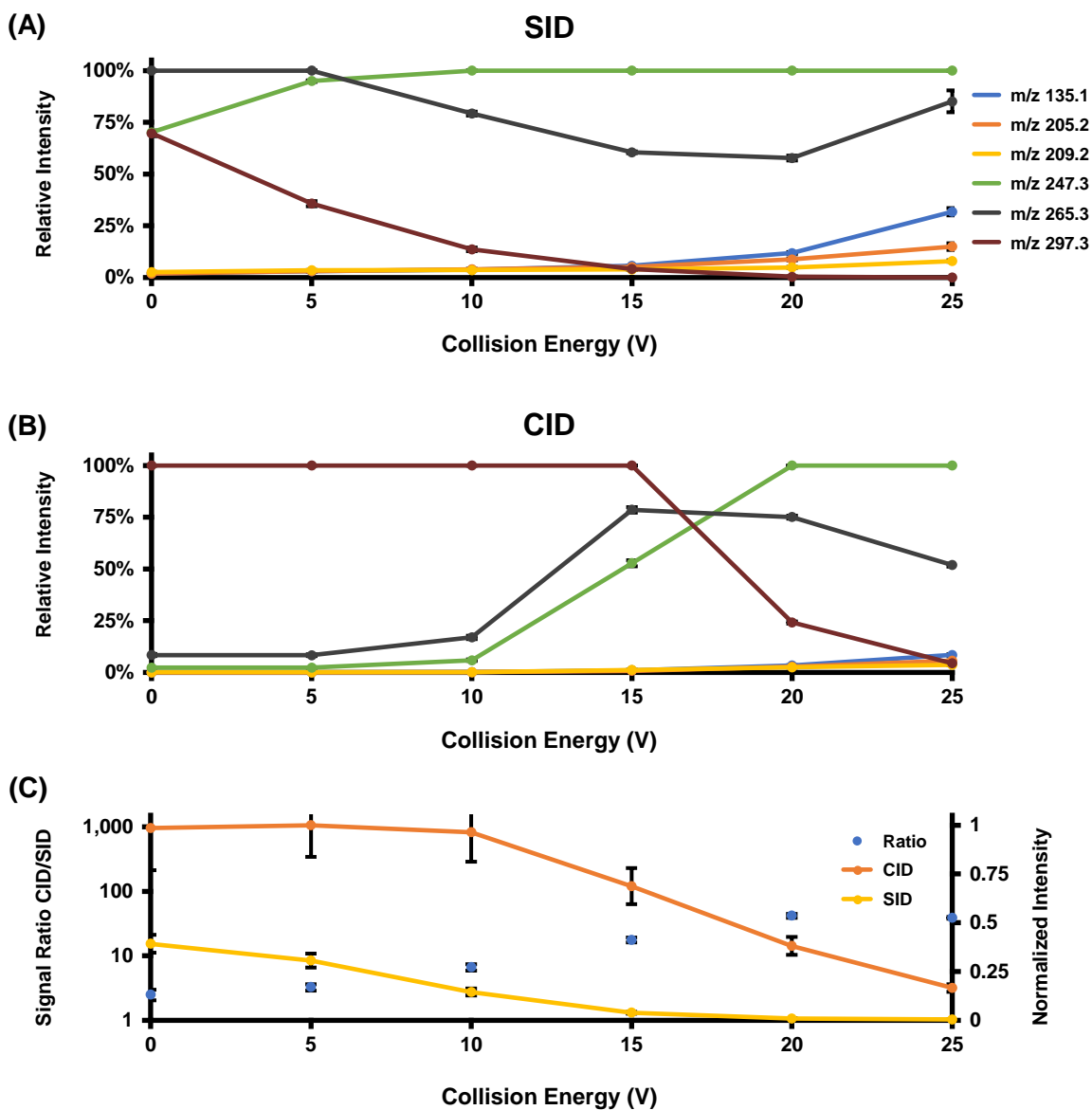
Figure C.10 (A) Relative ion intensity of SID precursor and predominant fragment ions as a function of collision energy for ST. **(B)** Relative ion intensity of CID precursor and predominant fragment ions as a function of collision energy for the same precursor ion as **(A)**. **(C)** Comparison of the normalized total ion intensity for CID and SID of ST as a function of collision energy, plotted alongside the ratio of the two normalized signals.
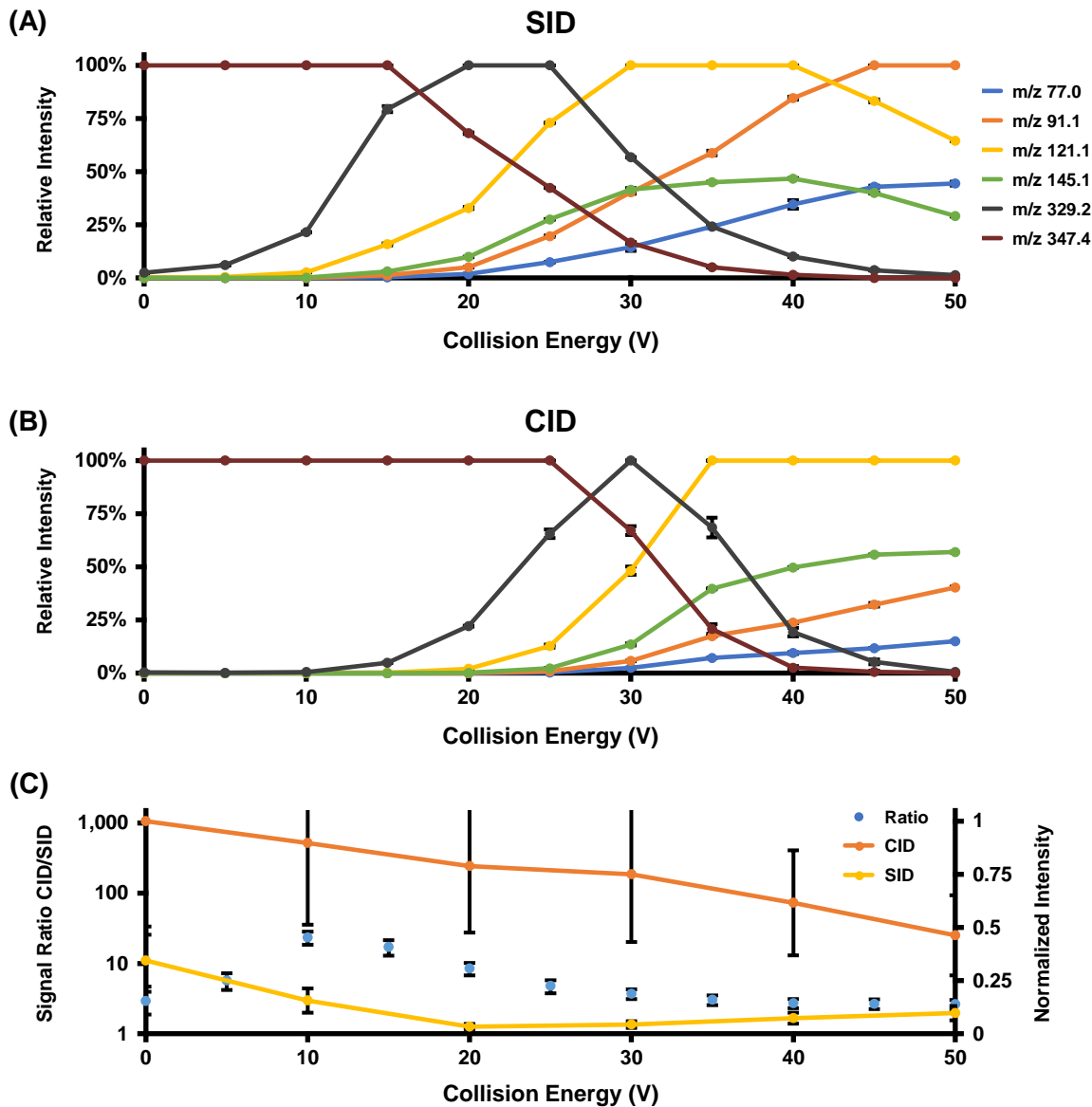
APPENDIX D

SUPPLEMENTARY MATERIALS FOR CHAPTER 4

D.1 Supplemental Materials for Mass Spectrometry and Ion Mobility Study of Polyurethanes

D.1.1 Synthesis Reagents and Reaction Schema

Methylene diphenyl diisocyanate, ethylene glycol, diethylene glycol, triethylene glycol and tetra ethylene glycol were purchased from Sigma-Aldrich and used without further purification. Toluene and Methylene chloride were purchased from Fischer Scientific. Trityl chloride was obtained from Oakwood Chemical, and tosyl chloride was obtained from Avocado Research Chemicals (Alfa Aesar). All NMR characterization was performed on a 400MHz Bruker NMR Spectrometer and chemical shifts were measured relative to tetramethylsilane (TMS).

The synthetic route utilized to synthesize mono-disperse hexa-, octa-, and deca-polyethylene glycols is shown in Scheme D.1. Mono-disperse tetra-polyethylene glycol (4) was tosylated to form the bis-tosylate (5). The mono-trityl-protected ethylene glycol was synthesized by reacting ethylene glycol (6a), diethylene glycol (6b), triethylene glycol (6c), or tetraethlyene glycol with trityl chloride to form the mono-tritylated derivatives (7a-d). Then the sodium salt of 7(a-c) was reacted with the bis-tosylate (5) to give the bis-trityl-protected hexa-, octa-, and deca-PEGs (8a-c). The trityl protecting groups were then removed using a biphasic system composed of methylene chloride and either concentrated hydrochloric acid or acetic acid to yield the monodisperse hexa-, octa-, and deca-PEGs (9a-c).
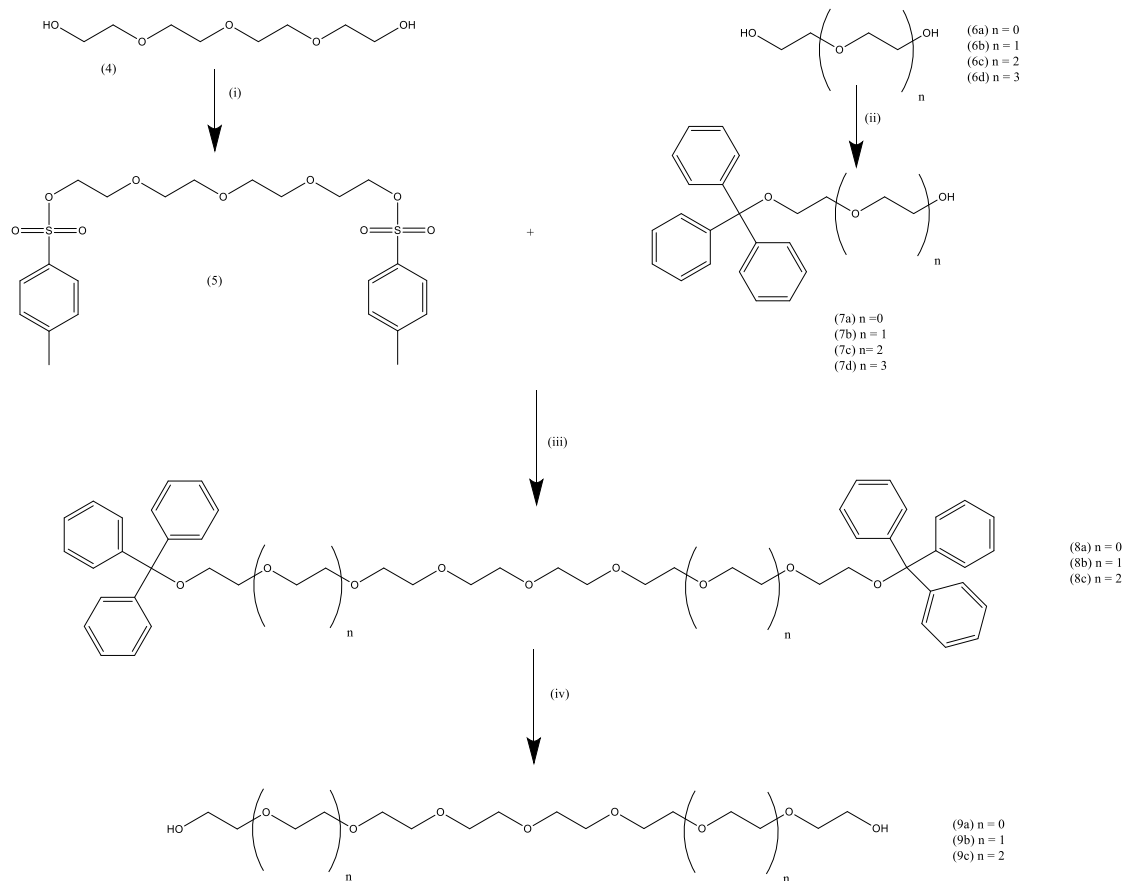
Scheme D.1 (i) Ts-Cl, THF, H_2O, KOH, 0ºC – 20ºC, 48 hrs; (ii) Trityl chloride, Et_3N, CH_2Cl_2, 0ºC - 20ºC, 24 hrs; (iii) NaH, THF, 40ºC, 72 hrs; (iv) AcOH or HCl, CH_2Cl_2, ambient temperature or 40ºC, 12 hrs.

136

The symmetrical MDI hexa-PEG oligomer derivative IDT747 (1) was synthesized as outlined in Scheme D.2.[1] MDI (12) was reacted with a 10-fold excess of hexa-PEG (11) by dripping a solution of MDI in toluene to a solution of the PEG in toluene containing a catalytic quantity of triethylamine to give IDT747 (1).

IDT764 (2) and IDT814 (3) were synthesized as outlined by Scheme D.3. Specifically, IDT764 (2) was synthesized by the addition of mono-trityl-tetraethylene glycol (7d) in toluene to a 3-fold excess of MDI (10) in toluene in the presence of a catalytic quantity of triethylamine. To give the mono-carbamates (11a) which was semi purified by adding hexanes to the toluene solution and crystalizing out unreacted MDI overnight in the refrigerator. Unreacted MDI was removed by filtration and the organic solution was evaporated under reduced pressure. The resultant intermediate (11a) was dissolved in methylene chloride and added to a solution containing an excess of octa-PEG dissolved in methylene chloride; the resultant solution was stirred at ambient temperature for 18 hours, evaporated and (12a) was semi purified by column chromatography on silica gel and deprotected by stirring a solution of (12a) in methylene chloride in the presence of concentrated hydrochloric acid to give IDT764 (2).

A sample of IDT814 (3) was synthesized in a similar fashion by reacting mono-trityl-protected deca-PEG with 5 equivalents of MDI and subsequently adding the crude mixture to 220 equivalents of diethylene glycol. The mono-trityl-protected intermediate was purified by column chromatography and deprotected using the same protocol as was used for the synthesis of IDT764 (2). Attempts to synthesize mono-tritylated deca-PEG using the protocol outlined for the synthesis of the mono-trityl tetra-PEG (7d) were low yielding and an alternative methodology was developed. The mono-trityl-protected tetra-PEG was synthesized by 2 different routes either directly from dodecyl PEG by reacting an excess of dodecyl-PEG with trityl alcohol in toluene

(12)

(11) n =5

(i)

(1) IDT 747 n = 5
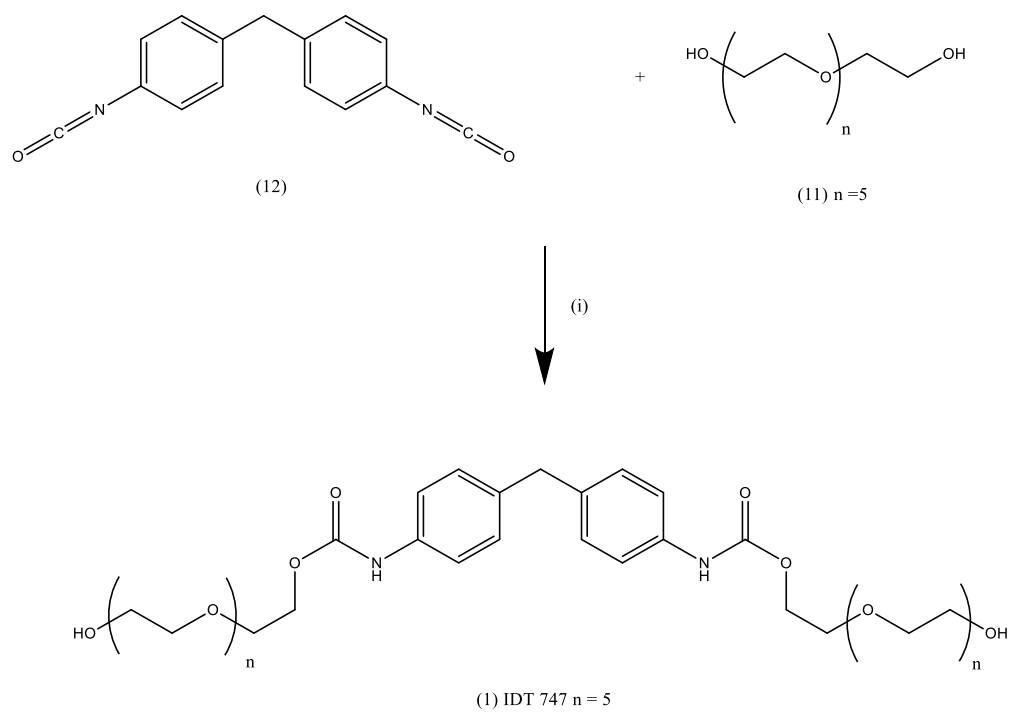
Scheme D.2 (i) toluene, Et$_3$N (cat)

(route A) using a catalytic quantity of para-toluene sulfonic acid with azeotropic removal of the resultant water to give the desired mono-tritylated deca-peg in a 43% yield or the mono-tritylated deca-peg (7e) was synthesized by converting mono-tritylated tetra PEG (7d) into the tosylate (13) and reacting this intermediate with an excess of the mono-sodium salt of hexa-peg (7c) (route B) to give the desired mono-tritylated deca-peg (7e) in a 50% yield.

D.1.2 Detailed Description of Compound Syntheses outlined in Schemes D.1, D.2, and D.3

Bis(17-hydroxy-3,6,9,12,15pentaoxaheptadecyl) (methylenebis(4,1-phenylene))dicabamate IDT747 (1)

Hexa-polyethylene glycol (2.82g, 0.01mols) was added to toluene (10ml) in a 3-necked flask equipped with a magnetic follower. Then triethylamine (1 drop) was added and the mixture was stirred at ambient temperature for 5 minutes. After which methylene diphenyl diisocyanate (MDI) (0.25g, 0.001mols) dissolved in toluene (50ml) was added dropwise over 1 hour. The resultant solution was stirred at ambient temperature for 18 hours and subsequently evaporated under reduced pressure. Then the residue was dissolved in methylene chloride (50ml) and this solution was washed with saturated sodium bicarbonate (50ml) and deionized water (50ml). After drying over magnesium sulphate the organic solution was filtered and evaporated and the product was purified by column chromatography on silica eluted with methylene chloride 95%: methanol 5%. This gave 0.263g of product in a 32% yield as a yellow oil. ^{1}H nmr (CDCl$_3$) δ 7.84 (brs, 2H), 7.32-7.28 (m, 4H), 7.09-7.02 (m, 4H), 4.29-4.28 (m, 4H), 3.86 (s, 2H), 3.60-3.58 (m, 44H), 3.35 (brs, 1H), 2.68 (brs, 1H); ^{13}C nmr (CDCl$_3$) δ 153.60, 136.17, 136.06, 129.25, 118.79, 72.61, 72.53, 70.49, 70.42, 70.34, 70.13, 70.08, 64.01, 61.52, 40.48
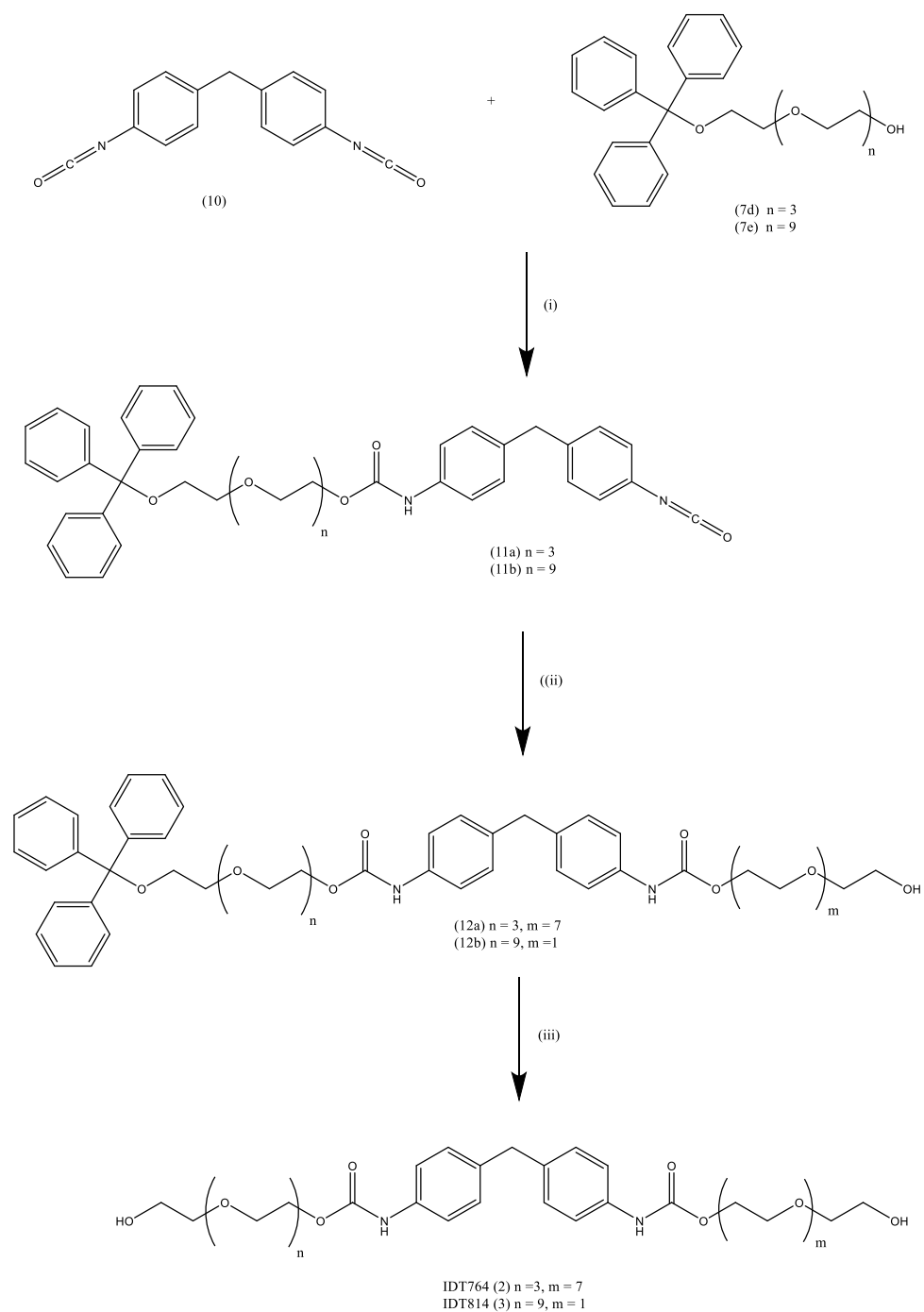
Scheme D.3. (i) toluene, triethylamine (cat), 18 hours 20ºC, (ii) methylene chloride, octa-ethylene glycol (excess), 20ºC, 18 hours; (iii) HCl, methylene chloride.

140

2-(2-(2-(2-hydroxyethoxy)ethoxy)ethoxy)ethyl 4-(4-((25-hydroxy-2,5,8,11,14,17,20,23-octaoxapentacosanoyl)amino)benzyl)phenyl carbamate IDT764 (2)

1,1,1-triphenyl-2,5,8,11-tetraoxatridecan-13-yl (4-(4-((25-hydroxy-2,5,8,11,14,17,20,23-octaoxapentacosanoyl)amino)benzyl)phenyl carbamate (0.8g, 0.0076mols) was dissolved in methylene chloride (100ml) and concentrated hydrochloric acid (2ml) was added. The resultant mixture was stirred at ambient temperature for 1 hour. Then it was washed with deionized water, dried over magnesium sulphate, filtered and evaporated to yield crude (2). This was purified by column chromatography on silica eluted with a gradient system running from methylene chloride 100% to methylene chloride 95%: methanol 5%. 0.35g of purified product was obtained from the column in a 56% yield as a pale-yellow oil. ^{1}H nmr (CDCl$_3$) δ 7.81 (brs, 1H), 7.66 (brs, 1H), 7.38-7.30 (m, 4H), 7.08-7.01 (m, 4H), 4.28 (t, 4H), 3.85 (s, 2H), 3.74-3.58 (m, 44), 3.47 (brs, 2H); ^{13}C nmr (CDCl$_3$) δ 153.53, 136.15, 136.11, 135.90, 135.87, 129.09, 118.8, 72.47, 72.36, 70.30, 70.25, 70.23, 70.17, 69.97, 69.94, 69.18, 63.77, 63.63, 62.24, 61.32, 40.37, 29.61

29-hydroxy-3,6,9,12,15,18,21,24,27-nonaoxanonacosyl (4-(4-(((2-(2-hydroxyethoxy)ethoxy)carbonyl)amino)benzyl)phenyl)carbamate IDT814 (3)

2-(2-(trityloxy)ethoxy)ethyl(4-(4-((31-hydroxy-2,5,8,11,14,17,20,23,26,29 decaoxahentriacontanoyl)amino)benzyl)phenyl)carbamate (0.37g, 0.00035 mols) was dissolved in methylene chloride (25ml) and concentrated hydrochloric acid (3 drops) was added. This mixture was stirred at ambient temperature for 30 minutes after which it was washed with deionized water (2 x 25ml) and dried over magnesium sulfate. The organic solution was filtered and evaporated and the product was purified on a silica gel column eluted with a gradient system running from methylene chloride (95%) / methanol (5%) to methylene chloride (80%) / methylene chloride (20%). This gave 0.25g of IDT814 (3) as a yellow tar in an 85.7% yield. 1H nmr (CDCl3) 7.58 (brS, 1H), 7.39 (brS, 1H) 7.30-7.26 (m, 4H), 7.08-7.02 (m, 4H), 4.31-4.25 (m, 4H), 3.76 (s, 2H),

3.71-3.55 (m, 40H), 3.45 (s, 4H), 2.23 (brS, 2H); 13C nmr (CDCl3) 153.60, 136.23, 136.17, 135.96, 129.21, 129.18, 129.08, 119.11, 118.81, 72.58, 72.39, 70.42, 70.39, 70.32, 70.29, 70.26, 70.01, 69.30, 63.87, 61.47, 61.43, 61.33, 50.46, 40.45.

((oxybis(ethane-1,2-diyl))bis(oxy))bis(ethane-1,2-diyl) bis(4-methylbenzenesulphonate) (5)

Tosyl chloride (29.4g, 0.154 mols) was added to a solution of tetraethylene glycol (10g, 0.0515 mols) in tetrahydrofuran (100ml) and cooled to 0ºC. Then potassium hydroxide (19g, 0.338 mols) dissolved in deionized water (20ml) was added dropwise over 30 minutes after which the solution was allowed to warm to ambient temperature and stirred for 48 hours. The solution was then partitioned between methylene chloride (200ml) and deionized water (200ml). The organic solution was separated and dried over magnesium sulphate. Then it was filtered and evaporated to give 25g of ((oxybis(ethane-1,2-diyl))bis(oxy))bis(ethane-1,2-diyl) bis(4-methylbenzenesulphonate) (5) in a 96% yield as a yellow oil. This was used in the next step without further purification. ^{1}H nmr (CDCl$_3$) 7.77 (d, 4H), 7.34 (d, 4H), 4.22 (t, 4H), 3.69 (t, 4H), 3.58-3.51 (m, 8H), 2.44 (s, 3H); ^{13}C nmr (CDCl$_3$) 144.80, 132.89, 129.80, 127.93, 70.68, 70.50, 69.23, 68.64, 21.61

2-(trityloxy)ethan-1-ol (7a)

Ethylene glycol (25.5g, 0.41 mols) was added to dimethyl formamide (50ml), pyridine (10ml) and dimethyl amino pyridine (1.2g). Then trityl chloride (22.9g, 0.082mols) was added and the solution was stirred at ambient temperature for 24 hours. Deionized water (160 ml) was then added. The resultant precipitant was removed by filtration and was dissolved in ethylacetate (100ml). The organic solution was washed with deionized water (50ml) and dried over magnesium sulphate. After which the solution was filtered and evaporated to yield crude product. Crystallization proceeded from a mixture of acetonitrile (125ml) and deionized water (100ml) to

give 17.6g of a white solid. Then the product was purified by column chromatography on silica gel eluted with a gradient system running from 100% methylene chloride to 95% methylene chloride / 5% methanol. This gave 15g of pure 2-(trityloxy)ethan-1-ol (7(a)) as a white solid in a 60% yield. ^{1}H nmr (CDCl$_3$) δ 7.46-7.40 (m, H), 7.33-7.22 (m, 9H), 3.73 (q, 2H), 3.25 (t, 2H), 2.01 (t, 1H); ^{13}C nmr (CDCl$_3$) δ 143.87, 128.62, 127.83, 127.21, 127.06, 86.60, 64.76, 62.33

2-(2-(trityloxy)ethoxy)ethan-1-ol (7b)

Diethylene glycol (188g, 1.772 mols), triethylamine (50ml) and methylene chloride (200ml) were cooled to 0ºC under nitrogen. The solution was stirred and trityl chloride (50g, 0.179g) dissolved in methylene chloride (50ml) was added over 30 minutes. The solution was then allowed to warm to ambient temperature and stirred for 24 hours. After which it was concentrated under reduced pressure and added to methylene chloride (200ml). This organic solution was washed with saturated sodium bicarbonate solution (200ml) and deionized water (3 x 150ml). Then the organic solution was dried over magnesium sulphate filtered and evaporated. The product was recrystallized from methylene chloride / hexanes to give 31.2g of the product as a white crystalline solid in a 50% yield. ^{1}H nmr (CDCl$_3$) δ 7.45-7.49 (m, 6H), 7.32-7.19 (m, 9H), 3.8-3.6 (m, 6), 3.33 (t, 1H); ^{13}C nmr (CDCl$_3$) δ 143.97, 128.66, 127.78, 126.97, 86.65, 72.23, 70.57, 63.31, 61.85

2-(2-(2-trityloxy)ethoxy)ethoxy)ethan-1-ol (7c)

Triethylene glycol (269g, 1.794 mols), triethylamine (50ml) and methylene chloride (400ml) were mixed and cooled to 0ºC with stirring. A solution of trityl chloride (50g, 0.1794 mols) in methylene chloride (50ml) was added dropwise over 30 minutes then the solution was allowed to warm to ambient temperature. Stirring was continued at ambient temperature for 24 hours. After which it was concentrated under reduced pressure and partitioned between methylene chloride (200ml) and saturated sodium bicarbonate (200ml). The organic solution was separated

and washed with deionized water (3 x 150ml) followed by drying over magnesium sulphate, filtration and evaporation. This gave 76g of the product as an oil which was used in the next step without further purification. ^{1}H nmr (CDCl$_3$) δ 7.47-7.45 (m, 6H), 7.30-7.19 (m, 9H), 3.69-3.62 (m, 8H), 3.48 (t, 2H), 3.24 (t, 2H), 2.56 (brs, 1H); ^{13}C nmr δ 143.92, 128.55, 127.64, 126.82, 86.45, 72.42, 70.66, 70.53, 70.35, 63.14, 61.58

2-(2-(2-(2-trityloxy)ethoxy)ethoxy)ethoxy)ethan-1-ol (7d)

Tetraethylene glycol (172g, 0.886mols), triethylamine (25ml) and methylene chloride (200ml) were mixed and cooled to 0°C with stirring. Trityl chloride (25g, 0.0897mols) dissolved in methylene chloride (25ml) was added dropwise over 30 minutes whilst maintaining the temperature at 0°C. Then the solution was allowed to warm to ambient temperature and stirred for 24 hours. After which it was concentrated under reduced pressure and the resultant slurry was partitioned between methylene chloride (200ml) and saturated sodium bicarbonate (200ml). The organic solution was separated and washed with deionized water (3 x 150ml), dried over magnesium sulphate filtered and evaporated to give 35.8g of product as a yellow oil. This was used in the next step without further purification. ^{1}H nmr (CDCl$_3$) δ 7.48-7.44 (m, 6H), 7.32-7.18 (m, 9H), 3.69-3.65 (m, 12H), 3.59 (t, 2H), 3.24 (t, 2H), 2.49 (brs, 1H); ^{13}C nmr (CDCl$_3$) δ 144.01, 128.68, 127.73, 126.90, 86.52, 72.44, 70.75, 70.69, 70.67, 70.38, 63.28, 61.73

1,1,1-triphenyl-2,5,8,11,14,17,20,23,26,29-decaoxahentraicontain-31-ol (7e)
Route A:

3,6,9,12,15,18,21,24,27-nonaoxanonacosane-1,29-diol (9c) (3.7g, 0.008 mols) was dissolved in toluene (100ml). Trityl alcohol (0.21g, 0.0008 mols) was added as well as para-toluene sulphonic acid (0.05g, 0.00026 mols). The solution was heated at reflux with stirring for 18 hours and water was removed by azeotropic distillation employing a dean and stark trap. Then

the solution was cooled to ambient temperature and evaporated under reduced pressure. The product was purified by column chromatography on silica gel eluted with methylene chloride (95%) / methanol (5%). This gave 0.24g of 1,1,1-triphenyl-2,5,8,11,14,17,20,23,26,29-decaoxahentraicontain-31-ol (7e) as an oil in a 43% yield.

Route B:

0.175g of sodium hydride (60% in mineral oil) was added to dry THF (30ml) and stirred under nitrogen. 3,6,9,12,15-pentaoxaheptadecane-1,17-diol (6(a), hexapolyethylene glycol) (6g, 0.021 mols) dissolved in dry THF (30ml) was added dropwise and the resultant solution was stirred at ambient temperature for 30 minutes under nitrogen. Then 1,1,1-triphenyl-2,5,8,11-tetraoxatridecan-13-yl 4-methylbenzenesulfonate (1.68g, 0.0028mols) dissolved in toluene (30 ml) and the resultant solution was heated at reflux for 18 hours with stirring. After which the solution was cooled to ambient temperature and toluene (20ml) was added. The organic solution was washed with brine (50ml) and water (50ml), dried over magnesium sulfate filtered and evaporated to give the crude product. This was purified by column chromatography on silica gel eluted with methylene chloride (95%) / methanol (5%) to give 1g of pure 1,1,1-triphenyl-2,5,8,11,14,17,20,23,26,29-decaoxahentraicontain-31-ol (7e) as an oil in a 50% yield. 1H nmr (CDCl3) δ 7.47 (d, 6H), 7.3-7.2 (m, 9H), 3.25-3.1 (m, 38H), 3.2 (t, 2H), 2.6 (brS, 1H); 13C nmr (CDCl3) δ 144.06, 128.64, 127.68, 126.84, 86.45, 72.50, 70.71, 70.63, 70.60, 70.54, 70.49, 70.25, 63.25, 61.65

1,1,1,21,21,21-hexaphenyl-2.5,8,11,14,17,20-heptooxahenicosane (8a)

Sodium hydride (60% in oil, 6.6g, 0.164mols) was washed with hexanes and dry tetrahydrofuran (100ml) was added. 2-(trityloxy)ethan-1-ol (25g, 0.082mols) was dissolved in dry tetrahydrofuran (100ml) and added to the sodium hydride suspension at ambient temperature with

stirring. The resultant suspension was stirred for 1 hour at ambient temperature then it was cooled to 0ºC. ((oxybis(ethane-1,2-diyl))bis(oxy))bis(ethane-1,2-diyl) bis(4-methylbenzenesulphonate) (20.6g, 0.041 mols) was dissolved in dry THF (50ml) and added dropwise to the cooled solution at 0ºC with stirring over 30 minutes. Then the solution was warmed to 40ºC and stirred for 80 hours. After which it was poured into an ice/water mix (300ml) and extracted with methylene chloride (2x150ml). The organic solution was dried over magnesium sulphate, filtered, and then evaporated to give crude product. This was purified by column chromatography on silica gel eluted with a gradient system running from 100% methylene chloride to 98% methylene chloride: 2% methanol, to give 24g of the desired product in a 76% yield as an orange oil. ^{1}H nmr (CDCl$_3$) δ7.47-7.44 (m, 12H), 7.30-7.18 (m, 18H), 3.68-3.62 (m, 20H), 3.22 (t, 4H); ^{13}C nmr (CDCl$_3$) δ 144.09, 128.68, 127.73, 126.88, 86.48, 70.74, 70.66, 70.63, 70.58,3.28, 53.41

1,1,1,27,27,27-hexaphenyl-2,5,8,11,14,17,23,23,26-nonaoxaheptacosane (8b)

Sodium hydride (60% in oil, 7.24g) was washed with hexanes and added to dry THF (200ml). 2-(2-(trityloxy)ethoxy)ethan-1-ol (31.2g, 0.09mols) was dissolved in dry THF (100ml) and added in 1 portion to the suspension of sodium hydride in THF. This mixture was then stirred at ambient temperature for 4 hours after which it was cooled to 0ºC and ((oxybis(ethane-1,2-diyl))bis(oxy))bis(ethane-1,2-diyl) bis(4-methylbenzenesulphonate) (22.59g, 0.045mols) dissolved in dry THF (100ml) was added dropwise with stirring over 30 minutes. The resulting suspension was warmed to 40ºC and this temperature was maintained for 5 days. After which the suspension was added to an ice/water mix (300ml), extracted into methylene chloride and dried over magnesium sulphate. The organic solution was filtered and evaporated to give crude product which was purified via column chromatography on silica eluted with a gradient system running from 100% methylene chloride to 98% methylene chloride: 2% methanol. This gave 28g of the

product as a yellow oil in a 73% yield. ^{1}H nmr (CDCl$_3$) δ 7.48-7.45 (m, 12H), 7.31-7.19 (m, 18H), 3.69-3.67 (m, 28H), 3.27 (t, 4H); ^{13}C nmr (CDCl$_3$) 144.10, 128.70, 127.74, 126.90, 86.50, 77.21, 70.76, 70.68, 70.65, 70.58, 70.53, 68.30

1,1,1,33,33,33-hexaphenyl-2,5,8,11,14,17,20,23.26,29,32-undecaoxatritriacontane (8c)

Sodium hydride (60% in oil, 6.4g) was washed with hexanes and added to dry THF (100ml). The resulting suspension was stirred and 2-(2-(2-trityloxy)ethoxy)ethoxy)ethan-1-ol (31.24g, 0.0796mols) dissolved in dry THF (100ml) was added. Then it was stirred at ambient temperature for 4 hours. After which it was cooled to 0ºC and ((oxybis(ethane-1,2-diyl))bis(oxy))bis(ethane-1,2-diyl) bis(4-methylbenzenesulphonate) (20g, 0.04mols) dissolved in dry THF (70ml) was added dropwise over 30 minutes. Upon complete addition of the bis-tosylate the temperature of the solution was raised to 40ºC and maintained at this temperature for 4 days with stirring. Then it was poured into an ice/water mix (300ml) and extracted into methylene chloride (3 x 200ml). The organic extracts were combined and dried over magnesium sulphate after which they were filtered and evaporated to give the crude product. This was purified by column chromatography on silica eluted with a gradient system running from 100% methylene chloride to 95% methylene chloride: 5% methanol. This gave 23.75g of the product as a yellow oil in a 63% yield. ^{1}H nmr (CDCl$_3$) δ 7.47-7.45 (m, 12H), 7.30-7.18 (m, 18H), 3.68-3.61 (m, 36H), 3.23 (t, 4H); ^{13}C nmr (CDCl$_3$) δ 144.01, 128.06, 127.65, 126.81, 86.40, 70.68, 70.60, 70.56, 70.50, 70.45, 63.21, 53.37, 30.82

3,6,9,12,15-pentaoxaheptadecane-1,17-diol (9a, hexa-polyethylene glycol)

1,1,1,21,21,21-hexaphenyl-2.5,8,11,14,17,20-heptooxahenicosane (23.5g, 0.031mols) was dissolved in methylene chloride (70ml) and acetic acid (276ml) was added. This was heated at 40ºC for 18 hours with stirring. Then it was cooled to ambient temperature and poured into an

ice/water mixture (400ml) and filtered. After which the filtrate was evaporated to give 6.6g of product as an oil in a 75% yield. ^{1}H nmr (CDCl$_3$) δ 4.4 (br s, 2H), 3.28-3.18 (m, 24H); ^{13}C nmr (CDCl$_3$) δ 72.52, 70.44, 70.32, 70.17, 69.85, 61.28

3,6,9,12,15,18,21-heptaoxatricosane-1,23-diol (9b, octa-polyethylene glycol)

1,1,1,27,27,27-hexaphenyl-2,5,8,11,14,17,23,23,26-nonaoxaheptacosane (28g, 0.0328mols) was dissolved in methylene chloride (150ml) and concentrated hydrochloric acid (15ml) was added. The mixture was stirred at ambient temperature for 1 hour then it was evaporated and deionized water (150ml). The aqueous PEG solution was filtered to remove trityl chloride and evaporated. This gave 7.4g of the desired product as an oil in a 62.5% yield. ^{1}H nmr (CDCl$_3$) δ 3.27-3.36 (m, 28H), 3.30 (brS, 4H); ^{13}C nmr (CDCl$_3$) δ 72.43, 70.43, 70.15, 61.49

3,6,9,12,15,18,21,24,27-nonaoxanonacosane-1,29-diol (9c, deca-polyethylene glycol)

1,1,1,39,39,39-hexaphenyl-2,5,8,11,14,17,20,23,26,29,32,35,38-tridecaoxanatriacontane (44.3g, 0.047mols) was dissolved in methylene chloride (100ml) and concentrated hydrochloric acid (8ml) was added. This mixture was stirred at ambient temperature for 1 hour then it was evaporated and deionized water (200ml) was added. The aqueous solution was filtered and evaporated to give product which was dissolved in methylene chloride (200ml), dried over magnesium sulphate, filtered and evaporated to give 16.9g of decyl PEG in a 78% yield as a yellow oil. ^{1}H nmr (CDCl$_3$) δ 3.74-3.60 (m, 40H), 3.19 (brs, 2H); ^{13}C nmr (CDCl$_3$) δ 72.46, 70.44, 70.39, 70.13, 61.49

1,1,1-triphenyl-2,5,8,11-tetraoxatridecan-13-yl (4-(4-((25-hydroxy-2,5,8,11,14,17,20,23-octaoxapentacosanoyl)amino)benzyl)phenyl carbamate (12a)

Methylene diphenyl diisocyanate (MDI) (3.75g, 0.015mols) was dissolved in toluene (20ml) and triethylamine (0.2ml) was added. Then mono-trityl-protected tetra-polyethylene glycol

(2.2g, 0.005mols) dissolved in toluene was added dropwise with stirring. Upon complete addition the solution was stirred for 18 hours at ambient temperature. After which hexanes (150ml) were added and unreacted MDI crystalized upon cooling to 0ºC. This was removed by filtration and the filtrate was evaporated under reduced pressure. The resultant mono-carbamate intermediate was dissolved in methylene chloride (40ml) and added dropwise to a solution of octa-PEG (11(b)) (7.4g, 0.08mols) in methylene chloride (10ml). The resultant solution was stirred at ambient temperature for 18 hours and then evaporated under reduced pressure to give crude (14(a)) which was purified by column chromatography on silica gel eluted with a gradient system running from methylene chloride 100% to methylene chloride 95%: methanol 5%. This gave 0.8g of 1,1,1-triphenyl-2,5,8,11-tetraoxatridecan-13-yl(4-(4-((25-hydroxy-2,5,8,11,14,17,20,23-octaoxapentacossanoyl)amino)benzyl)phenyl carbamate (12) as a tar in a 15.2% yield. [1]H nmr indicated that this was the correct material however it still contained some impurities so it was deprotected and further purified in the next step.

2-(2-(trityloxy)ethoxy)ethyl (4-(4-((31-hydroxy-2,5,8,11,14,17,20,23,26,29-decaoxahentriacontanoyl)amino)benzyl)phenyl)carbamate (12b)

Methylene diphenyl diisocyanate (MDI) (1.159g, 0.0046 mols) was dissolved in toluene (5ml) and triethylamine (3 drops) was added. The solution was stirred at ambient temperature and 1,1,1-triphenyl-2,5,8,11,14,17,20,23,26,29-decaoxahentraicontain-31-ol (0.65g, 0.00092 mols) dissolved in toluene was added dropwise over 1 hour. Then the solution was stirred at ambient temperature for 1 hour after which it was evaporated under reduced pressure and the crude mixture was dissolved in methylene chloride (50ml). Diethylene glycol (21.2g, 0.2 mols) was dissolved in methylene chloride (10ml) and stirred. The solution of the crude mixture was added dropwise to the PEG solution over 1 hour and stirring was continued at ambient temperature for 18 hours. Then deionized water (50ml) was added the resultant solid was removed by filtration and washed with

methylene chloride (2 x 100ml). The combined organic extracts were dried over magnesium sulfate, filtered and evaporated to give crude product. This product was purified by column chromatography on silica gel eluted with ethyl acetate (95%) / methanol (5%) to give 0.39g of the pure intermediate as a tar. 1H nmr (CDCl3) δ 7.45 (d, H), 7.31-7.03 (m, 17H), 4.30-4.24 (m, 4H), 3.87 (s, 2H), 3.75-3.48 (m, 42H), 3.22 (t, 2H), 2.75 (brS, 1H); 13C nmr (CDCl3) δ 153.47, 143.97, 136.19, 136.04, 135.97, 135.88, 129.17, 128.56, 127.62, 126.78, 118.76, 72.32, 72.23, 70.60, 70.52, 70.48, 70.45, 70.35, 69.28, 63.84, 63.16, 61.48, 40.42

1,1,1-triphenyl-2,5,8,11-tetraoxatridecan-13-yl 4-methylbenzenesulfonate (13)

Route A:

2-(2-(2-(2-trityloxy)ethoxy)ethoxy)ethoxy)ethan-1-ol (7d) (9.4g, 0.0215 mols) was dissolved in THF (30ml) and cooled to 0ºC with stirring. Then sodium hydroxide (3.44g, 0.086 mols) dissolved in deionized water (10ml) was added dropwise maintaining the temperature below 5ºC. After which the solution was stirred at 0ºC for 30 minutes. Then tosyl chloride (4.7g, 0.0245 mols dissolved in THF (10ml) was added dropwise to the stirred solution at 0ºC over 15 minutes. The resultant solution was stirred at 0ºC for 5 hours and then for a further 18 hours at ambient temperature. Deionized water (50ml) was added and the solution was extracted with methylene chloride (100ml). Then the organic extracts were washed with deionized water (50ml), dried over magnesium sulfate filtered and evaporated. The product was purified by column chromatography on silica eluted with ethyl acetate (30%) / hexanes (70%) to give 6g of pure 1,1,1-triphenyl-2,5,8,11-tetraoxatridecan-13-yl 4-methylbenzenesulfonate (13) in a 46.5% yield as a clear oil.

Route B:

2-(2-(2-(2-trityloxy)ethoxy)ethoxy)ethoxy)ethan-1-ol (7d) (41.9g, 0.096 mols) was dissolved in methylene chloride (200ml) and triethylamine (30ml) followed by dimethylamino

pyridine (0.2g). The resultant solution was cooled to 0ºC then para-toluene sulfonyl chloride (21.96g, 0.115 mols was added). The solution was stirred at 0ºC for 1 hour then allowed to warm to ambient temperature and stirring was continued for 18 hours. After which the solution was washed with deionized water (2 x 100ml), dried over magnesium sulfate filtered and evaporated. The product was purified as described in the synthesis via route A and this gave 37g of 1,1,1-triphenyl-2,5,8,11-tetraoxatridecan-13-yl 4-methylbenzenesulfonate (13) in a 65.6% yield as a clear oil. 1H nmr (CDCl3) δ7.79 (d, 2H), 7.46 (d, 6H), 7.34-7.21 (m, 11H), 4.14 (t, 2H), 7.34-7.21 (m, 12H), 3.25 (t, 2H), 2.42 (s, 3H); 13C nmr (CDCl3) δ 144.71, 144.08, 132.99, 129.76, 128.68, 127.94, 127.72, 126.89, 86.50, 70.74, 70.70, 70.64, 70.58, 69.19, 68.64, 63.28, 60.36
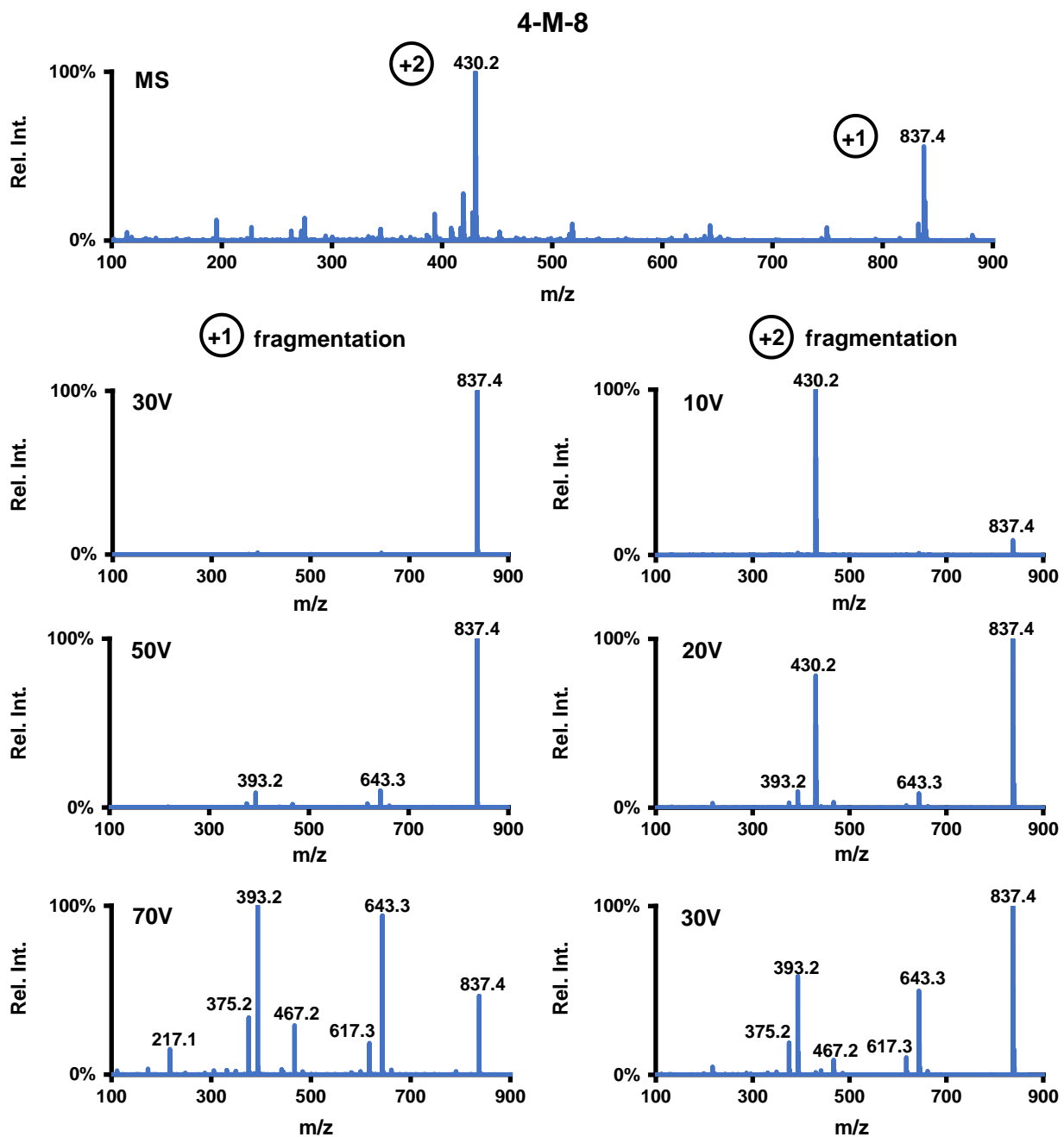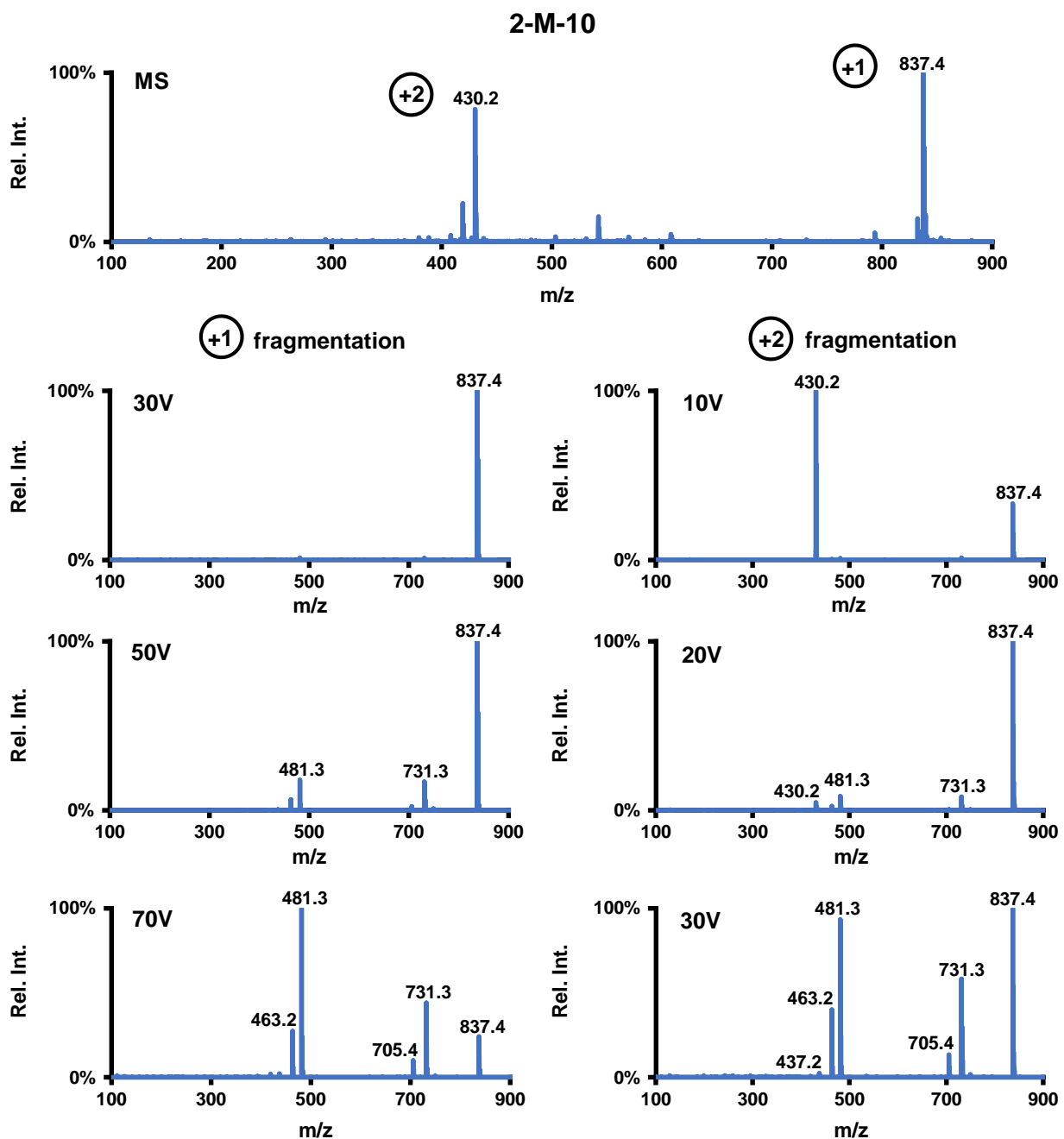
Supplemental Figure D.1 Mass spectra of 4-M-8 depicting the +1 and +2 species at m/z 837.4 and m/z 430.2, respectively. Both charge states were quadrupole-isolated and subjected to fragmentation at multiple collision energies, with the resulting fragmentation spectra shown for 30V, 50V, and 70V for the +1 species, and the 10V, 20V, and 30V for the +2 species. Both species produced the same fragment ions, with the +2 species first disassociating into the +1 species before further disassociation occurred.
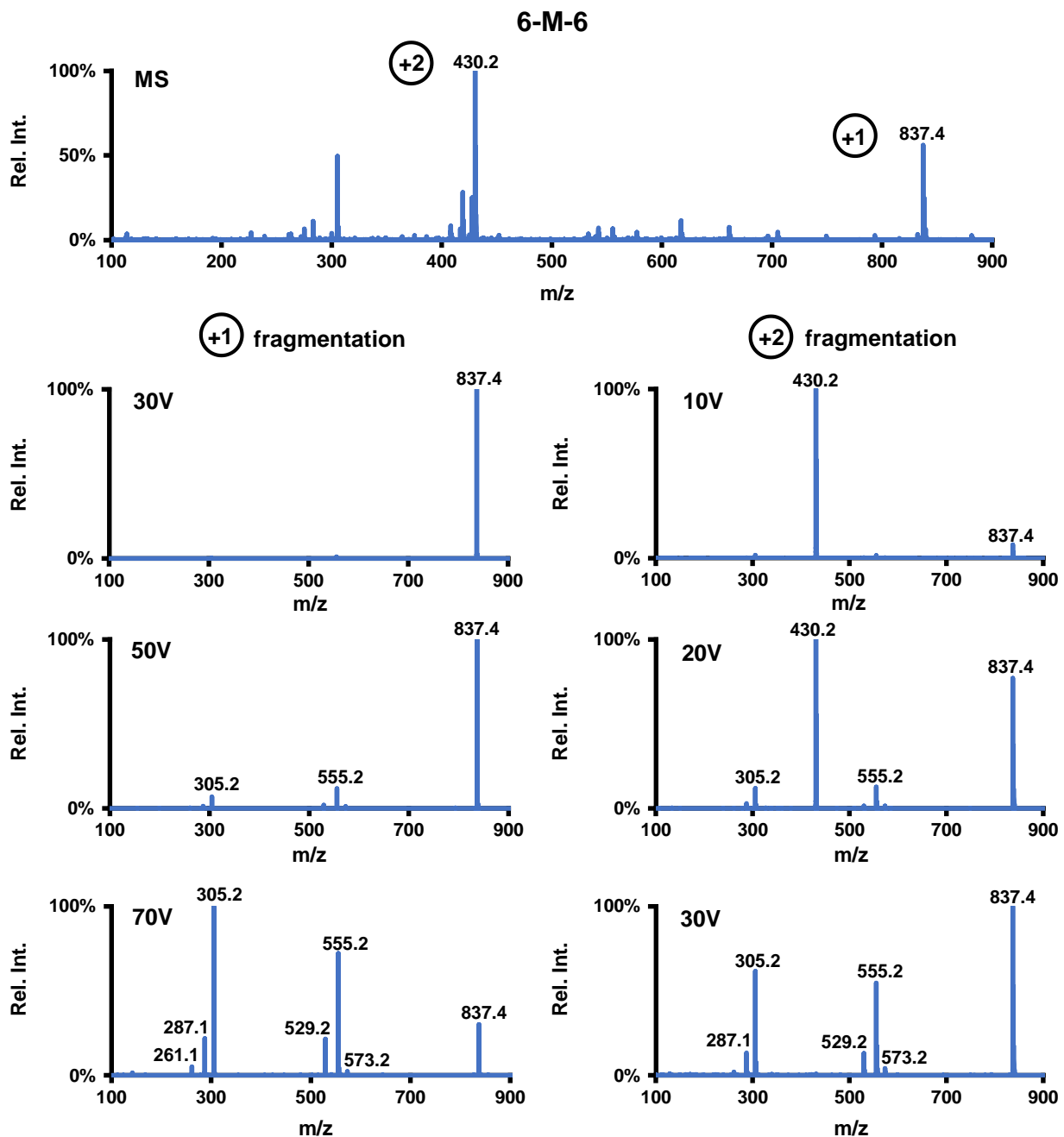
Supplemental Figure D.2 Mass spectra of 6-M-6 depicting the +1 and +2 species at m/z 837.4 and m/z 430.2, respectively. Both charge states were quadrupole-isolated and subjected to fragmentation at multiple collision energies, with the resulting fragmentation spectra shown for 30V, 50V, and 70V for the +1 species, and the 10V, 20V, and 30V for the +2 species. Both species produced the same fragment ions, with the +2 species first disassociating into the +1 species before further disassociation occurred.

Supplemental Figure D.3 Mass spectra of 2-M-10 depicting the +1 and +2 species at m/z 837.4 and m/z 430.2, respectively. Both charge states were quadrupole-isolated and subjected to fragmentation at multiple collision energies, with the resulting fragmentation spectra shown for 30V, 50V, and 70V for the +1 species, and the 10V, 20V, and 30V for the +2 species. Both species produced the same fragment ions, with the +2 species first disassociating into the +1 species before further disassociation occurred.
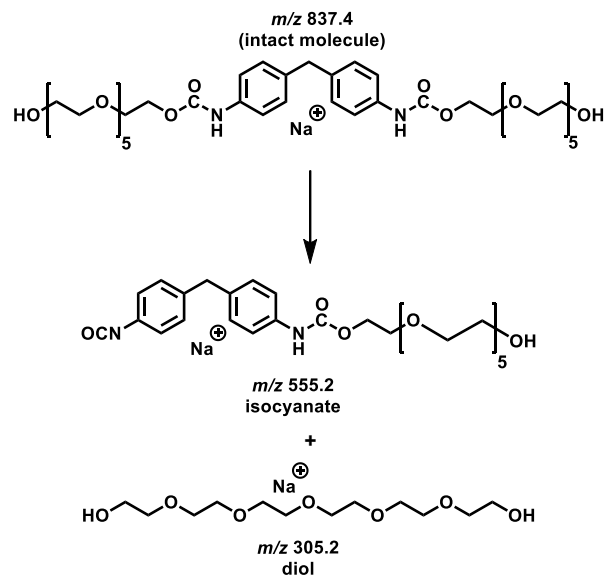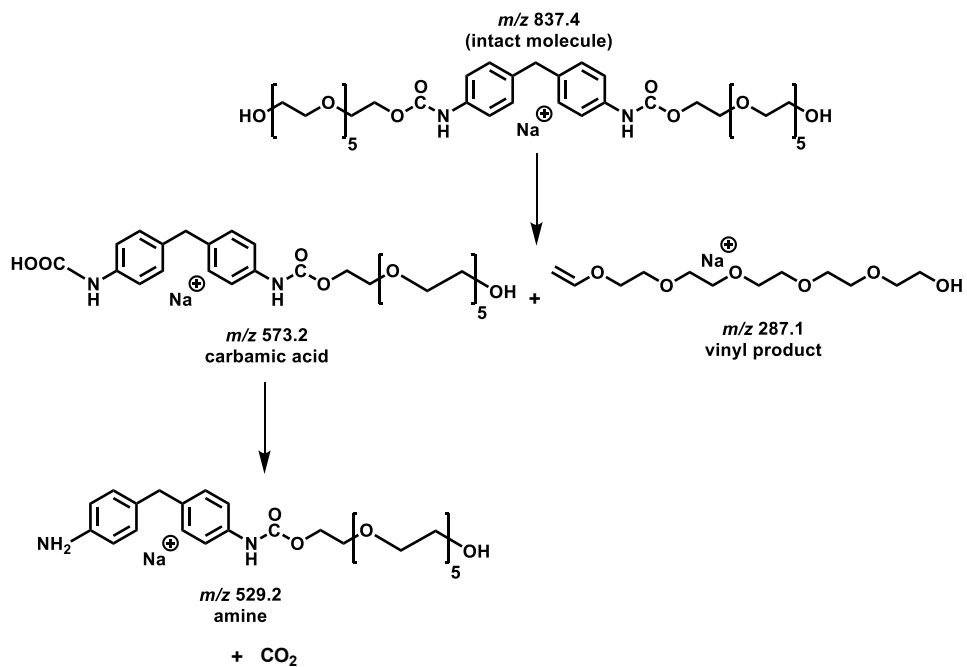
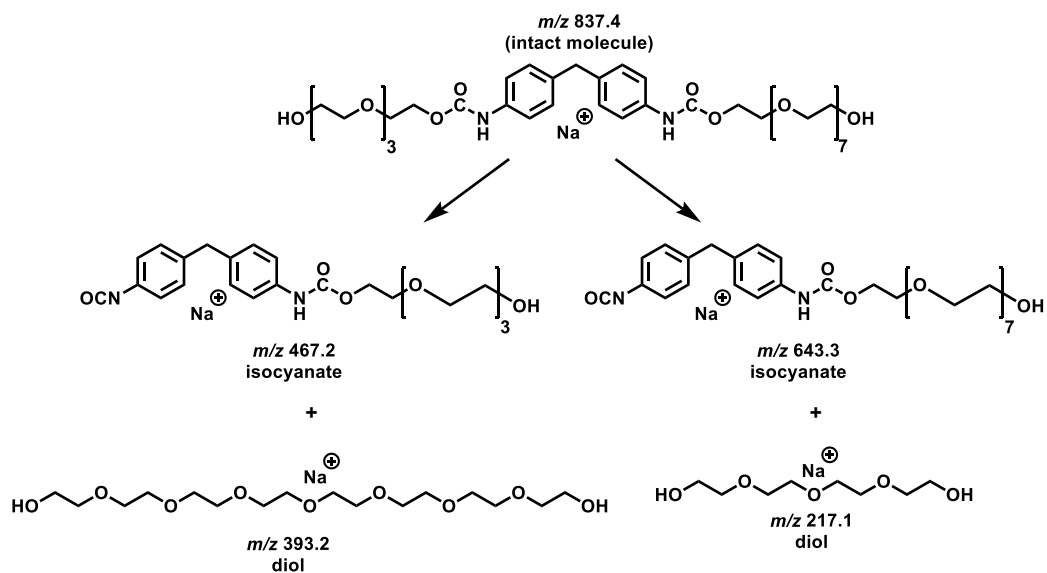**Supplemental Figure D.4** Illustrated 1,3-hydrogen shift reaction for the 6-M-6 oligomer with precursor and product masses labelled.

Supplemental Figure D.5 Illustrated 1,5-hydrogen shift reaction for the 6-M-6 oligomer with precursor and product masses labelled.

Supplemental Figure D.6 Illustrated 1,3-hydrogen shift reaction for the 4-M-8 oligomer with precursor and product masses labelled.

Supplemental Figure D.7 Illustrated 1,5-hydrogen shift reaction for the 4-M-8 oligomer with precursor and product masses labelled.
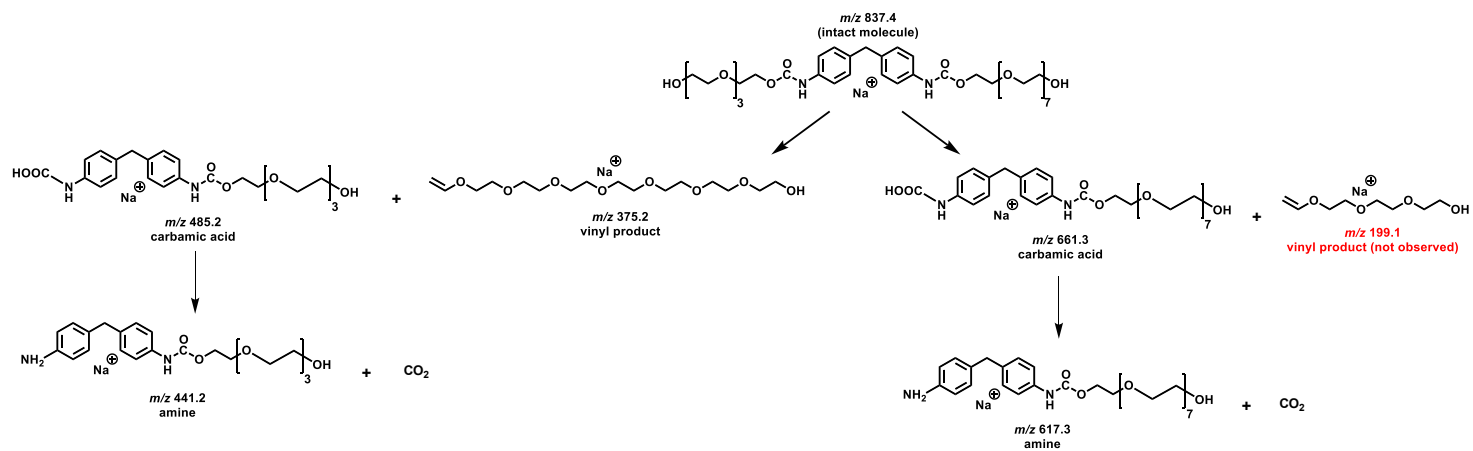
Supplemental Figure D.8 Illustrated 1,3-hydrogen shift reaction for the 2-M-10 oligomer with precursor and product masses labelled.

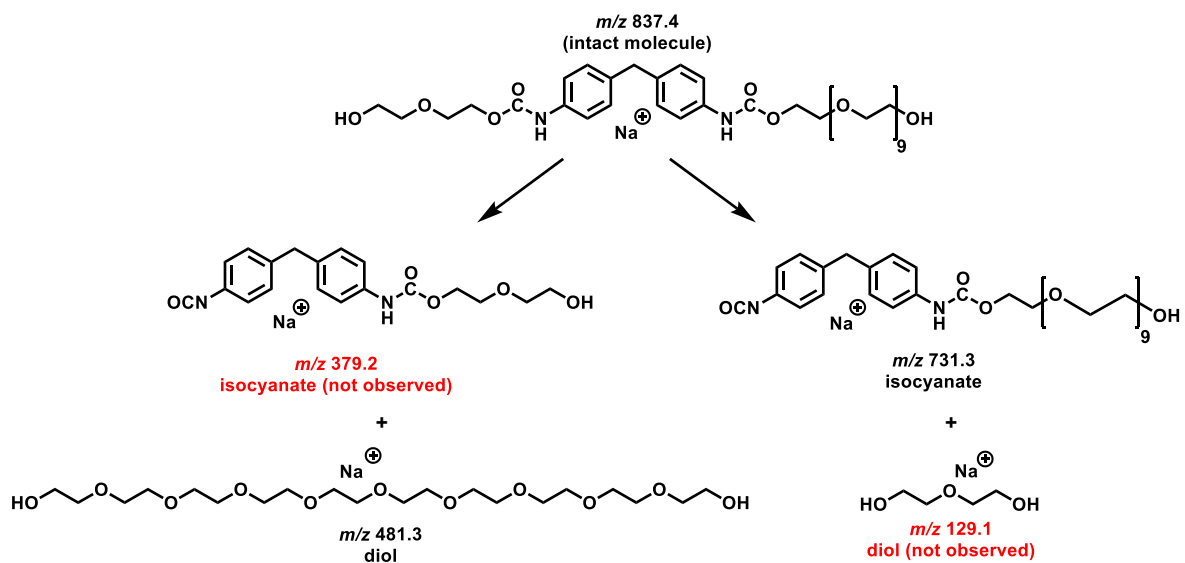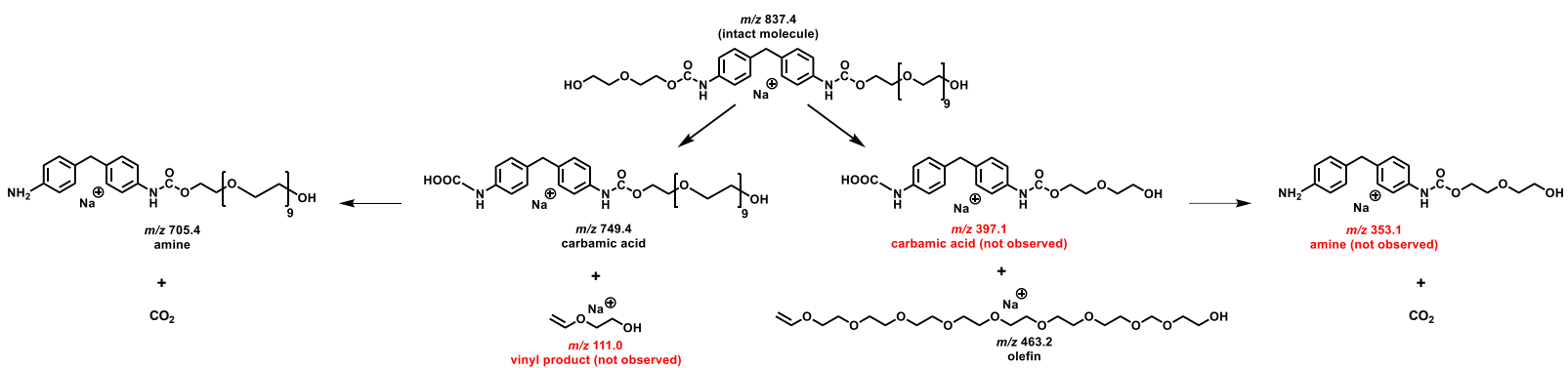**Supplemental Figure D.9** Illustrated 1,5-hydrogen shift reaction for the 2-M-10 oligomer with precursor and product masses labelled.
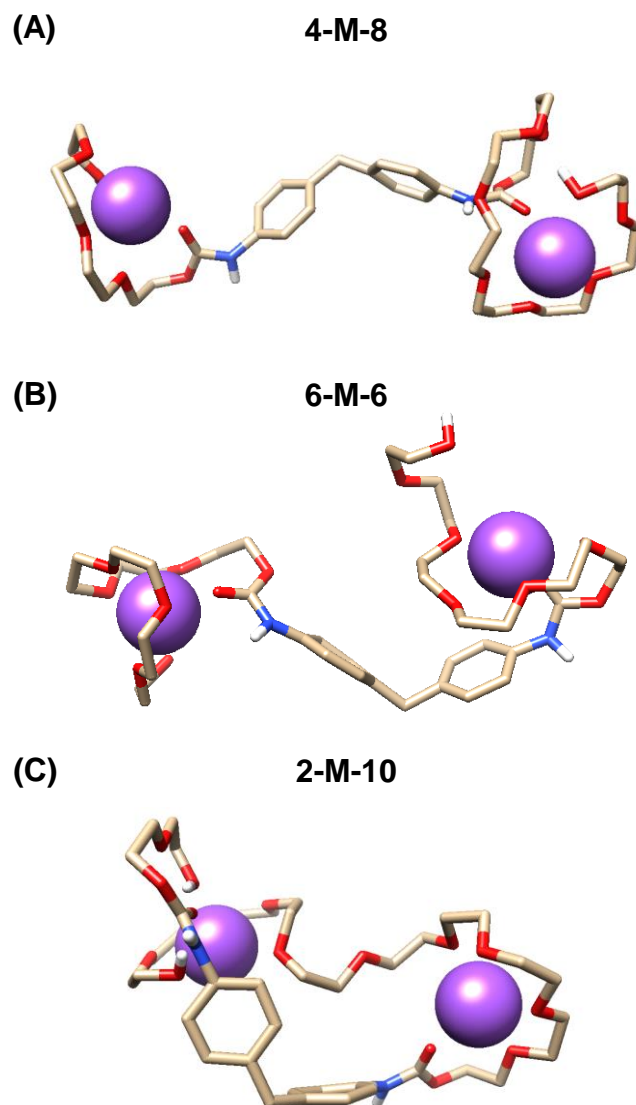
(A)   **4-M-8**

(B)   **6-M-6**

(C)   **2-M-10**

Supplemental Figure D.10 Example simulated structures for +2 species of the **(A)** 4-M-8, **(B)** 6-M-6, and **(C)** 2-M-10 oligomers.

D.1.4 References

(1)   Gothard, C. M.; Grzybowski, B. A. A Cost-Effective, Column-Free Route to Ethylene Glycol Oligomers EG$_6$, EG$_{10}$, and EG$_{12}$. *Synthesis (Stuttg).* **2012**, *44* (5), 717–722.

CURRICULUM VITAE

Rachel A. Harris

Permanent address:

6161 Slick Rock Drive

Conroe, TX 77304

rharris2343@gmail.com

936-522-6517

Present address:

110 Acklen Park Drive Apt 112

Nashville, TN 37203

rachel.a.harris@vanderbilt.edu

936-522-6517

EDUCATION

Vanderbilt University   Nashville, TN

Ph.D. in Chemistry   May 2021

Dissertation: Analysis of Biopolymers and Synthetic Polymers Using Structurally Selective Analytical Techniques in Combination with Mass Spectrometry

Advisor: Dr. John A. McLean

University of North Carolina at Chapel Hill   Chapel Hill, NC

B.S. Chemistry   May 2015

Advisor: Dr. Gary Glish

RESEARCH EXPERIENCE

Graduate Research Assistant   2015-2021

Department of Chemistry

Vanderbilt University

Nashville, TN

Principal Investigator: Dr. John McLean

Developed fragmentation techniques for improved lipid structural characterization, including online-ozonolysis and surface induced dissociation (SID). Optimized experimental conditions for maximized reaction yields, and identified novel fragment ions for greater structural coverage. Additional projects involved the analysis of polymer structural trends in ion mobility mass spectrometry.

Summer Research Intern   June-August 2015

NIH Eastern Regional Comprehensive Metabolomics Resource Core

RTI International

Research Triangle Park, NC

Supervisor: Dr. Suraj Dhungana

Established an untargeted LC-MS lipidomics platform for the identification of lipid species present in biological matrices. To reduce the false discovery rate (FDR), lipid standards from major classes were analyzed to determine retention time ranges, adduct preferences in positive and negative mode, and

fragmentation patterns for each class.

Undergraduate Research Assistant   2013-2015

Department of Chemistry

University of North Carolina at Chapel Hill

Chapel Hill, North Carolina

Principal Investigator: Dr. Gary Glish

Developed the technique of "linked scanning" of the compensation voltage and helium carrier gas simultaneously to improve the resolution and sensitivity of differential ion mobility spectrometry (DIMS/FAIMS) coupled to mass spectrometry.

Summer Undergraduate Research Assistant   June-August 2014

Department of Chemistry

University of North Carolina at Chapel Hill

Chapel Hill, North Carolina

Principal Investigator: Dr. Gary Glish

Designed method for the separation and identification of components present in e-cigarette liquids via GC-MS for the FDA Tobacco Center of Regulatory Science (TCORS).

Summer Research Intern   June-August 2013

Department of Experimental Radiation Oncology

The University of Texas MD Anderson Cancer Center

Houston, Texas

Principal Investigator: Dr. Junjie Chen

Used tandem affinity purification to identify potential protein interacting partners of the protein encoded by the TREX2 gene, which is thought to be involved in human DNA damage response pathways.

TEACHING EXPERIENCE

Teaching Assistant   2016-2021

Department of Chemistry

Vanderbilt University

Courses: General Chemistry Lab I, Physical Chemistry Lab, Analytical Lab, Forensics Lab, Capstone Advanced Integrated Lab

PUBLICATIONS

Harris, R. A.; McLean, J. A.; Robinson, R. A.; Verberne-Sutton, S. Determining the Concentration of CBD in Commercial Products using HPLC with Low Student Density at the Instrument. In Preparation for *J. Chem. Ed*, **2021**.

Harris, R. A.; May, J. C.; Harvey, S. R.; Wysocki, V. H.; McLean, J. A. Evaluation of Surface Induced Dissociation in Conjunction with Ion Mobility-Mass Spectrometry for Lipid Structural Characterization. In Preparation for *Analytical Chemistry*, **2021**.

Rose, B. S.; Leaptrot, K. L.; **Harris, R. A.**; Sherrod, S. D.; May, J. C.; McLean, J. A. A Shotgun Lipidomics Workflow for High-Confidence Lipid Analysis using a Drift Tube Ion Mobility-Tandem Mass Spectrometer. In *Shotgun Lipidomics: Methods and Protocols*. *In press,* **2021.**

Harris, R. A.; Picache, J. A.; Tomlinson, I. D.; Zlibut, E.; Ellis, B. M.; May, J. C.; Mclean, J. A.; Hercules, D. M. Mass Spectrometry and Ion Mobility Study of Poly(Ethylene Glycol)-based Polyurethane Oligomers. *Rapid Commun. Mass Spectrom*. **2020**, No. e8662, 1–8.

Harris R.A., Leaptrot K.L., May J.C., McLean J.A. New frontiers in lipidomics analyses using structurally selective ion mobility-mass spectrometry, *Trends Anal. Chem*., **2019**, *116*:316-323.

Harris R.A., May J.C., Stinson C.A., Xia Y., McLean J.A. Determining Double Bond Position in Lipids Using Online Ozonolysis Coupled to Liquid Chromatography and Ion Mobility-Mass Spectrometry, *Anal. Chem.* **2018**, *90*(3): 1915-1924.

Santiago, B. G., **Harris, R. A.**, Isenberg, S. L., & Glish, G. L. Resolving powers of >7900 using linked scans: how well does resolving power describe the separation capability of differential ion mobility spectrometry. *The Analyst*, **2015**, *140*(20), 6871–6878.

Santiago, B. G., **Harris, R. A.**, Isenberg, S. L., Ridgeway, M. E., Pilo, A. L., Kaplan, D. A., & Glish, G. L. Improved Differential Ion Mobility Separations Using Linked Scans of Carrier Gas Composition and Compensation Field. *Journal of The American Society for Mass Spectrometry*, **2015**, *26*(10), 1746–1753.

PRESENTATATIONS

Harris, R.A.; Buck, K.M.; Soni, S.; Picache, J.A.; Tomlinson, I.D.; Zlibut, E.; Ellis, B.M.; May, J.C.; McLean, J.A.; Hercules, D.M. Analysis of Synthesized Polyethylene Glycol-Based Polyurethane Oligomers Using Ion Mobility-Mass Spectrometry. Poster presented at the 68th ASMS Conference on Mass Spectrometry and Allied Topics. Virtual conference, 2020.

Harris, R.A.; May, J.C.; Harvey, S. R.; Wysocki, V.H.; McLean, J.A. Evaluation of Surface Induced Dissociation in Conjunction with Ion Mobility-Mass Spectrometry for Lipid Structural Characterization. Poster presented at the Waters Corporation Young Investigator's Summit. Beverly, MA, 2019.

Harris, R.A.; May, J.C.; Harvey, S. R.; Wysocki, V.H.; McLean, J.A. Evaluation of Surface Induced Dissociation in Conjunction with Ion Mobility-Mass Spectrometry for Lipid Structural Characterization. Poster presented at the 67th ASMS Conference on Mass Spectrometry and Allied Topics. Atlanta, GA, 2019.

Harris, R.A.; May, J.C.; Stinson, C.A.; Harvey, S.R.; Xia, Y.; Wysocki, V.H.; McLean, J.A. Evaluating New Fragmentation Technologies In Conjunction With Ion Mobility-Mass Spectrometry For Improved Lipid Structural Characterization. Oral presented at the 66th ASMS Conference on Mass Spectrometry and Allied Topics. San Diego, CA, 2018.

Harris, R.A.; Stinson, C.A.; Xia, Y.; May, J.C.; McLean, J.A. Development of a Flow-Cell Ozonolysis Device Coupled to Ion Mobility-Mass Spectrometry for Determining Double Bond Position in Lipids. Poster presented at the 65th ASMS Conference on Mass Spectrometry and Allied Topics. Indianapolis, IN, 2017.

Harris, R.A.; Stinson, C.A.; Xia, Y.; May, J.C.; McLean, J.A. Development of a Flow-Cell Ozonolysis Device Coupled to Ion Mobility-Mass Spectrometry for Determining Double Bond Position in Lipids. Poster presented at the 2017 Vanderbilt Institute of Chemical Biology Student Research Symposium. Nashville, TN, 2017.

Harris, R.; Jurneczko, E.; Harvey, S.; Wysocki, V.; McLean, J. A Critical Comparison of Collision Induced Dissociation and Surface Induced Dissociation for Metabolomics. Poster presented at the 64th ASMS Conference on Mass Spectrometry and Allied Topics. San Antonio, TX, 2016.

Harris R.; Jurneczko E.; Harvey S.; Wysocki V.; McLean J. A Critical Comparison of Collision Induced Dissociation and Surface Induced Dissociation for Metabolomics. Poster presented at the 10th Annual Q-Bio Conference. Nashville, TN, 2016.

Lackey, J.; **Harris, R**.; Spencer, S.; Reeber, S.; Glish, G. Liquid- and Vapor-Phase Analysis of E-Cigarette Liquids by Mass Spectrometry. Poster presented at the 63rd ASMS Conference on Mass Spectrometry and Allied Topics. St. Louis, MO, 2015.

Santiago, B.; **Harris, R.**; Glish, G. Improvement of Resolution and Peak Capacity for Differential Ion Mobility Spectrometry Scans using Linked Helium and Compensation Field Scans. Poster presented at the 63rd ASMS Conference on Mass Spectrometry and Allied Topics. St. Louis, MO, 2015.

 Spencer, S.; **Harris, R.**; Reeber, S.; Clapp, P.; Jaspers, I.; Glish, G. Evaluation of the Composition and Toxicity of Electronic Cigarette Liquids. Poster presented at the 63rd ASMS Conference on Mass Spectrometry and Allied Topics. St. Louis, MO, 2015.

Harris, R.; Santiago, B.; Isenberg, S.; Glish, G. A Novel Scan Method for Differential Ion Mobility Spectrometry Separations. Oral presented at the 249th ACS National Meeting & Exposition. Denver, CO, 2015.

Harris, R.; Santiago, B.; Isenberg, S.; Glish, G. Linked Scanning of He and Compensation Voltage to Improve the Resolving Power of Differential Ion Mobility Separations. Poster presented at the Eastern Analytical Symposium and Exposition. Somerset, NJ, 2014.

Harris, R.; Santiago, B.; Isenberg, S.; Glish, G. Linked Scanning of Helium and Compensation Voltage to Improve the Resolving Power of Differential Ion Mobility Spectrometry Separations. Poster presented at the 62nd ASMS Conference on Mass Spectrometry and Allied Topics. Baltimore, MD, 2014**.**

HONORS AND AWARDS

Vanderbilt Chemistry Warren Fellowship   2020

NSF-GRFP Honorable Mention   2016

Vanderbilt Institute of Chemical Biology Fellowship	2015
Harold Stirling Vanderbilt Graduate Scholarship	2015
Eastern Analytical Symposium Student Research Award	2014
National Merit Finalist	2011

PROFESSIONAL SOCIETIES /ORGANIZATIONS

American Chemical Society	2015-2021
American Society of Mass Spectrometry	2014-2021
Alpha Chi Sigma Chemistry Fraternity	2013-2021
Phi Beta Kappa – Alpha of North Carolina	2015-2021

COMMUNITY OUTREACH EXPERIENCE

Nashville Food Project	2016-2019
Vanderbilt/Fisk Universities Materials Research Society	2015-2019
Carolina Community Garden	2011-2015

EXTRACURRICULAR ACTIVITIES

Nashville Women's Rugby Football Club	2018-2021
Alpha Chi Sigma Professional Chemistry Fraternity	2013-2015
Gamma Sigma Epsilon Chemistry Honor Society	2013-2015